[redacted]

RESEARCH MEMORANDUM

for the

U. S. Air Force

INVESTIGATION OF A 1/22-SCALE MODEL OF THE REPUBLIC F-105 AIRPLANE IN THE LANGLEY 8-FOOT TRANSONIC TUNNEL

STATIC LONGITUDINAL STABILITY AND CONTROL AND PERFORMANCE CHARACTERISTICS AT TRANSONIC SPEEDS

By Arvo A. Luoma

Langley Aeronautical Laboratory
Langley Field, Va.

NATIONAL ADVISORY COMMITTEE
FOR AERONAUTICS

WASHINGTON

APR 26 1956

[redacted]
UNCLASSIFIED

NACA RM SL56D12

NATIONAL ADVISORY COMMITTEE FOR AERONAUTICS

RESEARCH MEMORANDUM

for the

U. S. Air Force

INVESTIGATION OF A 1/22-SCALE MODEL OF THE REPUBLIC F-105 AIRPLANE IN THE LANGLEY 8-FOOT TRANSONIC TUNNEL

STATIC LONGITUDINAL STABILITY AND CONTROL AND PERFORMANCE CHARACTERISTICS AT TRANSONIC SPEEDS

By Arvo A. Luoma

SUMMARY

A comprehensive investigation of the aerodynamic characteristics of various configurations of a 1/22-scale model of the Republic F-105 airplane has been made in the Langley 8-foot transonic tunnel at Mach numbers from 0.60 to 1.13. All the configurations except wing-off configurations were investigated with internal flow in the model. The results of the initial phase of the investigation are presented herein. These results include information of the static longitudinal stability and control characteristics of the model; on the effect of various configuration modifications on lift-drag ratio; on the effect of subsonic and supersonic inlets and of external stores on the aerodynamic characteristics; and on the effect of area-distribution modifications (on the basis of the area rule) on performance.

No serious pitch-up difficulties were apparent at a constant Mach number. An afterbody bump reduced the zero-lift drag coefficient by 0.006 at Mach numbers near 1.0 and by 0.004 to 0.005 at a Mach number of 1.13. The lift-drag characteristics were improved by several configuration modifications. The effective downwash derivative $d\epsilon/d\alpha$ decreased markedly at Mach numbers above 0.93.

INTRODUCTION

An extensive wind-tunnel investigation of the aerodynamic characteristics of the Republic F-105 airplane has been made by the National

Advisory Committee for Aeronautics at the request of the U. S. Air Force. A low-speed investigation of the static stability and control characteristics of a 1/4-scale model of the F-105 airplane was made in the Langley 19-foot pressure tunnel (refs. 1 and 2). A supersonic-speed investigation of the aerodynamic characteristics of a 1/22-scale model of the F-105 airplane was made in the Langley 4- by 4-foot supersonic pressure tunnel (results of preliminary tests are given in ref. 3). A transonic-speed investigation of the performance and static longitudinal, lateral, and directional stability and control characteristics of the 1/22-scale model of the F-105 airplane was made in the Langley 8-foot transonic tunnel.

The results of the initial phase of the investigation in the Langley 8-foot transonic tunnel are presented herein. These results include information on the static longitudinal stability characteristics; on the effectiveness of the horizontal tail and of the rudder; on the effect of leading-edge flaps, of inlet modifications, and of wing-tip extensions on lift-drag ratio; on the effect of subsonic and supersonic inlets and of external stores on the aerodynamic characteristics; and on the effect of area-distribution modifications (on the basis of the area rule) on performance.

SYMBOLS

The aerodynamic force and moment data are referred to the stability axes, with the origin at the center-of-gravity location shown in figure 1. This location coincided with the 25-percent point of the mean aerodynamic chord of the basic ($A = 3.18$) wing. All the data presented herein, including those for the configurations with the extended wing tips ($A = 3.69$) and with the wing removed, were based on the plan-form dimensions of the basic wing.

The term "complete model" as used herein refers to the combination of wing (including air inlets), body (including canopy), vertical tail, and horizontal tail. The symbols used are defined as follows:

A aspect ratio of wing, b^2/S

b span (projected) of wing

C_D external drag coefficient, $\frac{\text{External drag}}{qS}$

C_{D_o} zero-lift external drag coefficient

[redacted]

C_L lift coefficient, $\frac{\text{Lift}}{qS}$

C_Y lateral-force coefficient, $\frac{\text{Lateral force}}{qS}$

C_l rolling-moment coefficient, $\frac{\text{Rolling moment}}{qSb}$

C_m pitching-moment coefficient, $\frac{\text{Pitching moment}}{qS\bar{c}}$

C_n yawing-moment coefficient, $\frac{\text{Yawing moment}}{qSb}$

$\bar{c}$ mean aerodynamic chord of wing, $\frac{2}{3} c_r\left(\frac{1 + \lambda + \lambda^2}{1 + \lambda}\right)$

c_e nominal tip chord of wing, obtained by extending leading and trailing edges of wing to plane which is perpendicular to chord plane of wing, parallel to root chord of wing, and tangent to tip of wing

c_r root chord of wing, obtained by extending straight portions of leading and trailing edges of wing to plane of symmetry of model

i_t incidence of horizontal tail, determined by angle between plane of horizontal tail and reference line of body; positive direction when trailing edge is down

$(L/D)_{max}$ maximum value of lift-drag ratio

M Mach number of undisturbed stream

m/m_o inlet mass-flow ratio, measured by ratio of mass flow in model duct to mass flow through free-stream tube with area equal to inlet throat area (see table I for inlet throat areas)

q dynamic pressure of undisturbed stream

R Reynolds number of tests, based on mean aerodynamic chord of basic wing

S area (projected) of wing, $(b/2)(c_r + c_e)$

α angle of attack of model, based on reference line of body

[redacted]

δ control-surface deflection, measured in plane perpendicular to hinge line of control surface; positive direction when trailing edge is down in case of flaperon, when leading edge is up in case of leading-edge flaps, or when trailing edge is to the left in case of rudder

ϵ effective downwash angle in region of horizontal tail, determined from tests of complete model and complete model less horizontal tail or from tests of complete model less wing and complete model less wing and less horizontal tail

λ taper ratio of wing, c_e/c_r

$C_{L_\alpha} = \frac{dC_L}{d\alpha}$ per degree

$C_{L_{\delta_f}} = \frac{dC_L}{d\delta_f}$ per degree

$C_{l_{\delta_f}} = \frac{dC_l}{d\delta_f}$ per degree

$C_{l_{\delta_r}} = \frac{dC_l}{d\delta_r}$ per degree

$C_{m_{C_L}} = \frac{dC_m}{dC_L}$

$C_{m_{i_t}} = \frac{dC_m}{di_t}$ per degree

$C_{m_{\delta_f}} = \frac{dC_m}{d\delta_f}$ per degree

$C_{n_{\delta_f}} = \frac{dC_n}{d\delta_f}$ per degree

$C_{n_{\delta_r}} = \frac{dC_n}{d\delta_r}$ per degree

[redacted]

$$C_{Y_{\delta_f}} = \frac{dC_Y}{d\delta_f} \text{ per degree}$$

$$C_{Y_{\delta_r}} = \frac{dC_Y}{d\delta_r} \text{ per degree}$$

Subscripts:

f value for flaperon

n value for leading-edge flaps

r value for rudder

APPARATUS

Tunnel

The tests were made in the Langley 8-foot transonic tunnel. This tunnel operates at a stagnation pressure approximately equal to atmospheric pressure.

Model

Basic model.- The model used in the present investigation was a sting-supported, 1/22-scale model of the Republic F-105 airplane. This airplane is of the fighter-bomber type and is designed for supersonic flight. The airplane is turbojet powered, and has wing-root air inlets. The wing and tail surfaces have 45° of sweepback. The airfoil sections (parallel to the body reference line) of the wing are NACA 65A005.5 at the 0.38b/2 station and NACA 65A003.7 at the tip. The basic model is shown in figure 1, and the geometric characteristics are given in table I.

The model was designed for internal flow. Ducting from the wing-root inlets led into a single duct which had an exit at the body base. A supersonic inlet and a transonic inlet were tested on the model and these are shown in figure 2. Boundary-layer diverters were used with both inlets. The supersonic inlet had two interchangeable throats: one for the high-speed condition and one for the cruise condition. The area of the throat for the cruise condition was 25 percent greater than that for the high-speed condition. The throat areas of the inlets (scaled down from full-scale values) are given in table I and the duct exit areas used with the various inlets are given in figure 3. The duct exit area could be changed by replacement of a bushing at the end of the body.

[redacted]

The dimensions and location on the basic wing of leading-edge flaps and a single flaperon (located on right-wing panel) are shown in figure 4. The dimensions and location of pylon-mounted wing tanks (2) are shown in figure 5. The fineness ratio of the tanks was 7.65. The thickness ratio of the pylons was 0.06.

Area-rule modifications.- The longitudinal distributions of normal cross-sectional area of the complete model with the supersonic inlet (cruise condition) with and without modifications are shown in figure 6(a). An area of 1.40 square inches, which corresponded to 90 percent of the inlet area of the supersonic inlet (cruise condition), was subtracted from the area plots to compensate for the internal flow in the model. Various body modifications were made to improve the area distribution; these included a long nose, a modified canopy, an $M = 1$ afterbody bump, and a modified $M = 1$ afterbody bump. The contours of the modifications are shown in figure 6(b). Photographs of the modified canopy, the $M = 1$ bump, and the modified $M = 1$ bump are shown as figures 6(c), 6(d), and 6(e), respectively. The $M = 1$ bump was modified (essentially by eye) into the modified $M = 1$ bump in an attempt to improve the supersonic drag characteristics.

Modifications for improving $(L/D)_{max}$ characteristics.- Various configuration modifications were made on the model with the supersonic inlet (cruise condition) in an attempt to improve the lift-drag characteristics, particularly at the cruising Mach number of approximately 0.9 of the F-105 airplane. These modifications are enumerated as follows. The wing tips together with the leading-edge flaps were extended spanwise as shown in figure 7; the geometric characteristics of this modified wing are given in table I. The wing-inlet fairing (designated as wing modifications 2 and 3 of table II) was revised as shown in figures 7 and 6(e). The supersonic inlet (cruise condition) was drooped -5°. The drooped inlet was obtained by cutting the undrooped supersonic inlet (cruise condition) along a lateral plane located closely ahead of the leading edge of the wing and then drooping the inlet -5° about an axis at the bottom of the cut. The location of the droop axis and a cross section of the drooped inlet are shown in figure 2. The drooped inlet is included in the configurations shown in figures 6(c), 6(d), and 6(e).

The wing on the F-105 airplane has a small amount of negative camber in the region of the inlets as a result of a buildup of the lower surface to accommodate the landing gear. The major portion of the model tests was made with the wing in this condition. For two test runs, the model wing in the region of the inlets was modified into a symmetrical section by building up the upper surface of the wing. This modification is designated as wing modification 1 (table II). The radius of the upper lip and the contour of the upper surface (adjacent to the lip) of the drooped supersonic inlet (cruise condition) were reshaped slightly, and

some refairing was made on the external lower surface of the inlet. This modification is designated as inlet modification 1 (table II).

Instrumentation

Balance.- A six-component strain-gage balance housed within the fuselage was used for determining the overall forces and moments on the model.

Pressure instrumentation.- Two static-pressure orifices were located within the chamber surrounding the strain-gage balance and two others on the sides of the sting adjacent to the base of the body. A rake, attached to the sting, was used at the duct exit for mass-flow and internal-drag determinations. The rake consisted of 2 static-pressure tubes and of either 12 total-pressure tubes for the configurations with the transonic inlet and the supersonic inlet (high-speed condition) or of 16 total-pressure tubes for the configurations with the supersonic inlet (cruise condition).

Angle-of-attack indicator.- A strain-gage, pendulum-type attitude transmitter was used for getting the no-load angle of attack of the model. The attitude transmitter was housed in the extension of the model sting and was located approximately 61 inches downstream of the model center-of-gravity location. Flexibility under aerodynamic load of the balance, model sting, and sting extension between the model and the attitude transmitter required a correction to the reading of the attitude transmitter to obtain the model angle of attack.

METHODS

Test Configurations and Procedure

The identification number and description of the configurations tested and a listing of the control deflections are given in table II. Most of the configurations included the supersonic inlet (cruise condition), either drooped or undrooped. All the tests were made with the model in the smooth condition. All the configurations were investigated through an angle-of-attack range at generally eight or nine Mach numbers from 0.60 to 1.13. The angle-of-attack range varied from approximately -2° to 16° at the lowest Mach number to -2° to 9° at the highest Mach number. The angle of sideslip was 0°. The average Reynolds number of the investigation is shown plotted against Mach number in figure 8.

All the configurations except the wing-off configurations were investigated with internal flow in the model. No attempt was made to regulate the internal mass flow for a given configuration.

[redacted]

Measurement of Overall Forces and Moments

The overall aerodynamic forces and moments of the various configurations were determined from strain-gage readings. The mass-flow rake was detached from the sting during these measurements.

Internal-Flow Measurements

The static pressure in the chamber surrounding the strain-gage balance and at the sides of the sting at the body base was measured for all configurations.

The internal mass flow and internal drag were measured for three configurations. These configurations consisted of the complete model at a horizontal-tail incidence of -3° equipped with the transonic inlet, the supersonic inlet (high-speed condition), and the undrooped supersonic inlet (cruise condition), and are listed as configurations 1, 4, and 5 in table II. Internal-flow data were obtained through the angle-of-attack and Mach number ranges of the investigation. The mass-flow and internal-drag measurements were made separately from the force and moment measurements.

CORRECTIONS AND ACCURACY

Pressure Correction to Drag

No internal flow in model.- The drag coefficient C_D of the wing-off configurations, which had no internal flow in the model, has been adjusted for the difference between the actual measured static pressure at the base of the body and that in the undisturbed stream, so that the drag coefficient C_D corresponds to a static pressure at the base of the body equal to that of the undisturbed stream.

Internal flow in model.- The external drag coefficient C_D of the configurations with internal flow in the model includes corrections for the internal drag coefficient and for the deviation from the free-stream value of the static pressure in the balance chamber and at the rim of the body base. The same correction for internal drag was used for all configurations equipped with the same inlet.

No corrections were included herein for the effects of internal flow on lift, pitching-moment, rolling-moment, yawing-moment, and lateral-force coefficients. The maximum effect of internal flow on lift coefficient occurred at the highest angles of attack and amounted to only 0.005.

Tunnel-Boundary Interference

Subsonic Mach numbers.- At subsonic Mach numbers, the interference effects of a tunnel boundary on the flow over a model in the test region near the center line of a tunnel have been made negligible by means of a slotted test section (ref. 4).

Supersonic Mach numbers.- Data are presented herein at supersonic Mach numbers of 1.03 and 1.13. Boundary interference (tunnel-boundary-reflected compression and expansion disturbances) on the data at a Mach number of 1.03 was probably small and is believed to have been confined primarily to affecting the drag data. No data are presented herein between Mach numbers of 1.03 and 1.13, where the effects of boundary interference may have been large. It is believed that the data at a Mach number of 1.13 were not significantly affected by boundary interference.

No corrections have been made to the data for tunnel-boundary interference except to the extent of the partial correction for tunnel-boundary interference inherent in the base-pressure correction, which was made by using the actual measured value of base static pressure.

Sting-Interference Corrections

No sting-interference corrections have been made to the data except to the extent of the partial correction for sting interference inherent in the base pressure correction, which was made by using the actual measured value of base static pressure.

Precision of Data

The estimated accuracy of the data based primarily on the repeatability of the data was as follows:

C_L	±0.01
C_D	±0.0015
C_m	±0.003
C_l	±0.0003
C_n	±0.0004
C_Y	±0.002
α, deg	±0.1
M	±0.003

[redacted]

RESULTS AND DISCUSSION

Presentation of Results

Basic force and moment results.- The basic force and moment results for the various configurations are presented in figures 9 to 39. An index of these figures together with the identification number and description of the configurations and a listing of the control deflections are given in table II. Horizontal-tail incidences are included in the titles of the basic figures; other control deflections are included in the titles of the basic figures only when the deflections were different from 0°.

The inlet mass-flow ratio m/m_o (based on inlet throat areas; see table I for area values) was approximately 0.90 for all inlets at most of the test conditions (data not presented herein). The inlet mass-flow ratio at a given Mach number decreased at the highest angles of attack; for example, the decrease amounted to approximately 20 percent at an angle of attack of 17° at a Mach number of 0.60. The inlet mass-flow ratio at a given angle of attack generally varied only slightly with change in Mach number. The actual mass flow in the configurations with the transonic inlet and the supersonic inlet (high-speed condition) was less than that in the configurations with the supersonic inlet (cruise condition) because of the smaller inlet throat areas of the transonic inlet and the supersonic inlet (high-speed condition). See table I for inlet areas.

Summary force and moment results.- Summary plots derived from the basic force and moment data are shown in figures 40 to 55. An index of these plots is given in table III. Control deflections are included in the titles of the summary figures only when the deflections were different from 0°.

The trim data of figure 42 and the neutral-point-location data of figure 43 were worked up from the basic results for configurations 5, 6, and 11. The effective downwash data of figures 54 and 55 for the model with the supersonic inlet (cruise condition) were determined from the basic results for configurations 5 to 9 and 11. Configuration 11 included wing modification 1 (see table II) which was not present on configurations 5 to 9. The effect of this configuration difference, however, was indicated by a comparison of the results for configurations 5 and 10 to be small. The effective downwash data for the model with the transonic inlet were determined from the results for configurations 1 to 3, and for the complete model less wing from the results for configurations 27 to 31.

[redacted]

Lift Characteristics

An increase in lift-curve slope with increase in angle of attack at moderate angles of attack was characteristic of all configurations tested. The lift-curve slope C_{L_α} is presented herein at lift coefficients of 0 and 0.4, and is the average value from 0.1 below to 0.1 above the specified lift coefficient. The variation of lift-curve slope with Mach number was generally characterized by a small "bucket" type of variation at Mach numbers near 1.0, particularly at lifting conditions (fig. 40, for example). This type of variation has been shown by other investigations (refs. 5 and 6, for example).

Most of the configuration modifications for which comparisons are shown in the summary plots had less than 5-percent effect on lift-curve slope. The leading-edge flaps (fig. 45) and the $M = 1$ bump added to configuration 14 (fig. 49) increased the lift-curve slope by approximately 8 percent at a lift coefficient of 0 at transonic Mach numbers. The addition of the $M = 1$ bump to configuration 14 made the variation of lift coefficient with angle of attack more nearly linear at transonic Mach numbers (figs 22(a) and 27(a)). The wing-tip extensions increased the lift-curve slope by approximately 15 percent at a lift coefficient of 0 (fig. 51); based on true wing areas, however, the increase amounted to approximately 8 percent.

Pitching-Moment Characteristics

The variation of pitching-moment coefficient with lift coefficient was generally nonlinear for the various configurations tested. The pitching-moment derivative $C_{m_{C_L}}$ is shown herein at lift coefficients of 0 and 0.4, and is the average value from 0.1 below to 0.1 above the specified lift coefficient.

Pitch-up tendencies.- The variation of pitching-moment coefficient with lift coefficient for the complete model less horizontal tail became unstable at the higher lift coefficients at all test Mach numbers except 1.13 (figs. 11(a) and 17(a)). The lift coefficient at which the pitching moment became unstable at these higher lift coefficients varied from approximately 0.5 at a Mach number of 0.60 to approximately 0.7 at a Mach number of 1.03. Unstable variations of pitching-moment coefficient with lift coefficient also occurred over a small range of lift coefficients at several Mach numbers for some of the complete-model configurations, but at lift coefficients which were considerably out of trim (fig. 15, for example). No serious pitch-up difficulties were apparent for the complete model at a constant Mach number, although some decreases in stability, tending toward pitch-up characteristics, were evident at several Mach numbers (figs. 9 and 10, 13 and 14). Furthermore, a tendency toward pitch-up characteristics exists during maneuvers at transonic

speeds where rapid speed decreases may occur and where a decrease in Mach number normally results in a forward movement of the aerodynamic center as shown by the present results. The significance of such possible pitch-up characteristics may be determined by calculations of the airplane motions by the methods of reference 7. These methods provide for the conversion of static nonlinear aerodynamic data into time histories of the longitudinal motions of the airplane and afford a detailed treatment of the pitch-up problem. Consideration is given in reference 7 to some of the factors which affect pitch-up behavior, such as pitching-moment variations with angle of attack and Mach number, rate and amount of control deflection, dynamic pressure, airplane longitudinal moment of inertia, and aerodynamic damping.

Static longitudinal stability.- The derivative $C_{m_{C_L}}$ of the basic complete model at a horizontal-tail incidence of -3° and at a lift coefficient of 0 was approximately -0.12 at Mach numbers up to 0.93, and increased in magnitude at transonic speeds to approximately -0.30 at a Mach number of 1.13 (fig. 40(a)). This increase in magnitude of the derivative $C_{m_{C_L}}$ at transonic speeds corresponded to a rearward movement of the aerodynamic center from the $0.37\bar{c}$ point to the $0.55\bar{c}$ point. The $C_{m_{C_L}}$ results of figure 40(b) indicated that the aerodynamic center of the complete model less horizontal tail at a lift coefficient of 0 was at the $0.20\bar{c}$ point at a Mach number of 0.60 and moved rearward with increase in Mach number to the $0.37\bar{c}$ point at a Mach number of 1.13. The complete model less horizontal tail had static longitudinal stability at Mach numbers greater than 0.91 at a lift coefficient of 0 and at all test Mach numbers at a lift coefficient of 0.4.

Configuration modifications generally had small effect on the derivative $C_{m_{C_L}}$. The wing-tip extensions made the slope more negative by approximately 0.05 to 0.08 (fig. 51); based on true wing areas and dimensions, however, the changes were much less. Trim changes due to configuration changes were also generally small. The largest trim changes occurred with addition of the pylon stores to the configuration, and amounted to a change of 0.02 in pitching-moment coefficient at transonic speeds (figs. 22(a) and 23(a)).

Neutral point.- The stick-fixed neutral-point location of the model with the supersonic inlet (cruise condition) at a lift coefficient of 0 was at the $0.36\bar{c}$ point at Mach numbers up to 0.90 and moved rearward at transonic speeds to the $0.54\bar{c}$ point at a Mach number of 1.13 (fig. 43). Increasing the lift coefficient to 0.3 caused the neutral point to move rearward by an increment of approximately $0.06\bar{c}$.

[redacted]

Horizontal-tail effectiveness.- The horizontal-tail effectiveness $C_{m_{i_t}}$ shown in figure 44 is the average value for horizontal-tail incidences from -3° to -8°. The horizontal-tail effectiveness is presented at constant angles of attack of 0° and 6° for the complete model with the transonic inlet, the complete model with the supersonic inlet (cruise condition), and the complete model less wing.

The horizontal-tail effectiveness at an angle of attack of 0° increased by approximately 20 percent between Mach numbers of 0.60 and 0.92, and then decreased at the higher Mach numbers (fig. 44). At an angle of attack of 0°, the horizontal-tail effectiveness at a Mach number of 1.13 was essentially the same as that at a Mach number of 0.60. The effect of wing removal on horizontal-tail effectiveness was variable, and amounted to a maximum of approximately 10 percent at the angles of attack shown. The horizontal-tail effectiveness at an angle of attack of 6° was lower than that at an angle of attack of 0° at Mach numbers up to approximately 0.94, and was essentially the same at the higher Mach numbers.

Zero-Lift Drag Characteristics

Basic model.- The low-speed ($M = 0.60$) zero-lift drag coefficient of the basic complete model at a horizontal-tail incidence of -3° was approximately 0.015 for all inlets (fig. 40(a)). The zero-lift drags of the basic model with the transonic inlet and the supersonic inlet (high-speed condition) were the same at supersonic speeds.

The zero-lift drag coefficient of the configuration with the supersonic inlet (cruise condition) was less than that of the configuration with the supersonic inlet (high-speed condition) throughout the Mach number range. The decrement amounted to a maximum of approximately 0.002 which occurred at supersonic Mach numbers (fig. 40(a)). The mass flow in the configuration with the supersonic inlet (high-speed condition) was less than that in the configuration with the supersonic inlet (cruise condition). Generally, a reduction in mass flow in a duct system with an inlet of the type investigated would be expected to result in an increase in external drag because of the additional spillage from the inlet.

The zero-lift drag coefficient of the basic configuration with the supersonic inlet (cruise condition) was generally slightly less at trim conditions (fig. 42(b)) than at a fixed horizontal-tail incidence of -3° (fig. 40(a)). The horizontal-tail incidence corresponding to trim conditions at zero lift was near 0°, so that the drag contribution of the horizontal tail was less at trim conditions. The incremental drag coefficient of the horizontal tail at an incidence of -3° was approximately

[redacted]

0.004 at supersonic Mach numbers and approximately one-half of this at the lowest speeds (figs. 40(a) and 40(b)).

Effect of area-rule modifications.- Addition of the long nose to the basic configuration increased the fineness ratio of the equivalent body from 9.2 to 10.6, and reduced the zero-lift drag coefficient at supersonic Mach numbers by approximately 0.002 (fig. 48). The zero-lift drag coefficient at the low subsonic Mach numbers was increased by approximately the same amount. The canopy modification reduced the zero-lift drag coefficient by a small amount at Mach numbers near 1 and the differences were slight and inconsistent at supersonic Mach numbers (fig. 49; configurations 14 and 17, and 19 and 18). Addition of the M = 1 bump reduced the zero-lift drag coefficient by 0.006 at Mach numbers near 1 and from 0.004 to 0.005 at a Mach number of 1.13 (fig. 49; configurations 14 and 19, and 17 and 18). The M = 1 bump was modified in an attempt to improve the supersonic drag characteristics. This improvement was not realized at Mach numbers up to 1.13 (fig. 50). The present results showed that the greatest reductions in transonic drag occurred through improvement in the normal cross-sectional-area distribution rearward of the maximum area rather than through improvement forward of the maximum area.

Effect of extended wing tips.- The extended wing tips increased the zero-lift drag at subcritical speeds by a small amount but had essentially no effect at transonic speeds (fig. 51). The normal cross-sectional-area distribution was improved slightly by the extended wing tips (fig. 6(a)). Based on true wing areas, the extended wing tips reduced the zero-lift drag coefficient throughout the Mach number range.

Effect of pylon stores.- The pylon stores increased the zero-lift drag by 17 percent at the lowest Mach number and by 35 percent at the highest Mach number (fig. 53). The pylon stores increased the maximum normal cross-sectional area of the basic model by 27 percent.

Maximum Lift-Drag Ratio

Basic model.- The maximum lift-drag ratio of the configuration with the supersonic inlet (cruise condition) at a horizontal-tail incidence of -3° varied from 9.0 at a Mach number of 0.60 to 5.6 at a Mach number of 1.13 (fig. 40(a)). The maximum lift-drag ratio of the configuration with the supersonic inlet (cruise condition) at trim conditions was slightly more than that for the configuration at a horizontal-tail incidence of -3° at Mach numbers up to 0.93, and was less by approximately 0.5 at supersonic speeds (figs. 42(c) and 40(a)). The horizontal-tail incidence required for trim at maximum lift-drag conditions was approximately -2.5° at Mach numbers up to 0.93 and increased at transonic speeds to approximately -7° at a Mach number of 1.13 (fig. 42(c)).

[redacted]

The effect of inlet design on $(L/D)_{max}$ was largest at Mach numbers near 0.9, amounting to an increment of 1.0 at a Mach number of 0.90 between the configurations with the supersonic inlet (high-speed condition) and the transonic inlet, and was negligible at supersonic Mach numbers (fig. 40(a)). The lower zero-lift drag of the configuration with the supersonic inlet (cruise condition) at supersonic speeds was counterbalanced by a higher drag due to lift, so that there was no gain in $(L/D)_{max}$.

Configuration modifications which improved $(L/D)_{max}$.- The configuration modifications (made on the model with the supersonic inlet (cruise condition)) which resulted in a significant improvement in the maximum lift-drag ratio consisted of deflection of the leading-edge flaps, the wing-tip extensions, the afterbody bump and modified canopy, inlet droop, and the inlet-wing juncture fairing (wing modification 2, table II).

The leading-edge flaps at a deflection of -7.5° improved the maximum lift-drag ratio at all Mach numbers (fig. 45). Increasing the flap deflection from -7.5° to -15° increased $(L/D)_{max}$ by a small amount at Mach numbers of 0.6 and 0.8 but actually decreased $(L/D)_{max}$ at the higher Mach numbers. The flaps increased the maximum lift-drag ratio by approximately 1.2 at Mach numbers of 0.9 and less; the increase was approximately 0.4 at supersonic speeds. As shown in figure 45, the flaps increased the zero-lift drag. The improvement in $(L/D)_{max}$ resulted from the lower drag-due-to-lift characteristics of the flapped configurations. The extended wing tips increased $(L/D)_{max}$ by approximately 1.0 at Mach numbers up to 1.03. The increase was approximately 0.4 at a Mach number of 1.13 (fig. 51). The improvement in $(L/D)_{max}$ resulted from a reduction in the drag force due to lift force of the configuration with the extended wing tips.

The $M = 1$ bump increased the $(L/D)_{max}$ of the basic configuration by approximately 0.6 at Mach numbers near 1.0 and by approximately 0.4 at supersonic Mach numbers (fig. 49; configurations 14 and 19). There was a loss in $(L/D)_{max}$ at Mach numbers of 0.9 and less due to the $M = 1$ bump. The combination of the $M = 1$ bump and the modified canopy increased the $(L/D)_{max}$ of the basic configuration by approximately 1.3 at Mach numbers near 1.0 (fig. 49; configurations 14 and 18). This gain was substantially greater than the sum of the individual contributions of the $M = 1$ bump and the modified canopy, indicating favorable interference effects with the combination. The effect of the combination on $(L/D)_{max}$ at supersonic Mach numbers and at Mach numbers of 0.90 and less was essentially the same as that of the $M = 1$ bump alone. The configuration with the modified $M = 1$ bump gave $(L/D)_{max}$ values which were the same as those for the configuration with the $M = 1$ bump (fig. 50).

[redacted]

Inlet droop increased the maximum lift-drag ratio by approximately 0.6 at Mach numbers of 0.9 and less (fig. 41). The increase was small at supersonic Mach numbers. The inlet-wing juncture fairing (wing modification 2, table II) increased $(L/D)_{max}$ by approximately 0.6 at Mach numbers from 0.90 to 0.99. The gain was small at supersonic Mach numbers (fig. 52).

Other configuration modifications.- Various configuration modifications which resulted in no improvement in $(L/D)_{max}$ or in a loss in $(L/D)_{max}$ are discussed in this section. Deflection of the single flaperon from 0° to 5° decreased the maximum lift-drag ratio by approximately 0.4 at Mach numbers up to 0.95 (fig. 46(a)). The decrement was less at the higher Mach numbers. An increase in zero-lift drag due to the flaperon deflection outweighed a reduction in drag due to lift resulting from flaperon deflection. The long nose had no effect on $(L/D)_{max}$ at supersonic speeds but decreased the ratio by nearly 1.0 at the lowest test Mach numbers (fig. 48). The symmetrical buildup on the external upper surface of the wing in the region of the inlet (wing modification 1, table II) had no effect on $(L/D)_{max}$ characteristics. No comparison results are shown herein for the symmetrical buildup; the basic data are presented in figures 13 and 18. The pylon stores decreased $(L/D)_{max}$ by approximately 1.0 at supersonic speeds and 1.7 at subsonic speeds (fig. 53). The inlet upper-lip revision (inlet modification 1, table II) showed no gain in $(L/D)_{max}$ at supersonic speeds and at the lowest speed, and actually a loss in the Mach number range from approximately 0.90 to 0.95 (fig. 52).

Flaperon and Rudder Characteristics

Flaperon.- The derivatives $C_{l_{\delta_f}}$, $C_{m_{\delta_f}}$, $C_{n_{\delta_f}}$, $C_{l_{\delta_f}}$, and $C_{Y_{\delta_f}}$ shown in figures 46(b) to 46(d) are average values for flaperon deflections from 0° to 5°. The effect of angle of attack was greatest on the derivatives $C_{m_{\delta_f}}$ and $C_{l_{\delta_f}}$ (figs. 46(b) and 46(c)). The derivative $C_{m_{\delta_f}}$ became reversed (that is, changed sign) in the angle-of-attack range from 4° to 7° at a Mach number of 0.90 (fig. 46(b)). An increase in Mach number increased the extent of the angle-of-attack range in which reversal occurred, until at Mach numbers of 0.97 and higher the derivative was reversed at all test angles of attack. The derivative $C_{l_{\delta_f}}$ became reversed at the highest angles of attack at Mach numbers of 0.80 and 0.90 (fig. 46(c)). The effect of Mach number on the flaperon derivatives at an angle of attack of 0° was greatest on $C_{m_{\delta_f}}$ (fig. 46(d)).

Rudder.- The derivatives $C_{n_{\delta_r}}$, $C_{l_{\delta_r}}$, and $C_{Y_{\delta_r}}$ shown in figures 47(b) to 47(c) are average values for rudder deflections from 0° to 5°. The effect of angle of attack on the derivatives $C_{n_{\delta_r}}$ and $C_{Y_{\delta_r}}$ was slight; an increase in angle of attack reduced $C_{l_{\delta_r}}$ (fig. 47(b)). The magnitude of the derivatives $C_{n_{\delta_r}}$ and $C_{Y_{\delta_r}}$ decreased with increase in Mach number at Mach numbers above 0.93 (fig. 47(c)). The derivative $C_{l_{\delta_r}}$ was essentially invariant with change in Mach number.

Effective Downwash Characteristics

The effective downwash angle (figs. 54 and 55) was determined at a given model angle of attack by finding the horizontal-tail incidence at which the pitching-moment coefficient of the configuration including the horizontal tail was equal to that of the configuration less the horizontal tail. The sum of the horizontal-tail incidence thus found and the model angle of attack gave the effective downwash angle in the region of the horizontal tail.

The variation of effective downwash angle with angle of attack is shown in figure 54. The variation of the derivative $d\epsilon/d\alpha$ with Mach number is shown in figure 55. The derivatives shown are the average slopes for angles of attack from 0° to 4° for the complete model with the supersonic inlet (cruise condition) and for the complete model less wing, and for angles of attack from 4° to 6° for the complete model with the transonic inlet.

The variation with Mach number of the effective downwash derivative $d\epsilon/d\alpha$ was essentially the same for the complete model with the transonic and supersonic inlets (fig. 55). There was a marked decrease in the effective downwash derivative at Mach numbers above approximately 0.93, reaching a value of approximately 0.25 at a Mach number of 1.13. The results of reference 3 showed that the effective downwash derivative of the complete model at a Mach number of 2 was negative (effective upwash).

The effective downwash derivative of the complete model less wing was negative throughout the Mach number range. The variation with Mach number was similar to that of the complete model, indicating that the flow field of the complete model in the region of the horizontal tail was strongly influenced by the flow field of the body alone (fig. 55).

[redacted]

CONCLUSIONS

An investigation was made in the Langley 8-foot transonic tunnel of the static longitudinal stability and control and performance characteristics of various configurations of a 1/22-scale model of the Republic F-105 airplane. The Mach number range of the tests was generally from 0.60 to 1.13, and the Reynolds number based on the mean aerodynamic chord of the wing was approximately 2×10^6. All the configurations except wing-off configurations were investigated with internal flow in the model. The following conclusions are indicated:

1. No serious pitch-up difficulties were apparent for the complete model at a constant Mach number, although some decreases in stability, tending toward pitch-up characteristics, were evident at several Mach numbers. The variation of pitching-moment coefficient with lift coefficient was unstable over a small range of lift coefficients for several of the complete-model configurations but at lift coefficients which were considerably out of trim.

2. An afterbody bump to improve the area distribution reduced the zero-lift drag coefficient by 0.006 at Mach numbers near 1.0 and by 0.004 to 0.005 at a Mach number of 1.13. Increasing the fineness ratio from 9.2 to 10.6 by the addition of a long nose reduced the zero-lift drag coefficient at supersonic Mach numbers by approximately 0.002.

3. Significant improvement in maximum lift-drag characteristics resulted from deflection of wing leading-edge flaps, extension of wing tips, addition of an afterbody bump and a canopy modification, inlet droop, and a revised inlet-wing juncture fairing.

4. The effective downwash derivative $d\epsilon/d\alpha$ of the complete model decreased markedly at Mach numbers greater than 0.93. The effective downwash characteristics of the complete model appeared to be strongly modified by the effective downwash characteristics of the body alone, which had an effective downwash derivative that was negative (effective upwash) throughout the Mach number range.

Langley Aeronautical Laboratory,
National Advisory Committee for Aeronautics,
Langley Field, Va., April 12, 1956.

Arvo A. Luoma
Aeronautical Research Scientist

Approved: Eugene C. Draley
Eugene C. Draley
Chief of Full-Scale Research Division

rmw

[redacted]

REFERENCES

1. Kelly, H. Neale, and Cancro, Patrick A.: Investigation of a 1/4-Scale Model of the Republic F-105 Airplane in the Langley 19-Foot Pressure Tunnel - Longitudinal Stability and Control of the Model Equipped With a Supersonic-Type Elliptical Wing-Root Inlet. NACA RM SL54F28, U. S. Air Force, 1954.

2. Cancro, Patrick A., and Kelly, H. Neale: Investigation of a 1/4-Scale Model of the Republic F-105 Airplane in the Langley 19-Foot Pressure Tunnel - Influence of Trailing-Edge Flap Span and Deflection on Longitudinal Characteristics. NACA RM SL54H27, U. S. Air Force, 1954.

3. Spearman, M. Leroy, Driver, Cornelius, and Robinson, Ross B.: Aerodynamic Characteristics of Various Configurations of a Model of a 45° Swept-Wing Airplane at a Mach Number of 2.01. NACA RM L54J08, 1955.

4. Ritchie, Virgil S., and Pearson, Albin O.: Calibration of the Slotted Test Section of the Langley 8-Foot Transonic Tunnel and Preliminary Experimental Investigation of Boundary-Reflected Disturbances. NACA RM L51K14, 1952.

5. Polhamus, Edward C.: Summary of Results Obtained by Transonic-Bump Method on Effects of Plan Form and Thickness on Lift and Drag Characteristics of Wings at Transonic Speeds. NACA TN 3469, 1955. (Supersedes NACA RM L51H30.)

6. Bielat, Ralph P.: A Transonic Wind-Tunnel Investigation of the Aerodynamic Characteristics of Three 4-Percent-Thick Wings of Sweepback Angles 10.8°, 35°, and 47°, Aspect Ratio 3.5, and Taper Ratio 0.2 in Combination With a Body. NACA RM L52B08, 1952.

7. Campbell, George S., and Weil, Joseph: The Interpretation of Nonlinear Pitching Moments in Relation to the Pitch-up Problem. NACA RM L53I02, 1953.

[redacted]

TABLE I.- GEOMETRIC CHARACTERISTICS OF 1/22-SCALE MODEL OF REPUBLIC F-105 AIRPLANE

Body (basic):	
Length, in.	32.830
Maximum width, in.	2.387
Maximum depth (excluding canopy), in.	3.546
Frontal area (including canopy), sq ft	0.0510
Side area (including canopy), sq ft	0.698
Volume (including canopy), cu ft	0.106
Fineness ratio $\left(\frac{\text{Length}}{\sqrt{\frac{\text{Frontal area}}{0.7854}}}\right)$	10.7
$\frac{\text{Frontal area}}{\text{Wing (basic) area}}$	0.0643
$\frac{\text{Total base area}}{\text{Wing (basic) area}}$	0.0307
Body (long nose):	
Length, in.	37.740
Maximum width, in.	2.387
Maximum depth (excluding canopy), in.	3.546
Frontal area (including canopy), sq ft	0.0510
Fineness ratio $\left(\frac{\text{Length}}{\sqrt{\frac{\text{Frontal area}}{0.7854}}}\right)$	12.3
$\frac{\text{Frontal area}}{\text{Wing (basic) area}}$	0.0643
$\frac{\text{Total base area}}{\text{Wing (basic) area}}$	0.0307
Wing (basic):	
Airfoil section (parallel to body reference line):	
At 0.38b/2 station	NACA 65A005.5
Tip	NACA 65A003.7
Root chord c_r, in.	8.181
Incidence of root chord with respect to body reference line, deg	0
Location of root chord above body reference line, in.	0.614
Location of leading edge of root chord from nose of basic body, in.	11.758
Tip chord c_e, in.	3.818
Span b, in.	19.054
Area S, sq ft	0.794
Aspect ratio A	3.18
Taper ratio λ	0.467
Mean aerodynamic chord, in.	6.264
Location of mean aerodynamic chord above body reference line, in.	0.358
Location of leading edge of mean aerodynamic chord from leading edge of root chord, in.	4.666
Sweepback of projected 25-percent-chord line, deg	45
Dihedral, deg	-3.5
Twist, deg	0
Leading-edge flaps:	
Type	Drooped-plain flap
Area (two flaps), sq ft	0.0472
Span (one flap), in.	5.336
Sweepback at hinge line	49° 07' 26"
Chord (average), in.	0.638
Flaperon:	
Type	Trailing-edge flap
Area, sq ft	0.026
Span, in.	2.507

[redacted]

TABLE I.- GEOMETRIC CHARACTERISTICS OF 1/22-SCALE MODEL OF REPUBLIC F-105 AIRPLANE - Concluded

Wing (extended wing tips):	
Airfoil section (parallel to body reference line):	
At 0.341b/2 station	NACA 65A005.5
Tip	NACA 65A003.4
Root chord c_r, in.	8.181
Incidence of root chord with respect to body reference line, deg	0
Location of root chord above body reference line, in.	0.614
Location of leading edge of root chord from nose of basic body, in.	11.758
Tip chord c_e, in.	3.319
Span b, in.	21.232
Area S, sq ft	0.848
Aspect ratio A	3.69
Taper ratio λ	0.406
Mean aerodynamic chord, in.	6.093
Location of mean aerodynamic chord above body center line, in.	0.335
Location of leading edge of mean aerodynamic chord from leading edge of root chord, in.	5.082
Sweepback of projected 25-percent-chord line, deg	45
Dihedral, deg	-3.5
Twist, deg	0
Leading-edge flaps:	
Type	Drooped-plain flap
Area (two flaps), sq ft	0.0601
Span (one flap), in.	6.519
Sweepback at hinge line	49° 07' 26"
Chord (average), in.	0.664
Flaperon:	
Type	Trailing-edge flap
Area, sq ft	0.026
Span, in.	2.507
Horizontal tail:	
Airfoil section (parallel to body reference line):	
Root	NACA 65A006
Tip	NACA 65A004
Root chord, in.	4.091
Tip chord, in.	1.864
Span, in.	9.090
Area (total), sq ft	0.188
Aspect ratio	3.06
Taper ratio	0.456
Mean aerodynamic chord, in.	3.114
Location of leading edge of mean aerodynamic chord from leading edge of root chord, in.	2.231
Sweepback of 25-percent-chord line, deg	45
Dihedral, deg	0
Twist, deg	0
Vertical tail:	
Airfoil section (parallel to body reference line):	
Exposed root (1.591 in. above body reference line)	NACA 65A006
Tip	NACA 65A004
Root chord (at body reference line), in.	5.473
Tip chord, in.	2.000
Span (to body reference line), in.	5.955
Area (to body reference line), sq ft	0.155
Aspect ratio $\left(\frac{(\text{Span})^2}{\text{Area}}\right)$	1.60
Taper ratio	0.365
Mean aerodynamic chord, in.	4.003
Location of leading edge of mean aerodynamic chord from leading edge of root chord, in.	2.887
Location of mean aerodynamic chord from root chord, in.	2.514
Sweepback of 25-percent-chord line, deg	45
Rudder:	
Type	Trailing-edge flap
Chord (average), in.	0.902
Span, in.	3.726
Area (total), sq ft	0.0235
Aspect ratio	4.10
Sweepback of hinge line, deg	29° 21.5'
Duct areas:	
Inlet throat (scaled down from full-scale values):	
Transonic inlet, sq in.	1.260
Supersonic inlet (high-speed condition), sq in.	1.240
Supersonic inlet (cruise condition), sq in.	1.550
Capture (scaled down from full-scale value):	
Supersonic inlet (high-speed condition), sq in.	1.746
Supersonic inlet (cruise condition), sq in.	1.746
Exit:	
Transonic inlet, sq in.	1.507
Supersonic inlet (high-speed condition), sq in.	1.507
Supersonic inlet (cruise condition), sq in.	2.024

[redacted]

TABLE II.- CONFIGURATIONS AND INDEX OF BASIC FIGURES

Configuration															Figure
Number	Description	Control-surface deflection				Body			Wing		Inlet				
		i_t, deg	δ_n, deg	δ_f, deg	δ_r, deg	Nose	Canopy	Afterbody	Aspect ratio	Modifications	Type	Droop, deg	Modifications		
1	Complete model	-3	0	0	0	Basic	Basic	Basic	3.18	None	Transonic	0	None		9
2	↓	-8													10
3	Complete model less horizontal tail	---									↓				11
4	Complete model	-3									Supersonic (high speed)				12
5		↓									Supersonic (cruise)				13
6		-8													14
7		-16													15
8		-24													16
9	Complete model less horizontal tail	---								↓					17
10	Complete model	-3								[a]1					18
11		0	↓							↓					19
12		-3	-7.5							None					20
13			-15												21
14	↓		-7.5									-5			22
15	Complete model plus wing pylon stores					↓									23
16	Complete model					Long									24
17						Basic	Modified								25
18								Basic plus M = 1 bump							26
19							Basic								27
20									3.69						28
21								Basic plus modified M = 1 bump		↓					29
22										[a]2					30
23				↓						↓			[b]1		31
24			↓	5						[a]3			↓		32
25			0	0	↓					↓					33
26			↓	↓	6				↓		↓	↓			34
27	Complete model less wing	0	-----	-----	0			Basic	-----	-----	----------	--	-----		35
28		-3	-----	-----	↓				-----	-----	----------	--	-----		36
29		-8	-----	-----					-----	-----	----------	--	-----		37
30	↓	-16	-----	-----					-----	-----	----------	--	-----		38
31	Complete model less wing and less horizontal tail	---	-----	-----	↓	↓	↓	↓	-----	-----	----------	--	-----		39

[a]Wing modification description:
1. Symmetrical buildup on external upper surface of wing in region of inlet.
2. Revised fairing along leading edge from inlet to inboard end of leading-edge flap (δ_n = -7.5°).
3. Same as modification 2 but faired into undrooped leading edge (δ_n = 0°).

[b]Inlet modification description:
1. Revised radius of upper lip and contour of upper surface (adjacent to lip) of inlet; some refairing on external lower surface of inlet.

TABLE III.- INDEX OF SUMMARY PLOTS

Description	Figure
Effect of inlet design	40
Effect of inlet droop	41
Results at trim conditions	42
Neutral-point location	43
Horizontal-tail effectiveness	44
Effect of leading-edge flaps	45
Effect of wing flaperon	46
Effect of rudder deflection	47
Effect of body-nose extension	48
Effect of canopy modification and M = 1 bump	49
Comparison of afterbody bumps	50
Effect of wing-tip extensions	51
Effect of inlet-wing fairing (wing modification 2)	52
Effect of pylon stores	53
ϵ characteristics	54
$d\epsilon/d\alpha$ characteristics	55

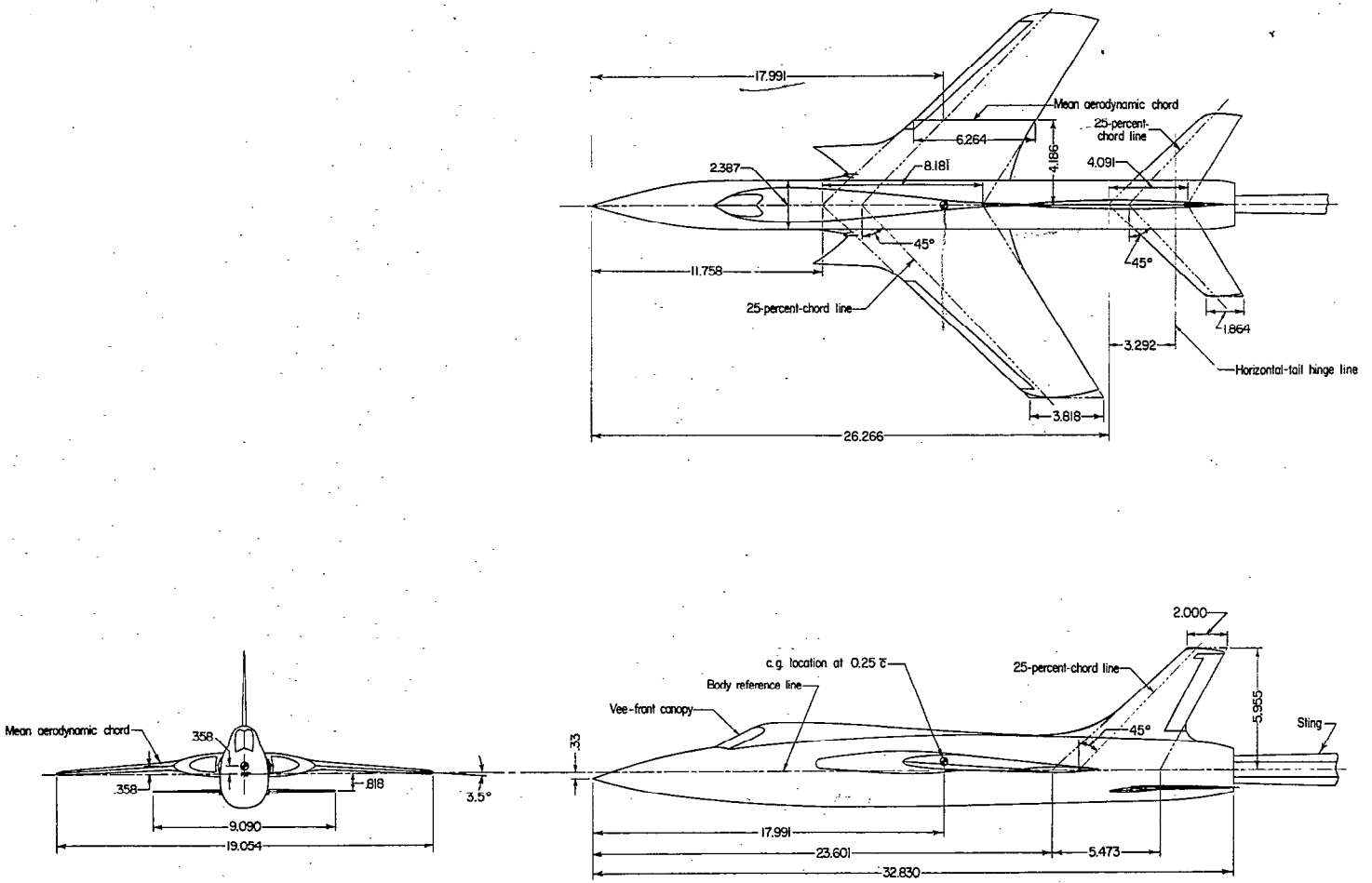

Figure 1.- General arrangement of 1/22-scale model of Republic F-105 airplane. Complete model; basic body nose, canopy, and afterbody; A = 3.18; supersonic inlet. All dimensions are in inches except as noted.

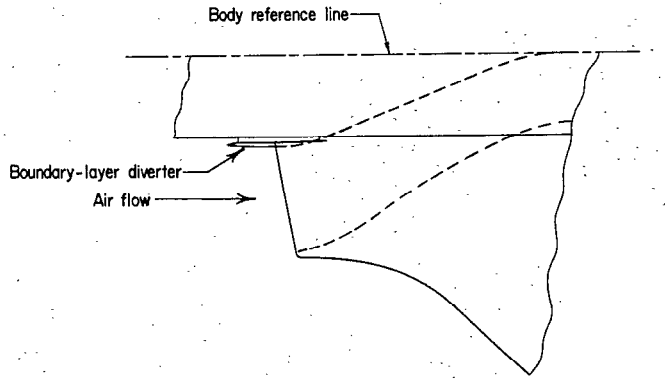

Transonic inlet

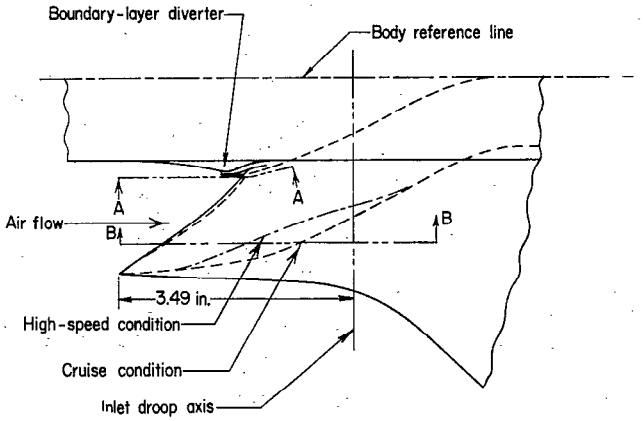

Supersonic inlet

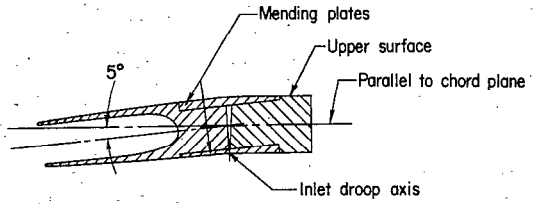

Section B–B Drooped supersonic inlet (cruise condition)

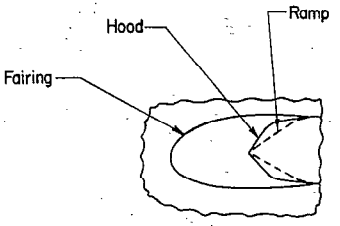

Section A–A

Figure 2.- Supersonic and transonic wing-root inlets on 1/22-scale model of Republic F-105 airplane. All dimensions are in inches except as noted.

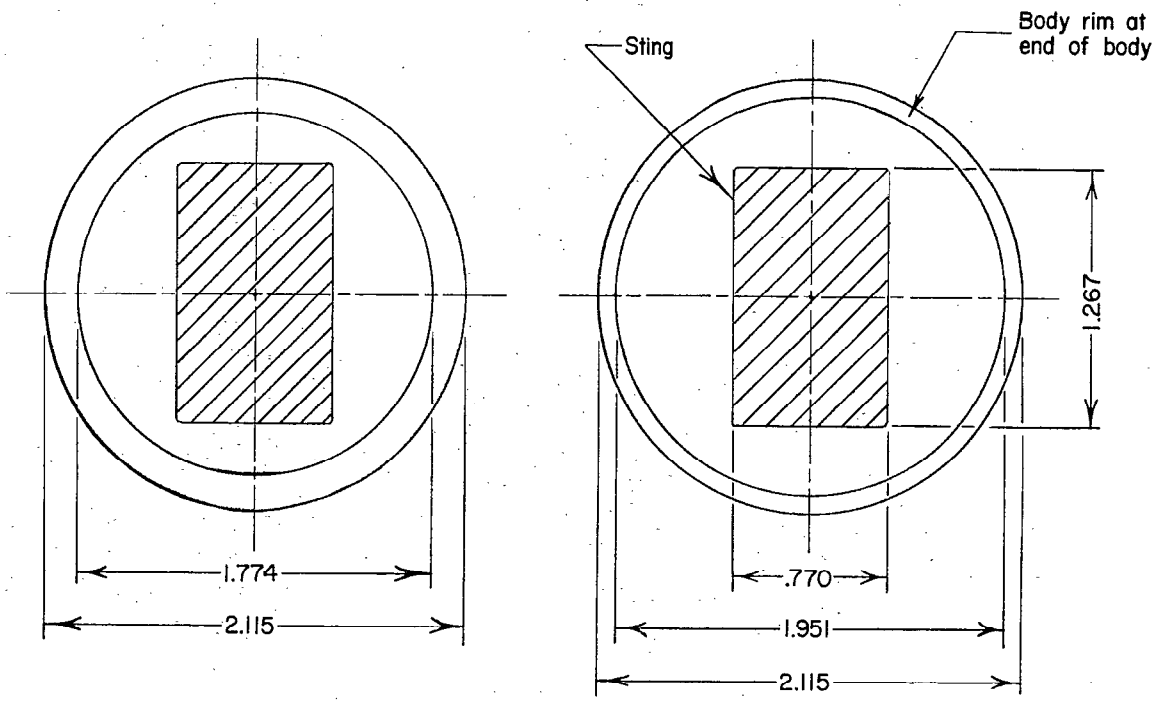

Inlet	Duct exit	Duct-exit area, sq in.
Transonic	A	1.507
Supersonic (high-speed condition)	A	1.507
Supersonic (cruise condition)	B	2.024

Figure 3.- Dimensions of duct exit for various inlets and of sting cross section at end of body. All dimensions are in inches except as noted.

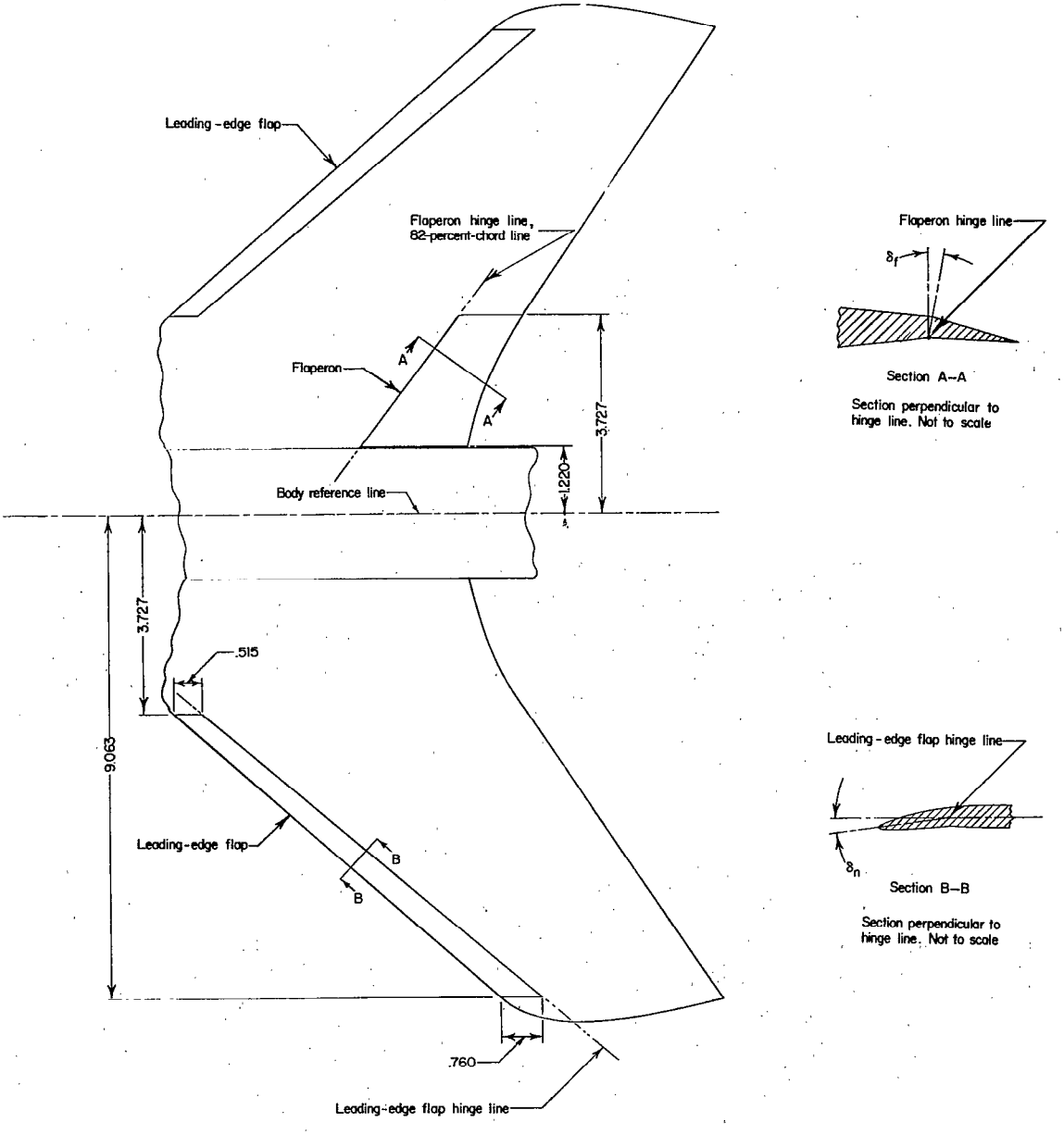

Figure 4.- Dimensions of wing leading-edge flaps and wing trailing-edge flaperon on 1/22-scale model of Republic F-105 airplane; A = 3.18. All dimensions are in inches.

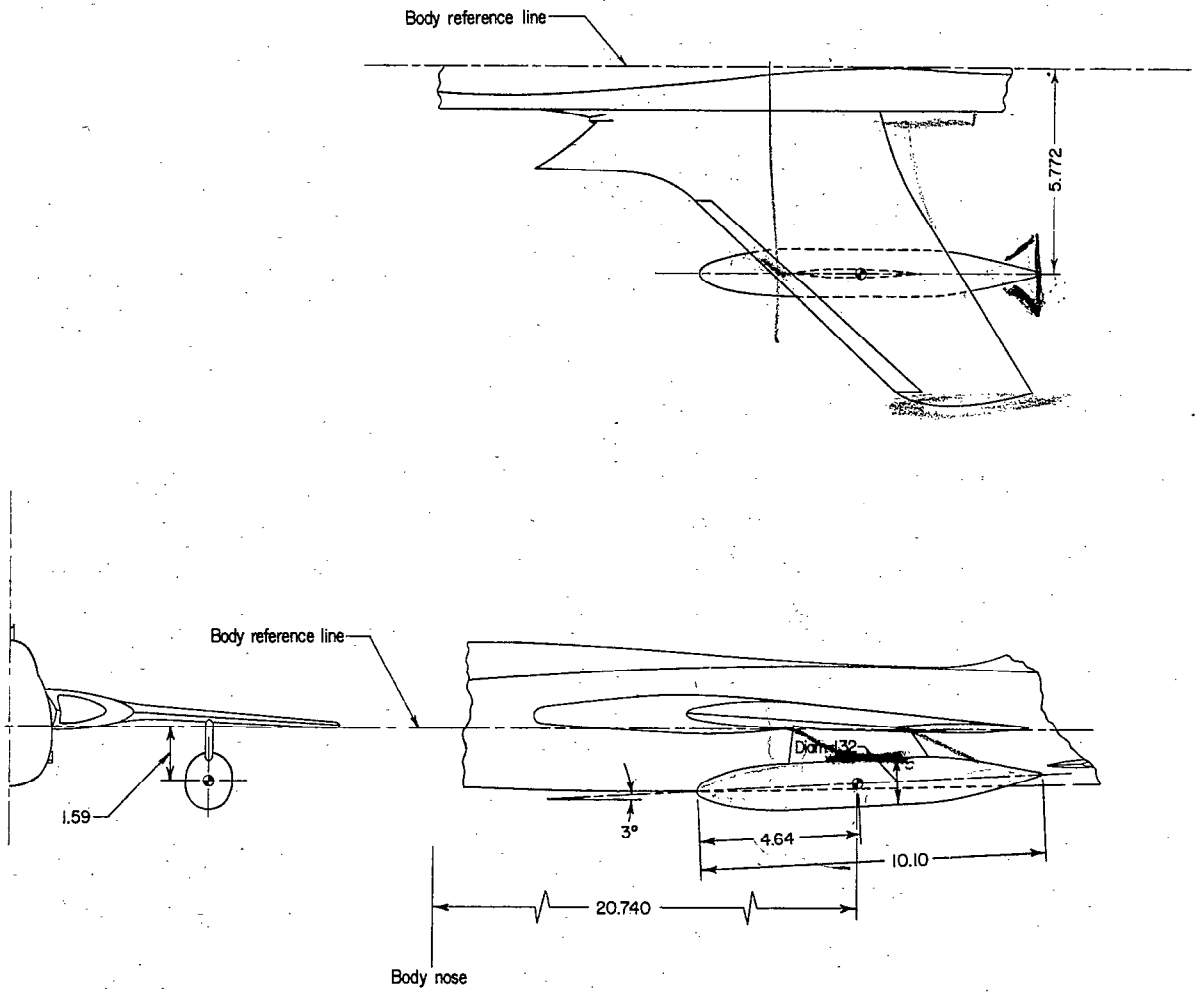

Figure 5.- Dimensions and location of 450-gallon (full-scale value) tanks mounted on inboard wing pylons on 1/22-scale model of Republic F-105 airplane. All dimensions are in inches except as noted.

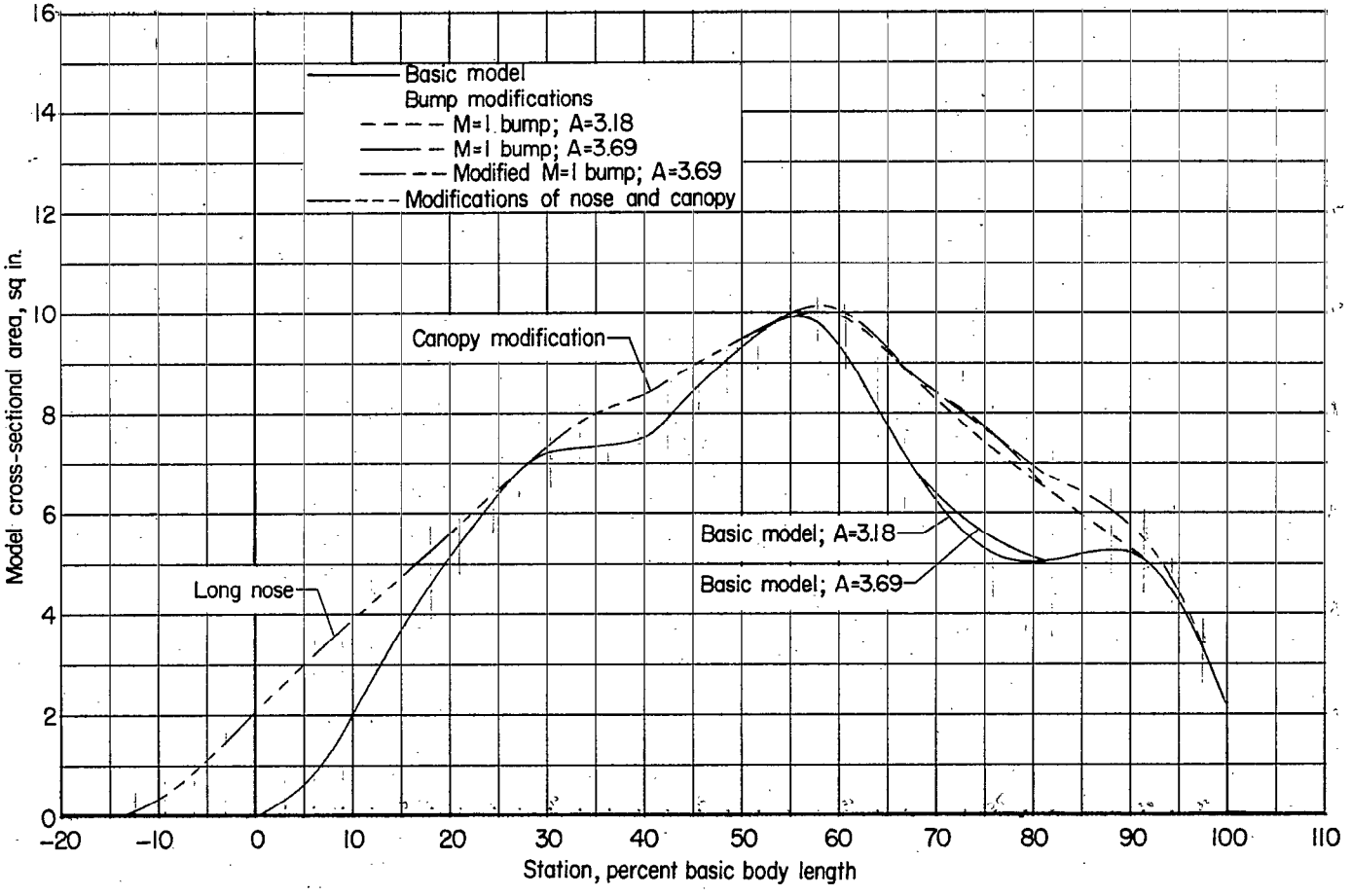

(a) Longitudinal area distribution.

Figure 6.- Longitudinal distribution of normal cross-sectional area of 1/22-scale model of Republic F-105 airplane, and various body modifications for improving the area distribution. Complete model; drooped supersonic inlet (cruise condition).

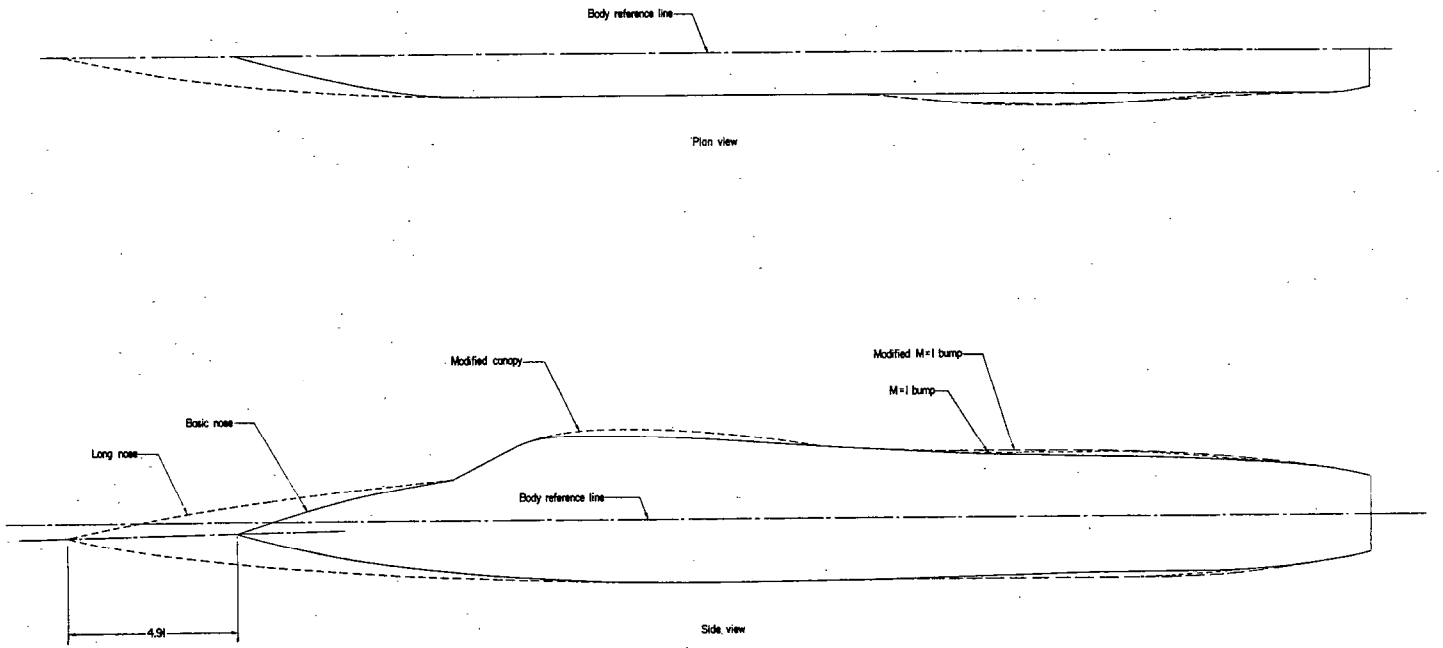

(b) Body modifications. All dimensions are in inches.

Figure 6.- Continued.

L-84419

(c) Configuration 17; body with modified canopy; A = 3.18.

Figure 6.- Continued.

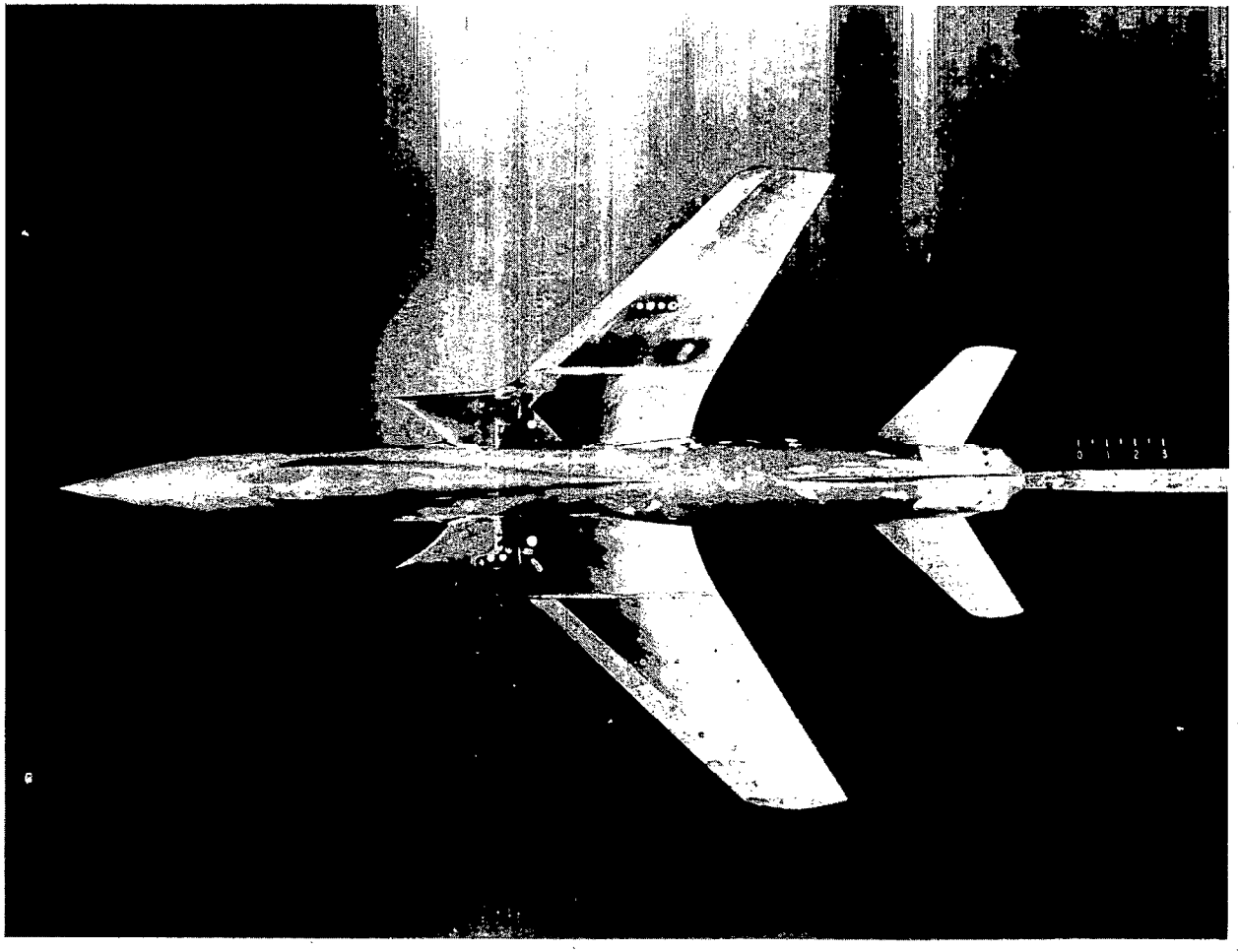

L-84493

(d) Configuration 20; body with M = 1 bump; A = 3.69.

Figure 6.- Continued.

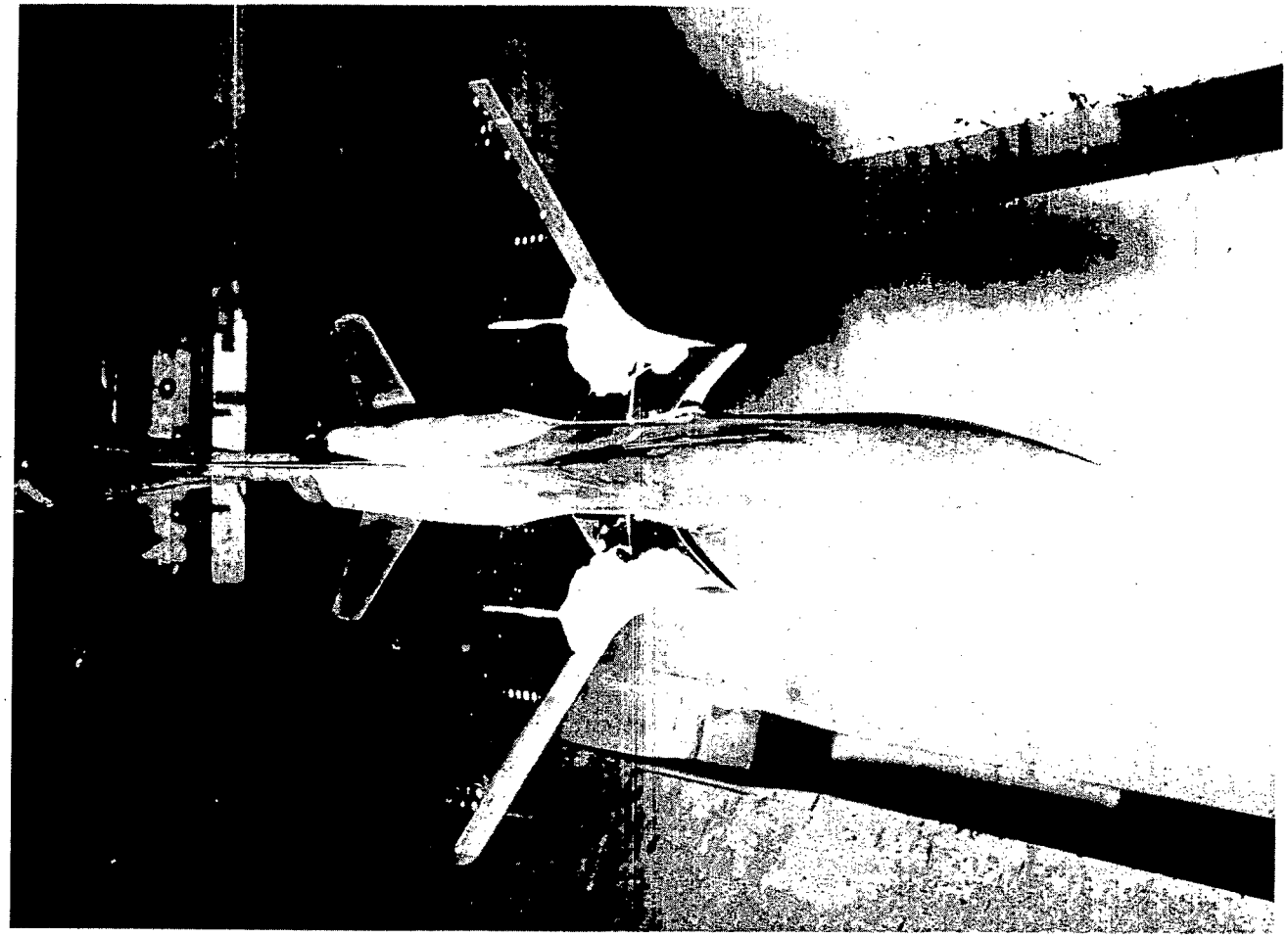

L-84512

(e) Configuration 22; body with modified M = 1 bump; A = 3.69; wing modification 2.

Figure 6.- Concluded.

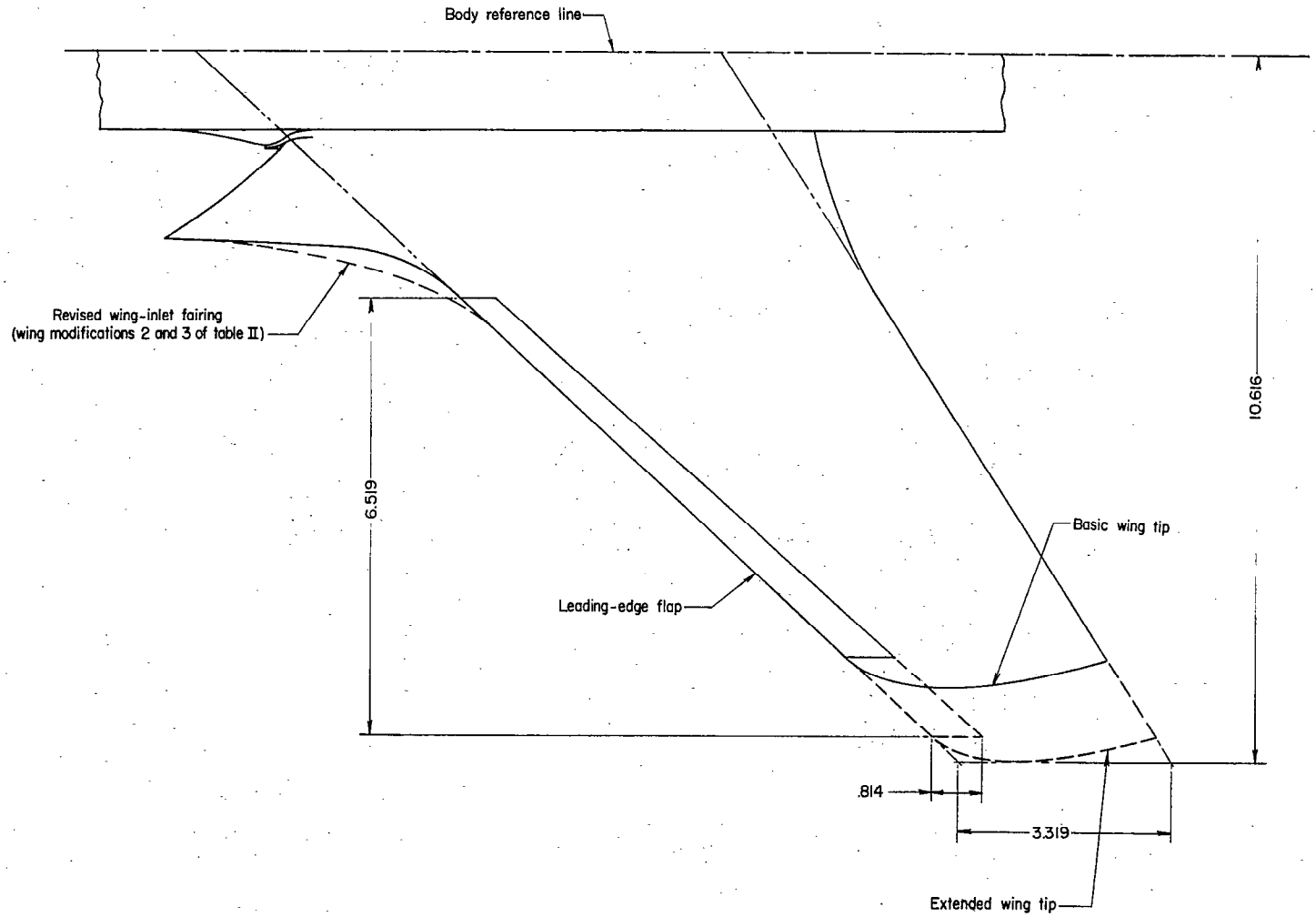

Figure 7.- Extended wing tips and revised wing-inlet fairing (wing modifications 2 and 3 of table II) on 1/22-scale model of Republic F-105 airplane. All dimensions are in inches.

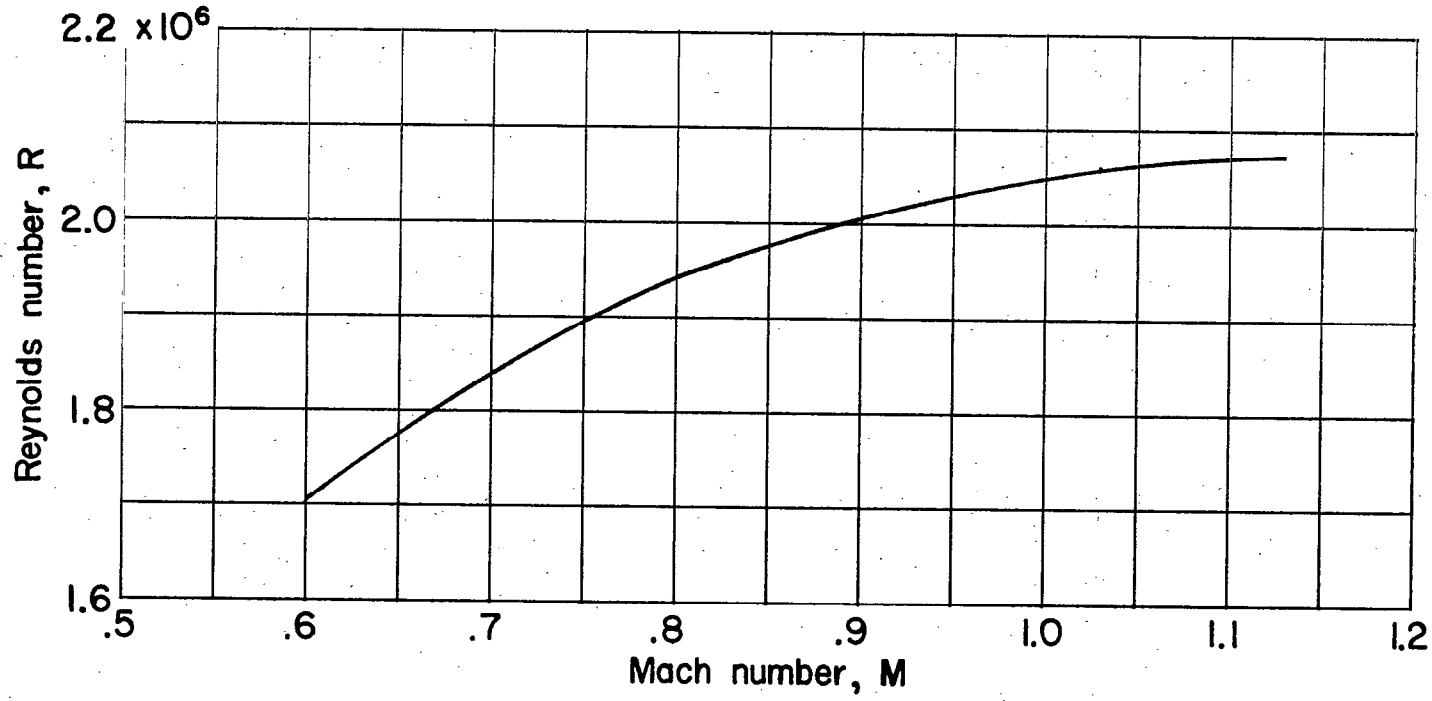

Figure 8.- Variation of Reynolds number (based on mean aerodynamic chord of 6.264 inches) with Mach number in tests of 1/22-scale model of Republic F-105 airplane in Langley 8-foot transonic tunnel.

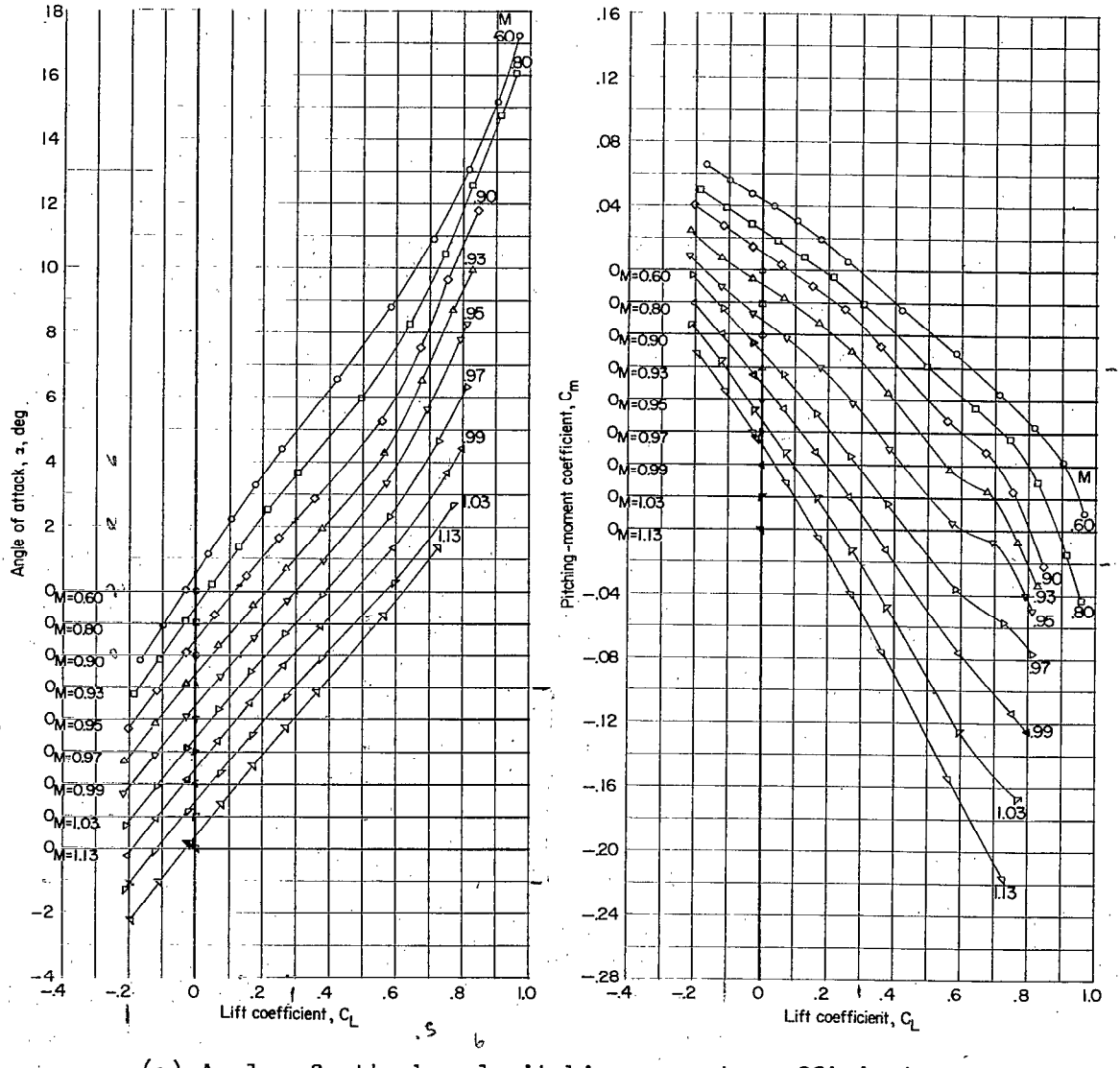

(a) Angle of attack and pitching-moment coefficient.

Figure 9.- Variation of aerodynamic characteristics with lift coefficient. Configuration 1; complete model; $i_t = -3^\circ$; A = 3.18; transonic inlet.

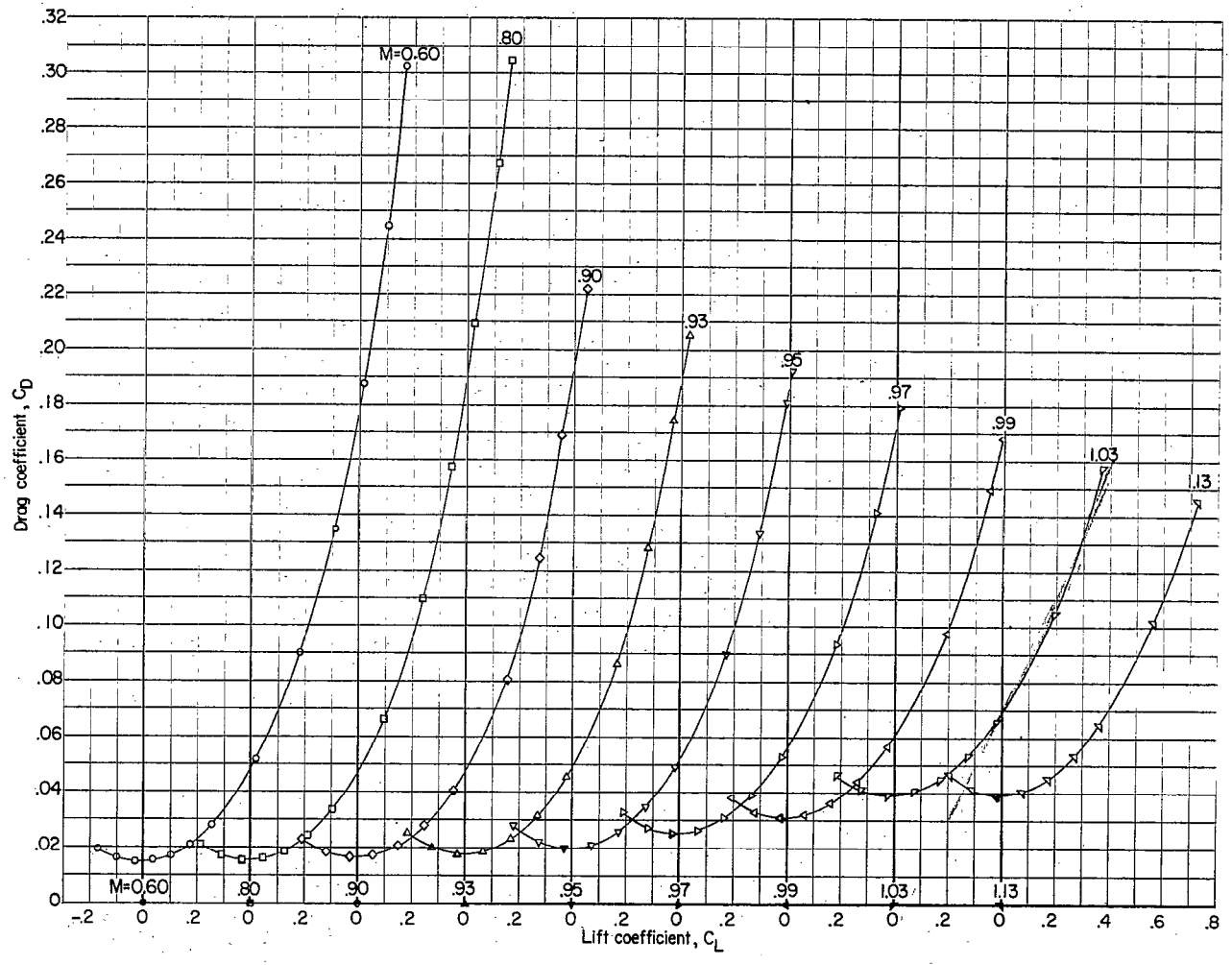

(b) Drag coefficient.

Figure 9.- Concluded.

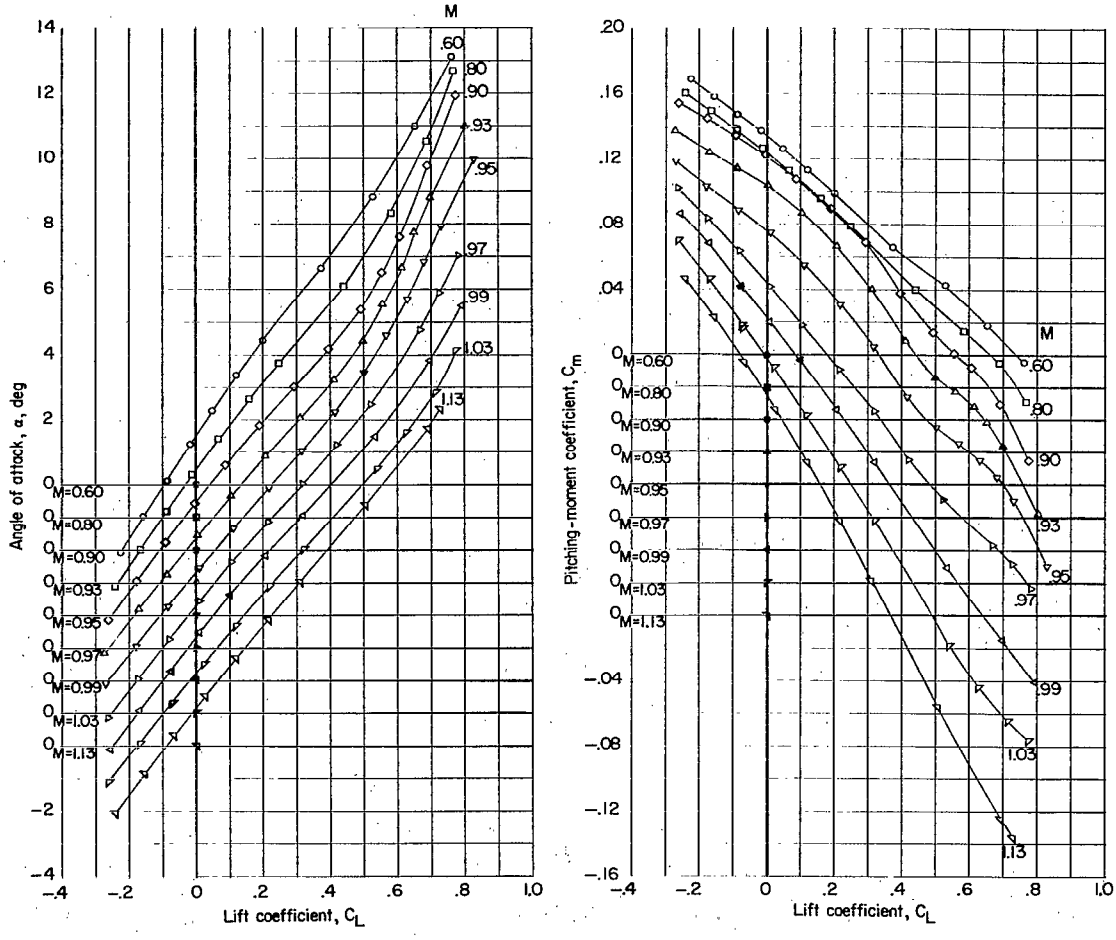

(a) Angle of attack and pitching-moment coefficient.

Figure 10.- Variation of aerodynamic characteristics with lift coefficient. Configuration 2; complete model; $i_t = -8^\circ$; A = 3.18; transonic inlet.

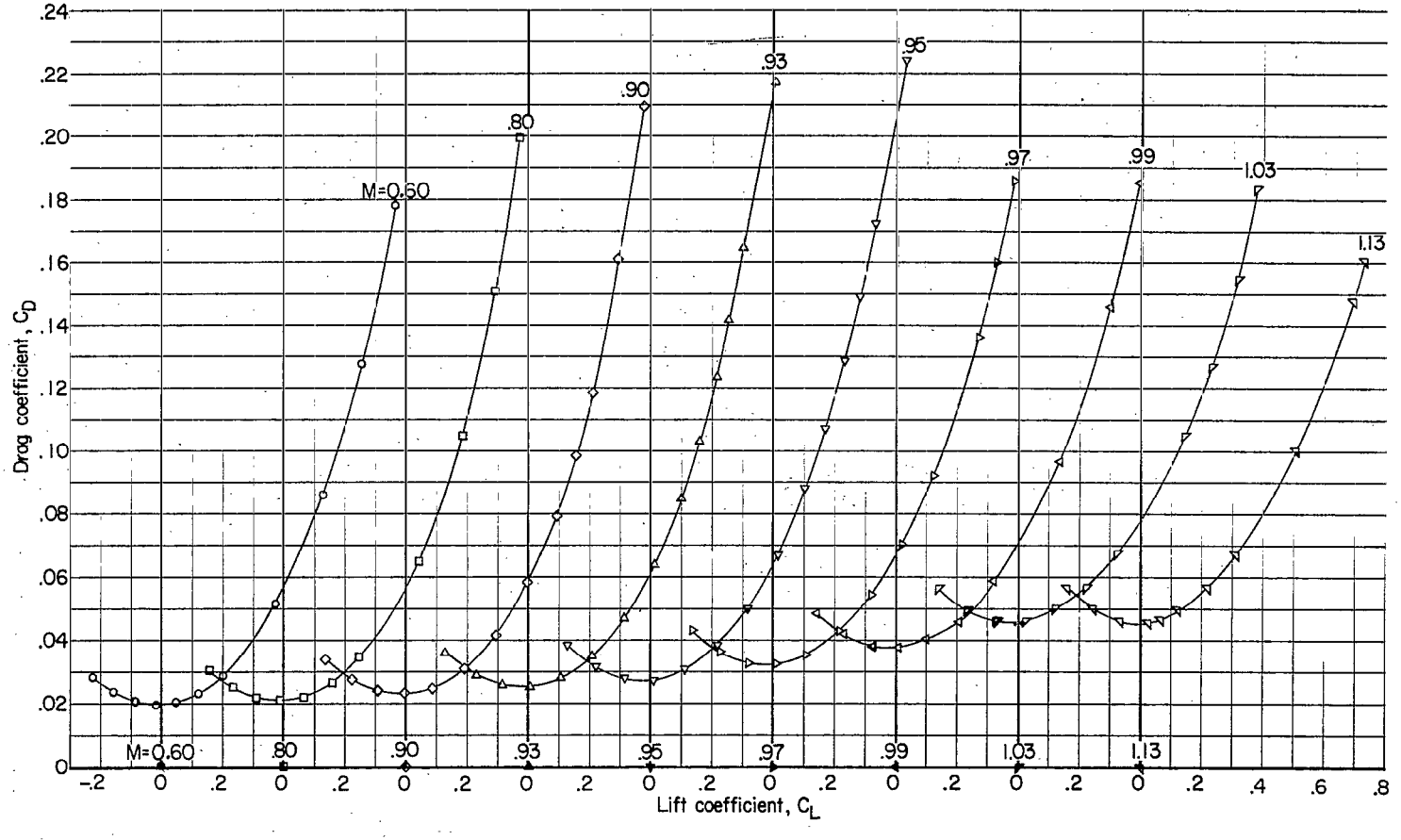

(b) Drag coefficient.

Figure 10.- Concluded.

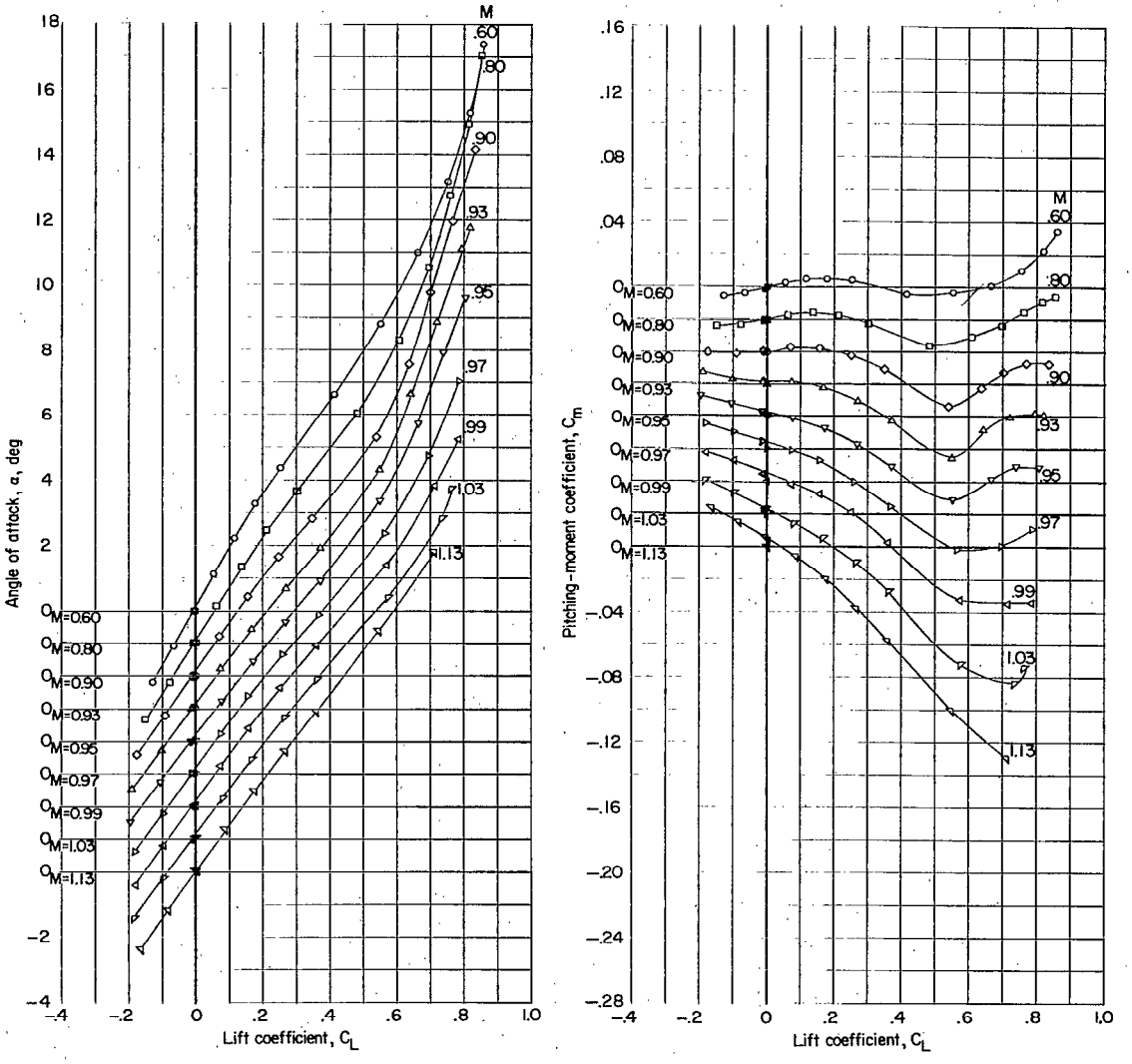

(a) Angle of attack and pitching-moment coefficient.

Figure 11.- Variation of aerodynamic characteristics with lift coefficient. Configuration 3; complete model less horizontal tail; A = 3.18; transonic inlet.

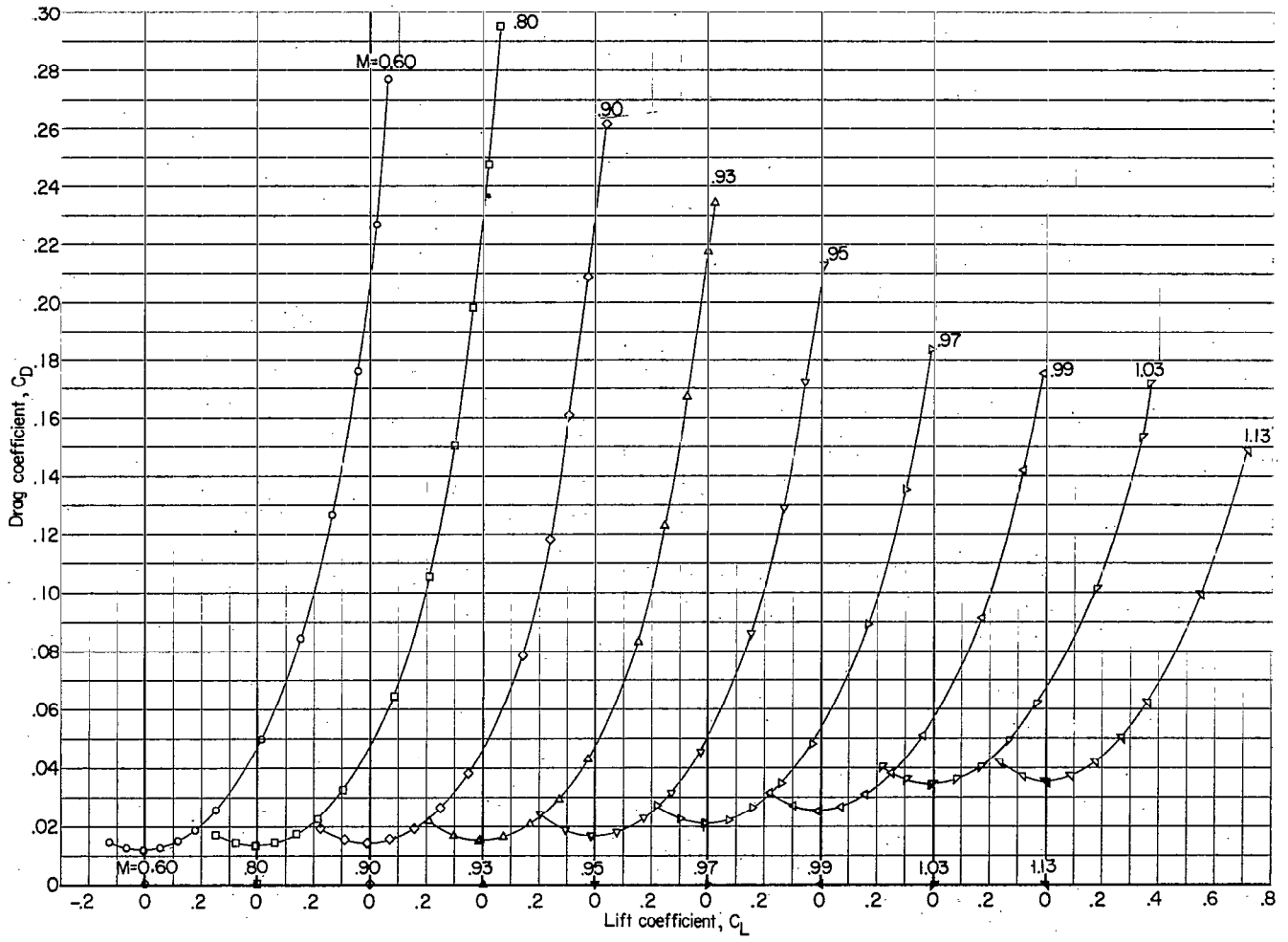

(b) Drag coefficient.

Figure 11.- Concluded.

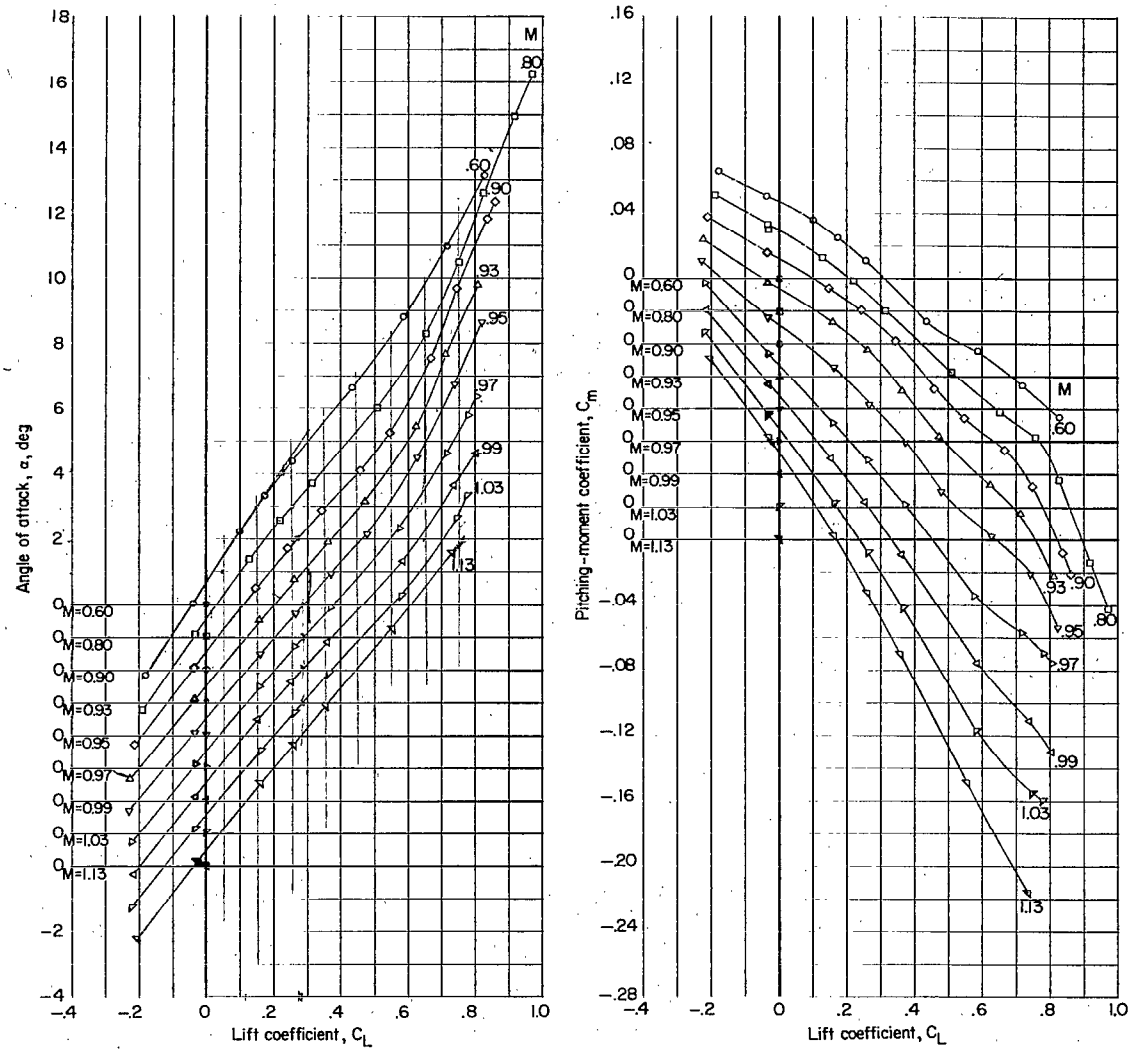

(a) Angle of attack and pitching-moment coefficient.

Figure 12.- Variation of aerodynamic characteristics with lift coefficient. Configuration 4; complete model; $i_t = -3^\circ$; A = 3.18; supersonic inlet (high-speed condition).

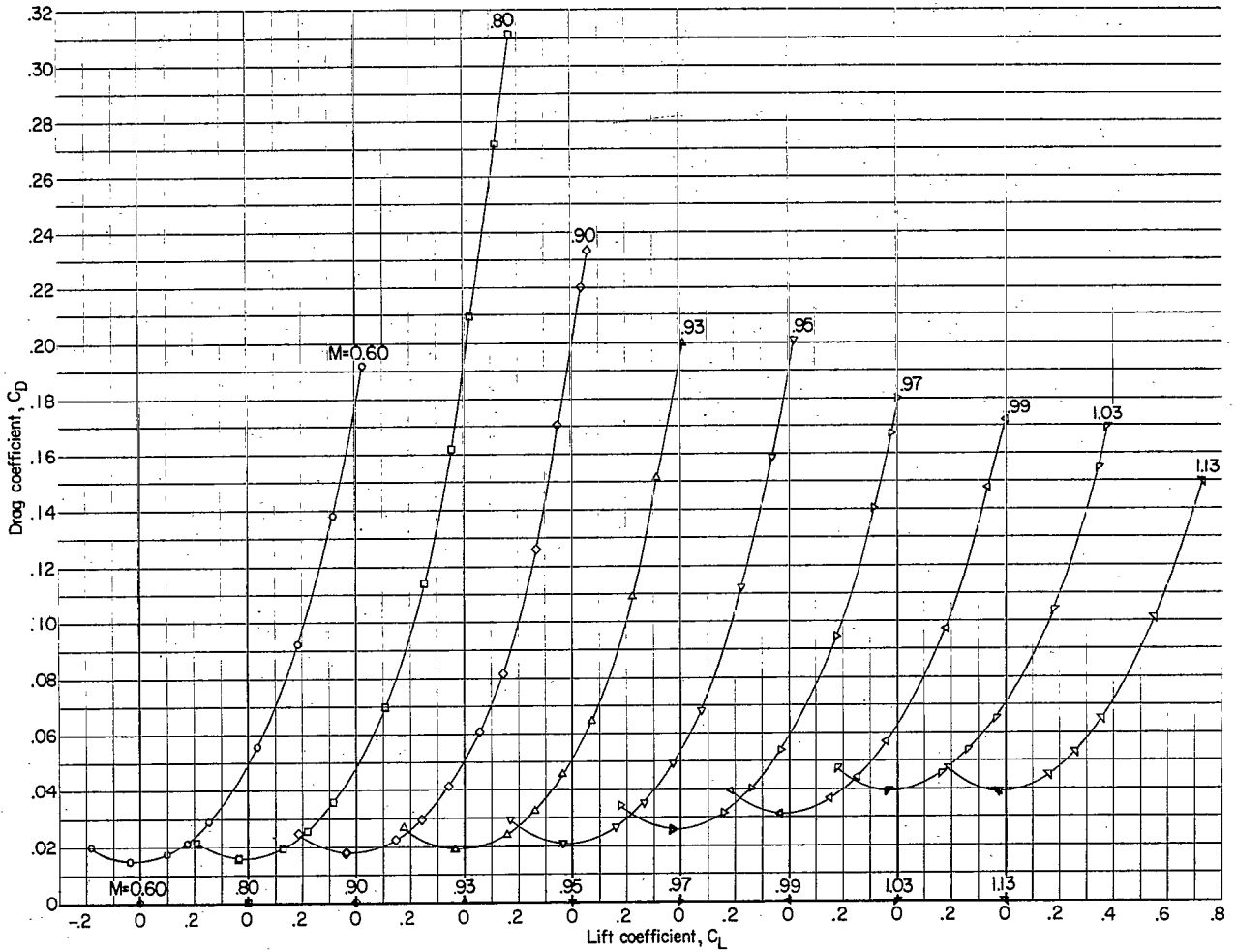

(b) Drag coefficient.

Figure 12.- Concluded.

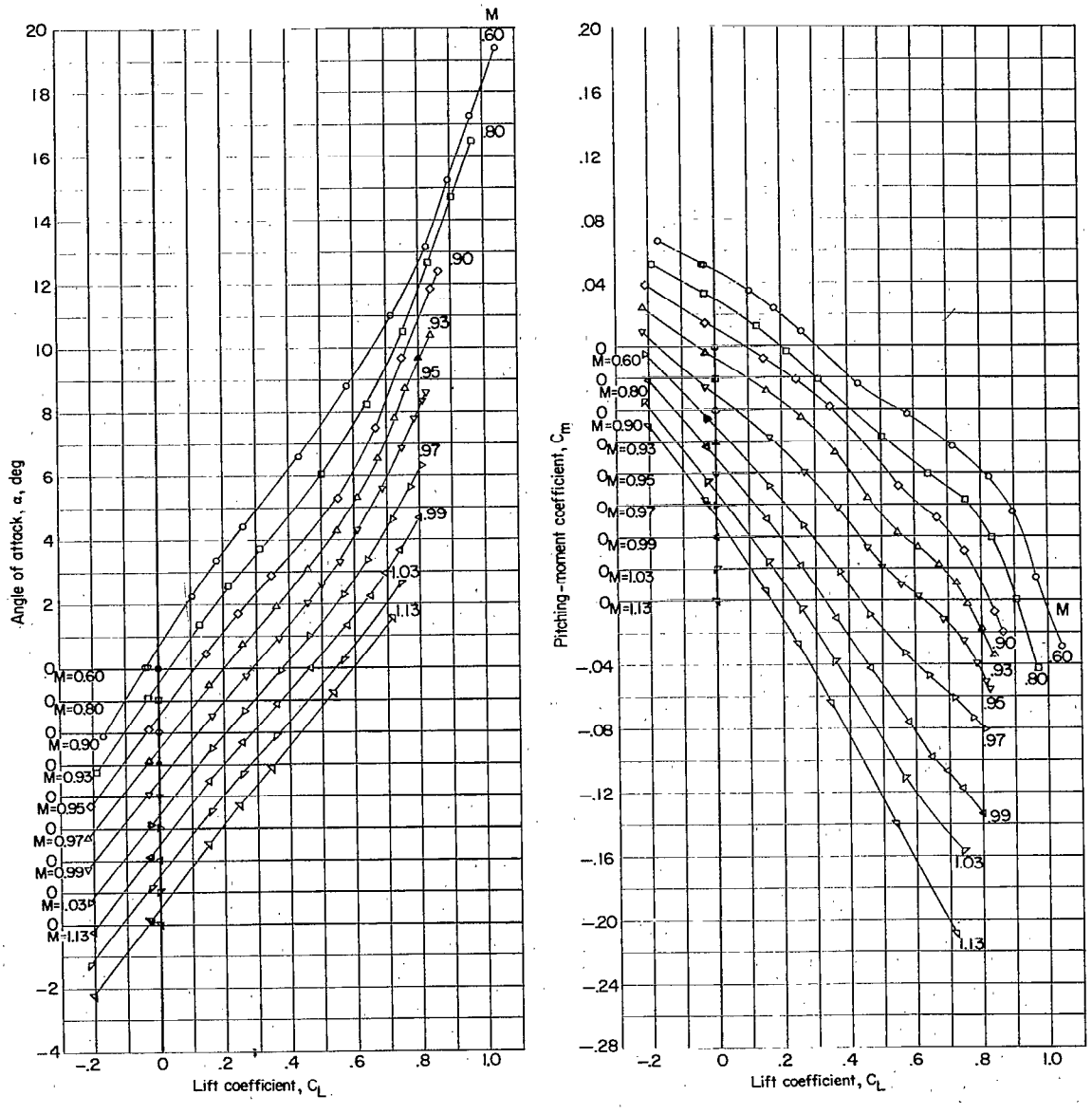

(a) Angle of attack and pitching-moment coefficient.

Figure 13.- Variation of aerodynamic characteristics with lift coefficient. Configuration 5; complete model; $i_t = -3^\circ$; A = 3.18; supersonic inlet (cruise condition).

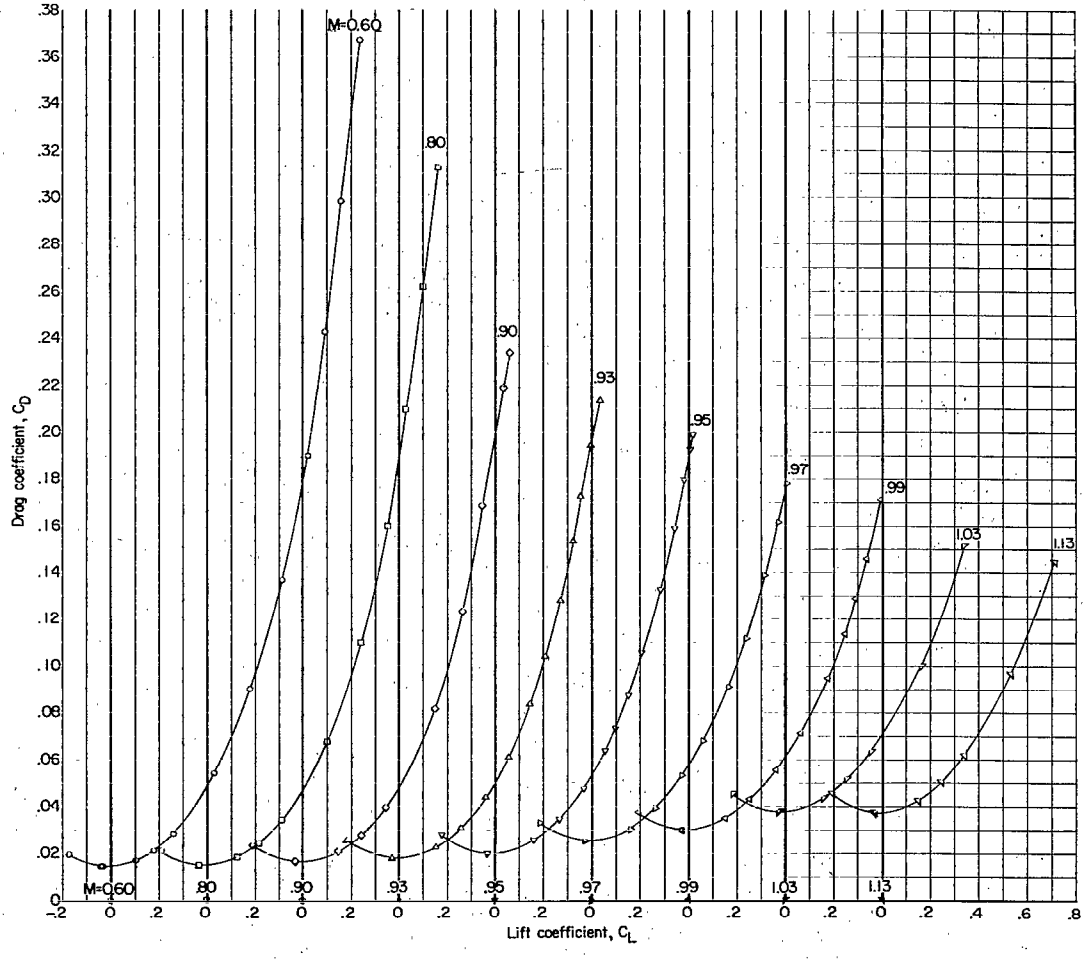

(b) Drag coefficient.

Figure 13.- Concluded.

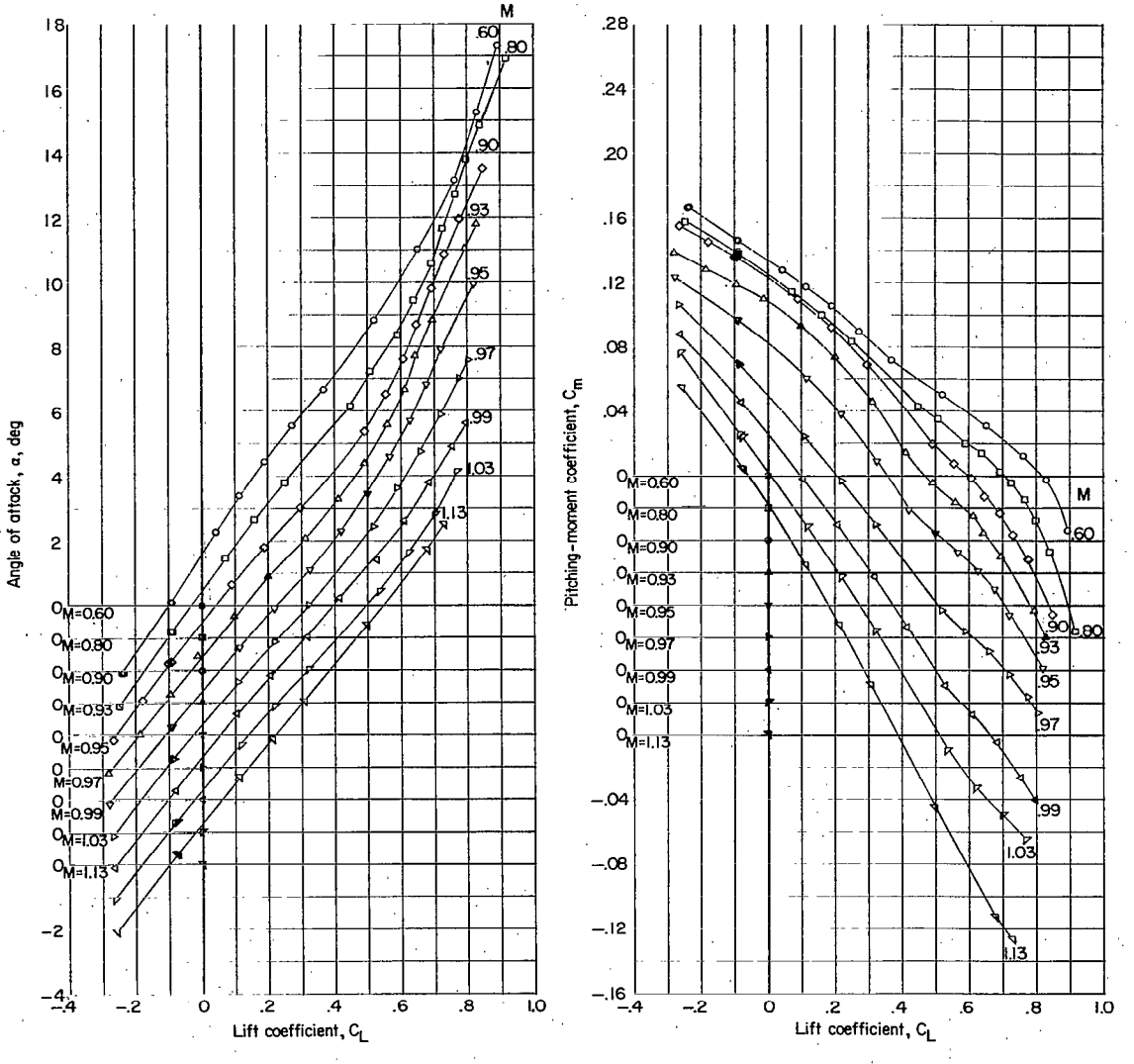

(a) Angle of attack and pitching-moment coefficient.

Figure 14.- Variation of aerodynamic characteristics with lift coefficient. Configuration 6; complete model; $i_t = -8^o$; A = 3.18; supersonic inlet (cruise condition).

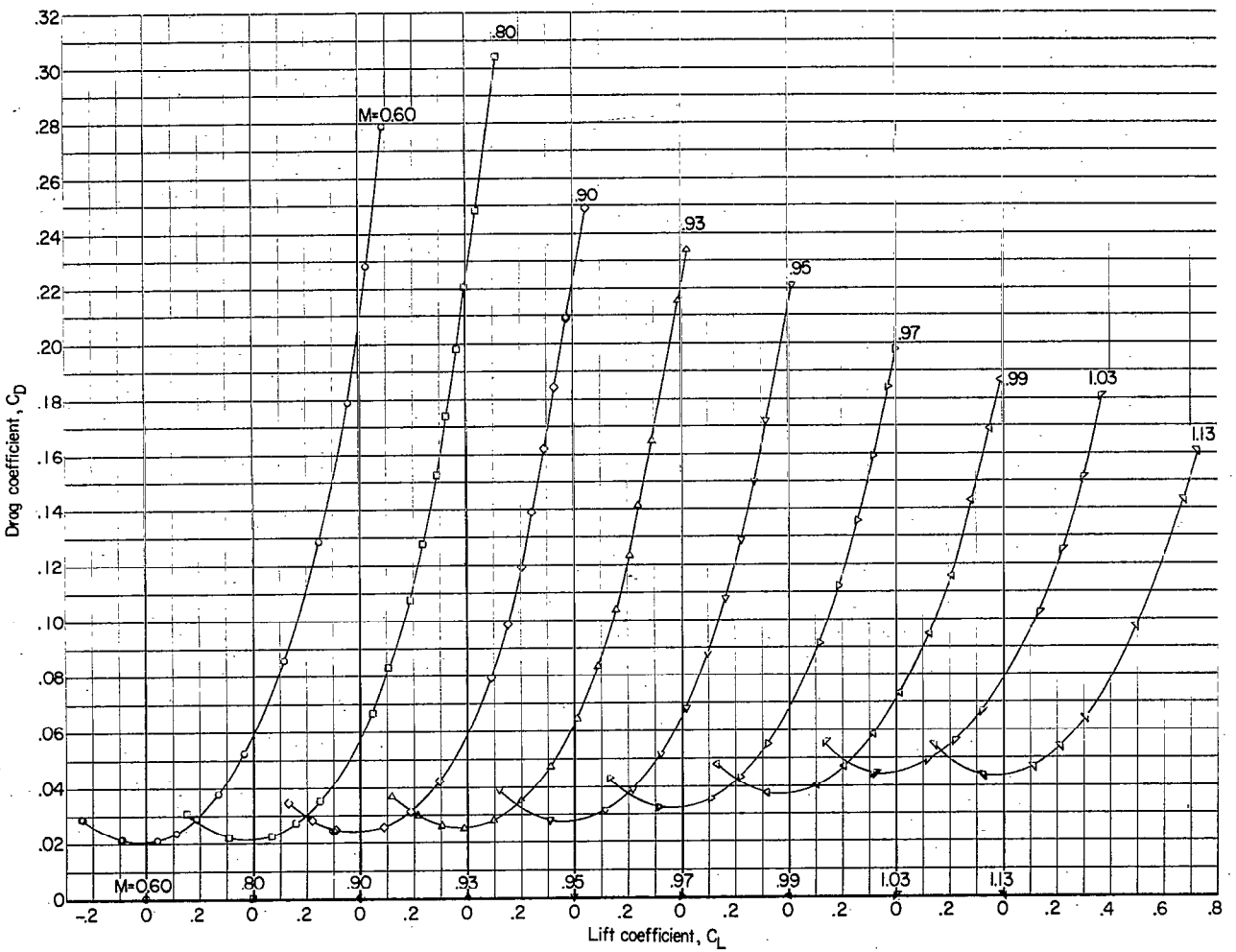

(b) Drag coefficient.

Figure 14.- Concluded.

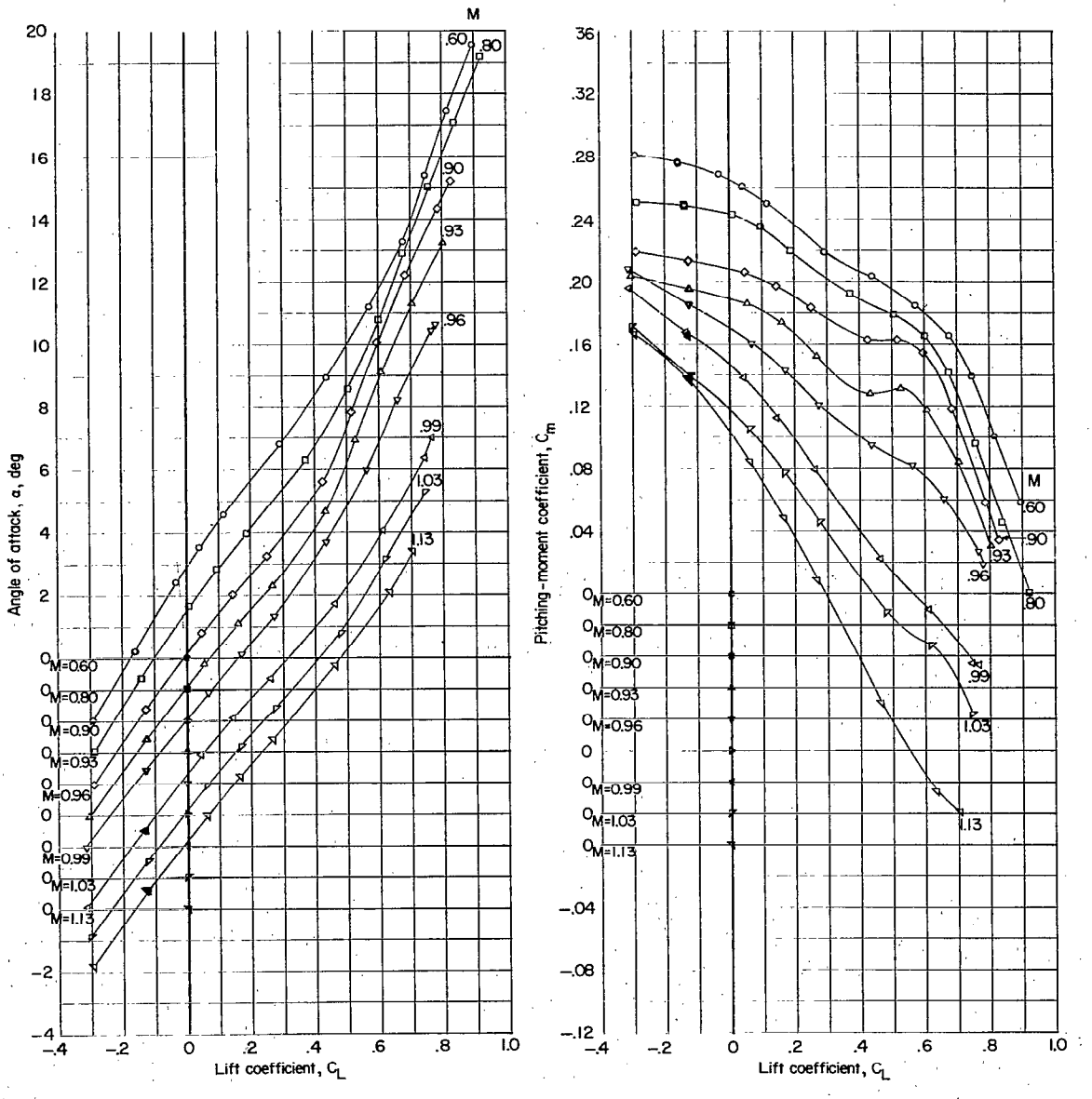

(a) Angle of attack and pitching-moment coefficient.

Figure 15.- Variation of aerodynamic characteristics with lift coefficient. Configuration 7; complete model; $i_t = -16^\circ$; A = 3.18; supersonic inlet (cruise condition).

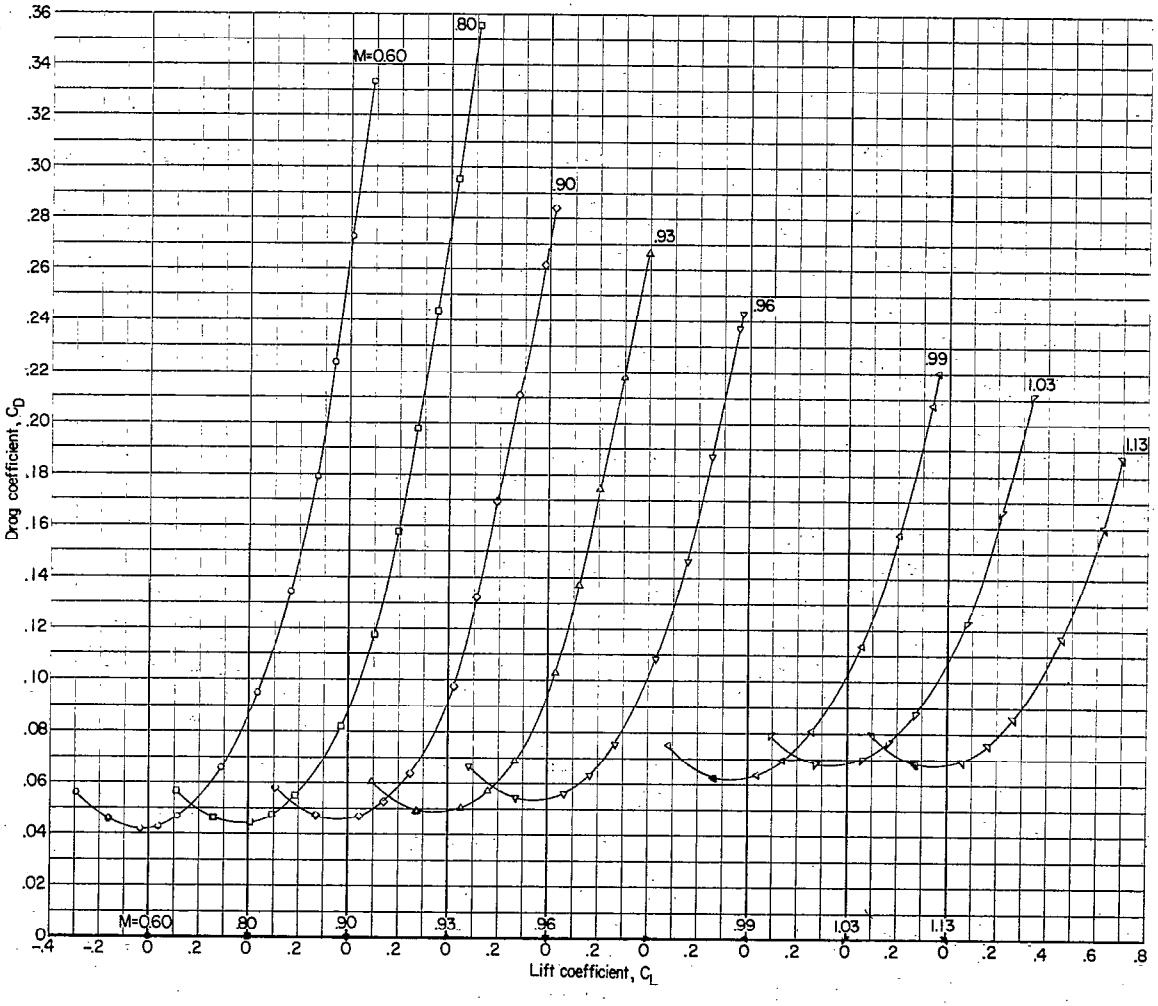

(b) Drag coefficient.

Figure 15.- Concluded.

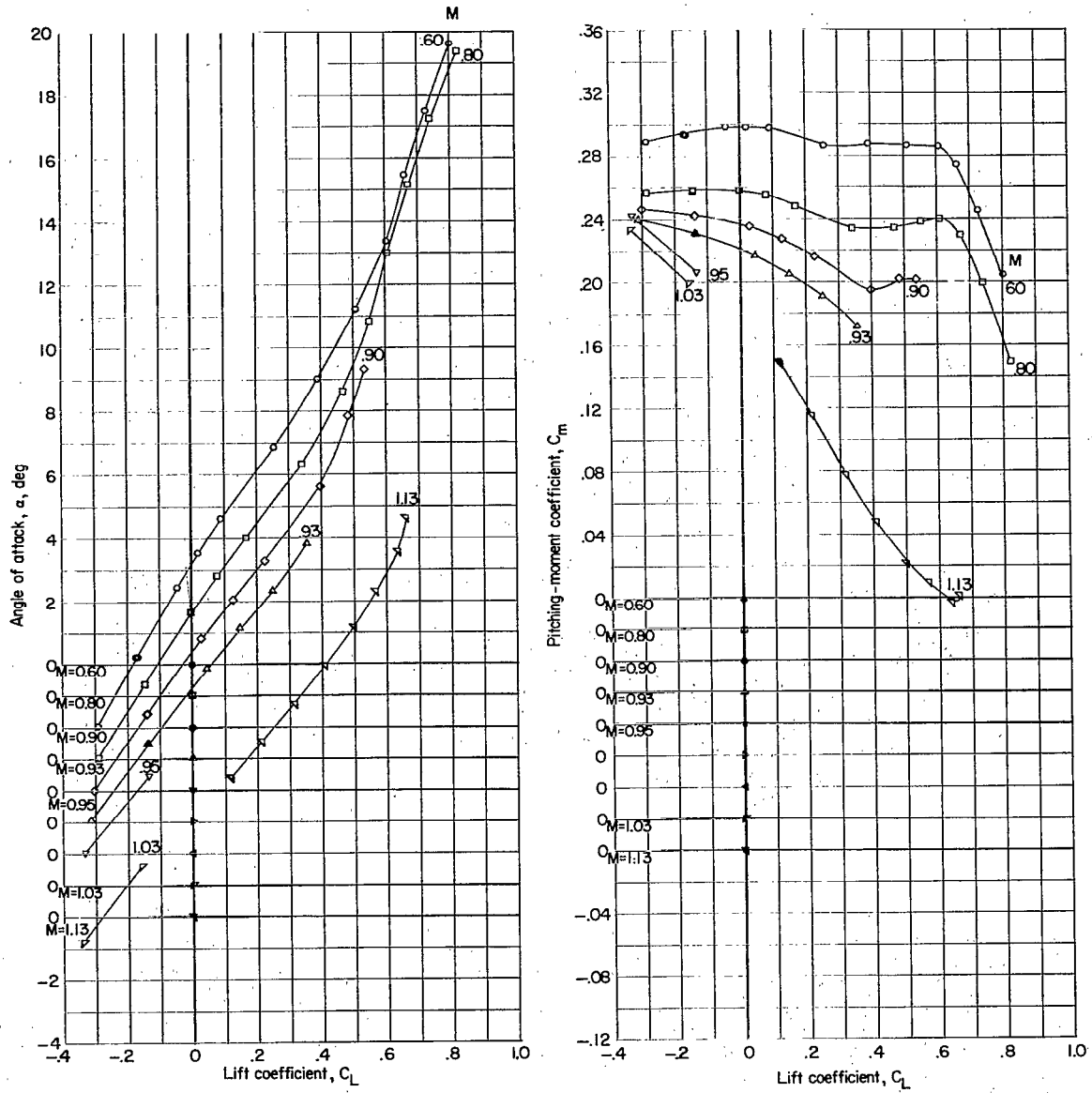

(a) Angle of attack and pitching-moment coefficient.

Figure 16.- Variation of aerodynamic characteristics with lift coefficient. Configuration 8; complete model; $i_t = -24^\circ$; A = 3.18; supersonic inlet (cruise condition).

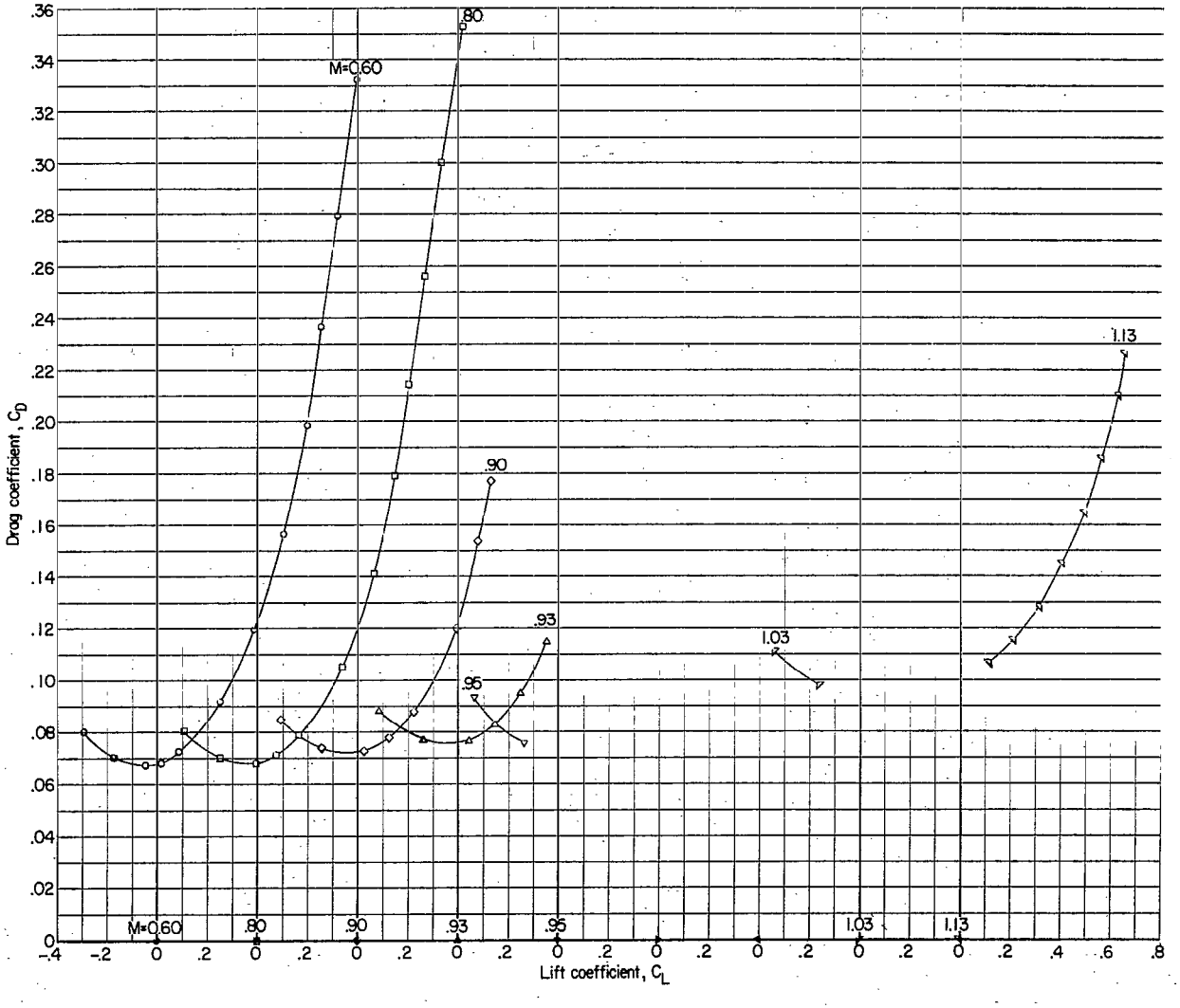

(b) Drag coefficient.

Figure 16.- Concluded.

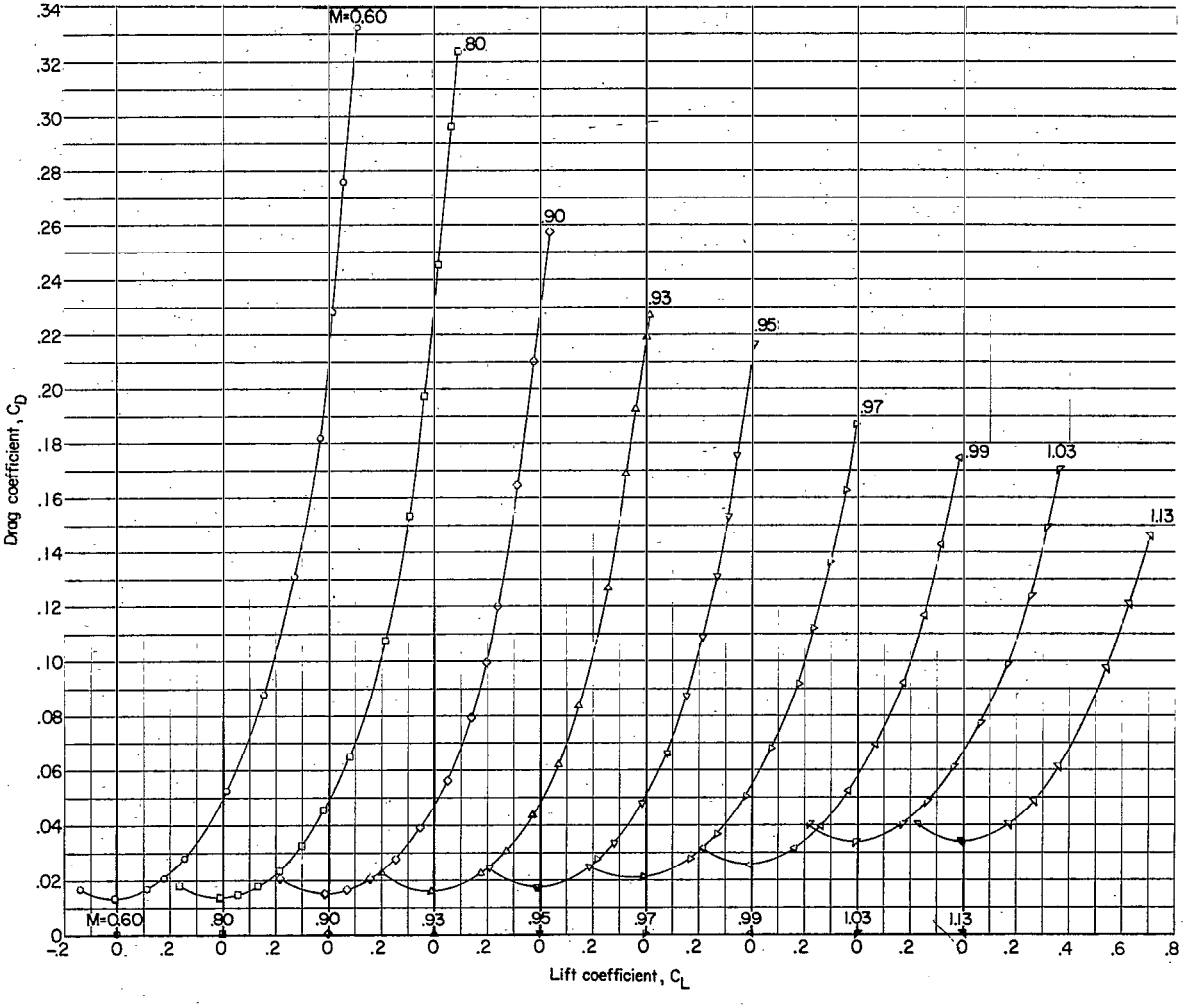

(b) Drag coefficient.

Figure 17.- Concluded.

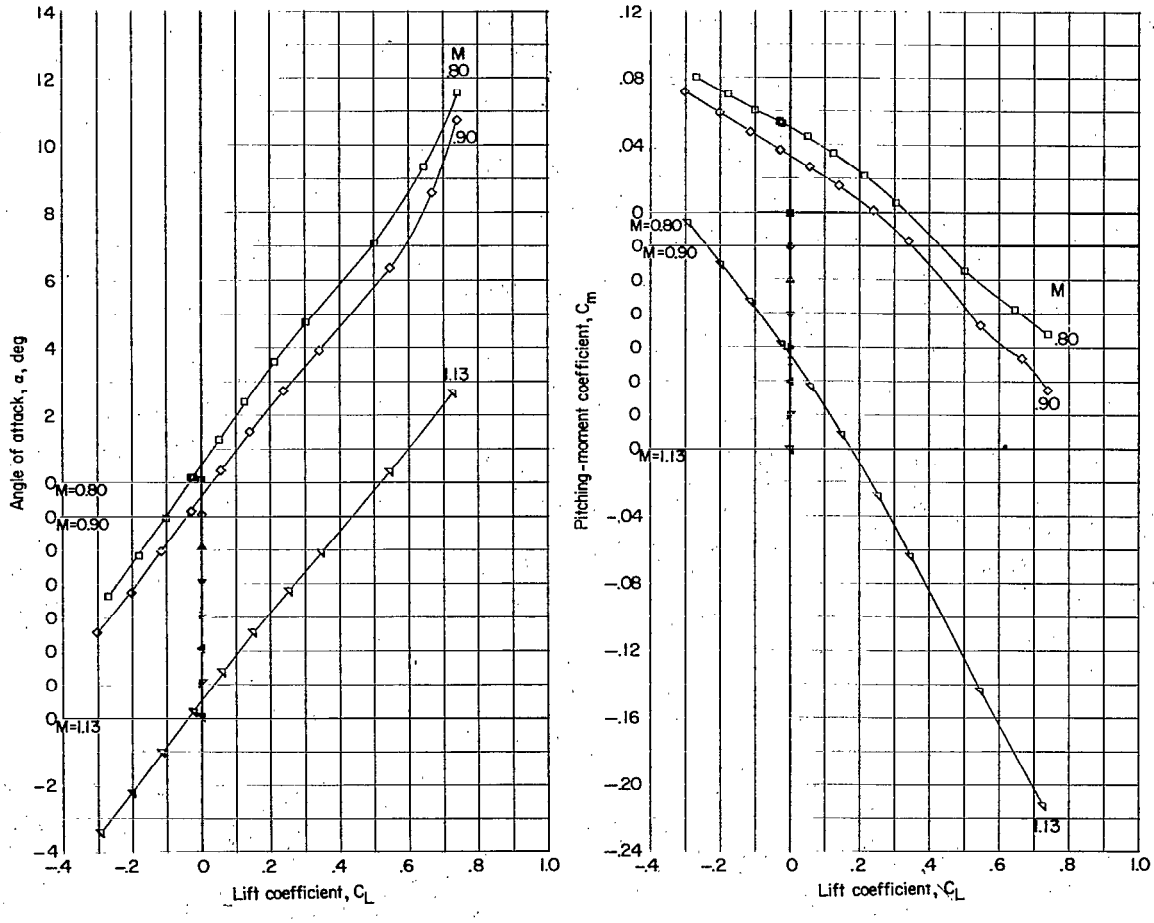

(a) Angle of attack and pitching-moment coefficient.

Figure 18.- Variation of aerodynamic characteristics with lift coefficient. Configuration 10; complete model; $i_t = -3^\circ$; A = 3.18; wing modification 1; supersonic inlet (cruise condition).

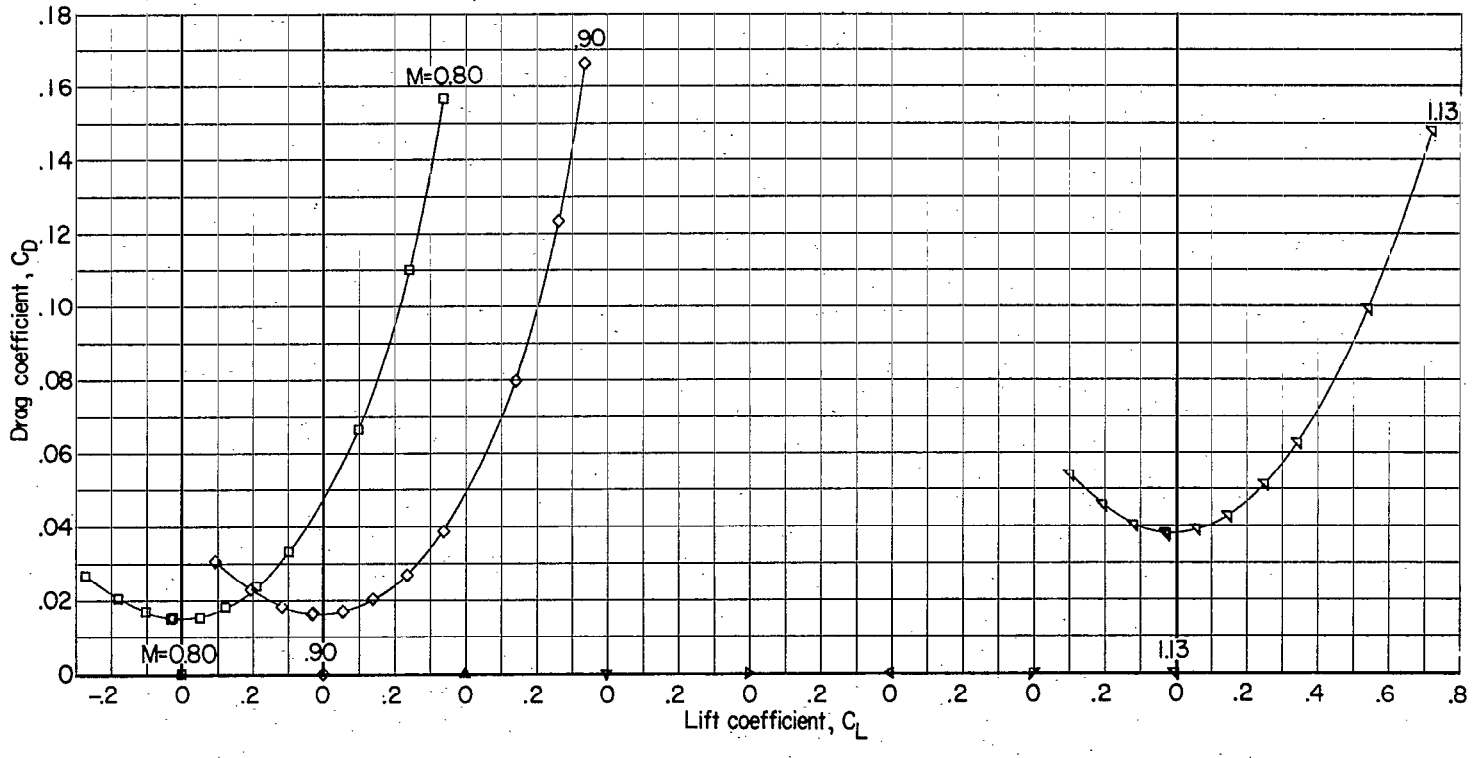

(b) Drag coefficient.

Figure 18.- Concluded.

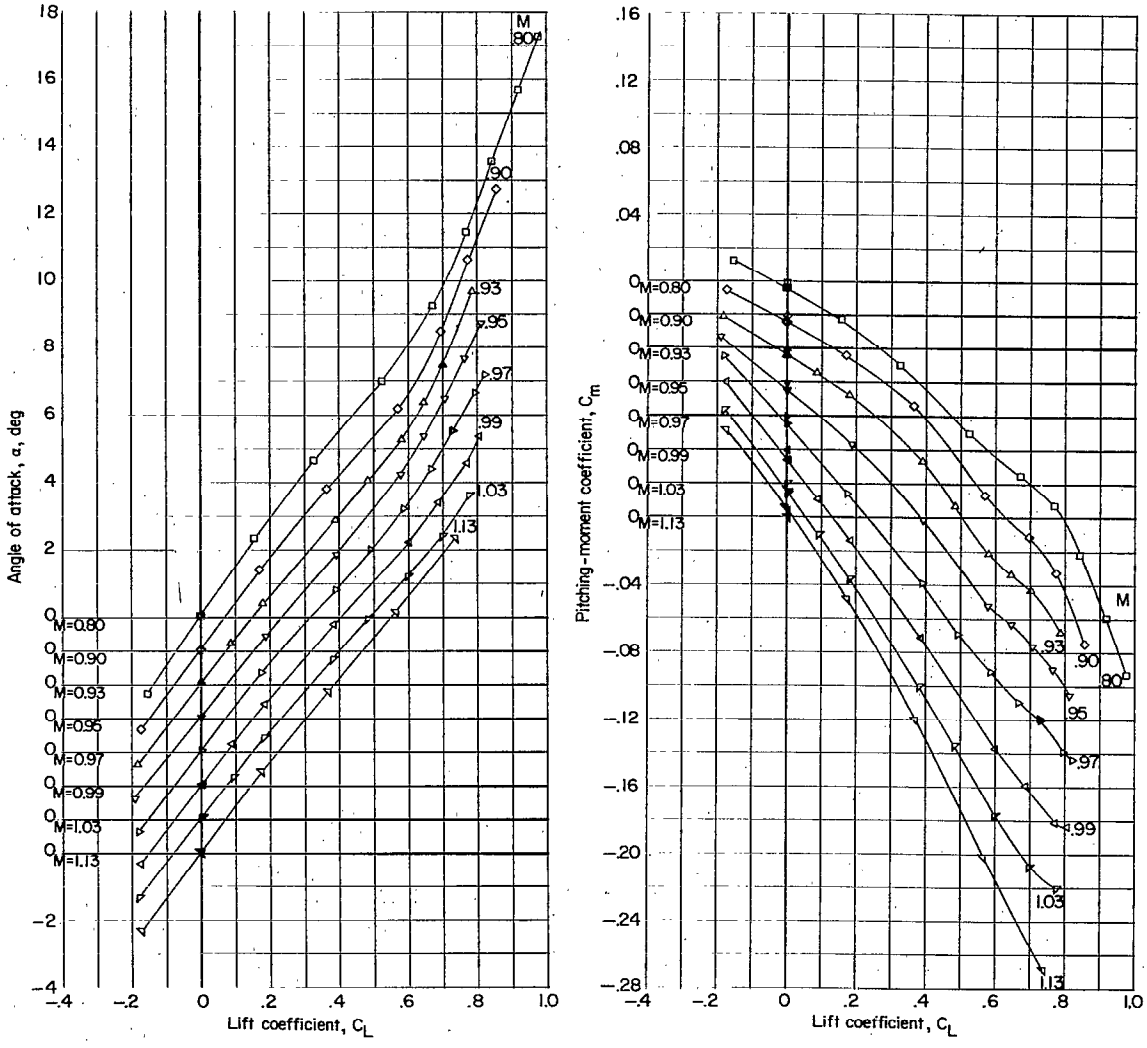

(a) Angle of attack and pitching-moment coefficient.

Figure 19.- Variation of aerodynamic characteristics with lift coefficient. Configuration 11; complete model; $i_t = 0^\circ$; A = 3.18; wing modification 1; supersonic inlet (cruise condition).

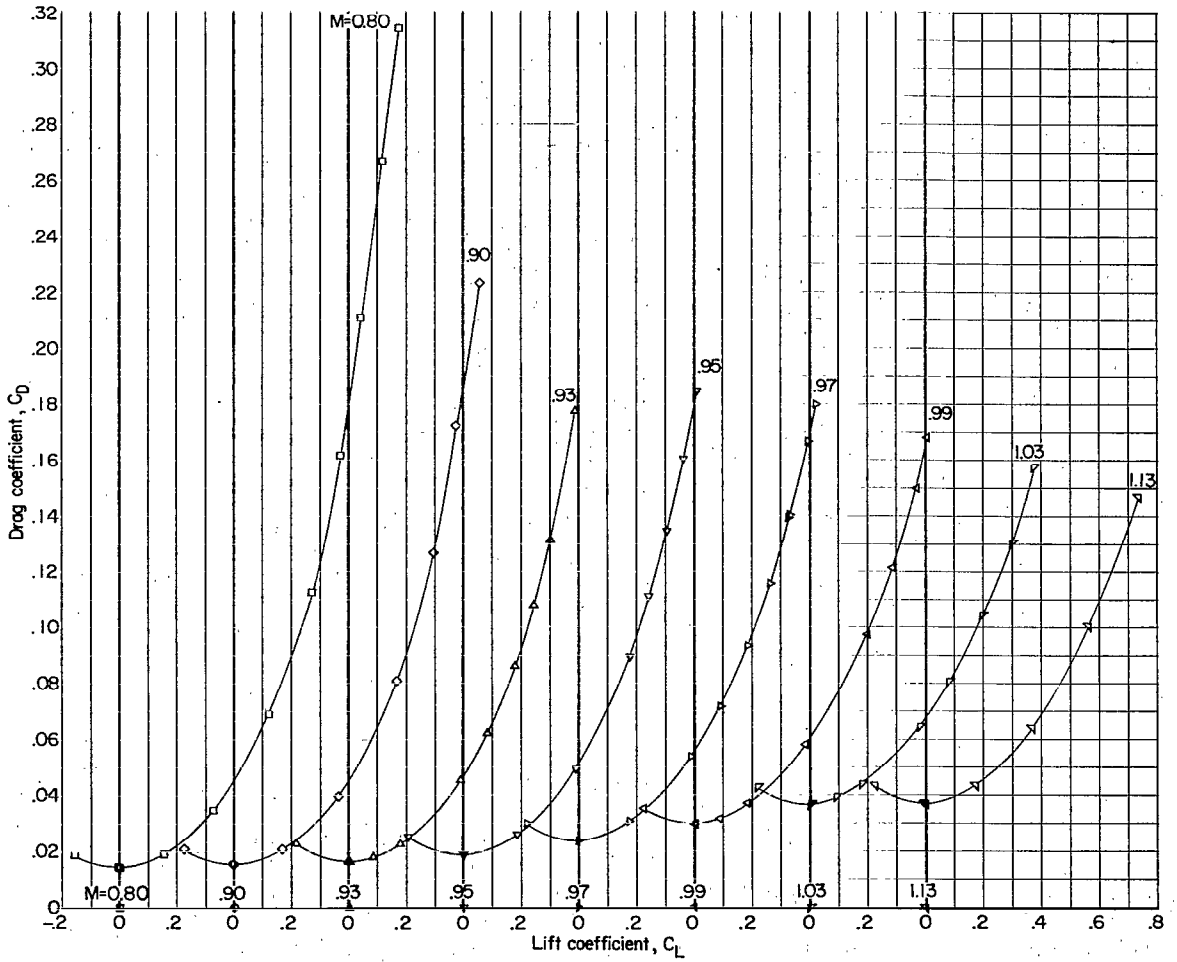

(b) Drag coefficient.

Figure 19.- Concluded.

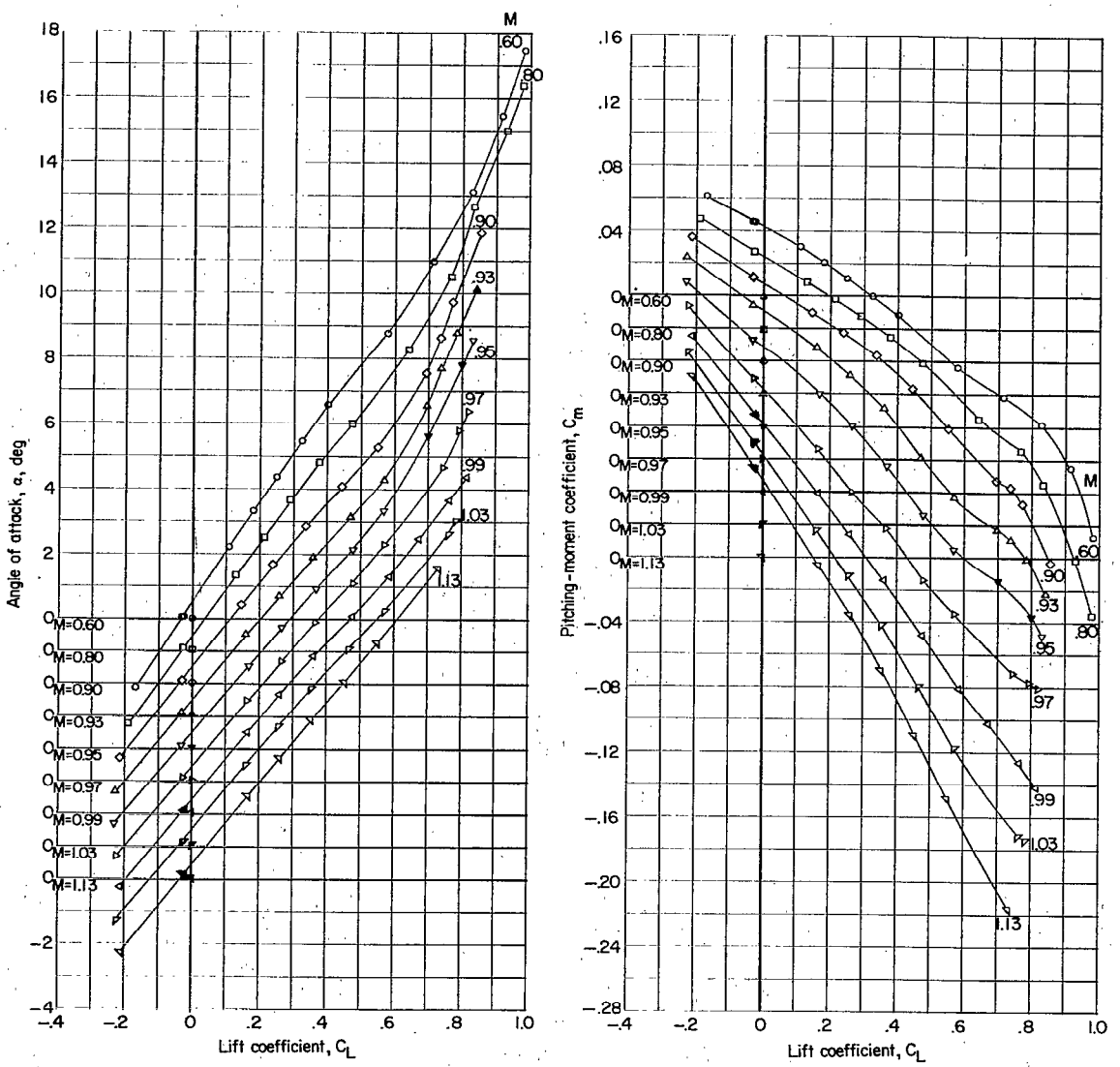

(a) Angle of attack and pitching-moment coefficient.

Figure 20.- Variation of aerodynamic characteristics with lift coefficient. Configuration 12; complete model; $i_t = -3^\circ$; $\delta_n = -7.5^\circ$; A = 3.18; supersonic inlet (cruise condition).

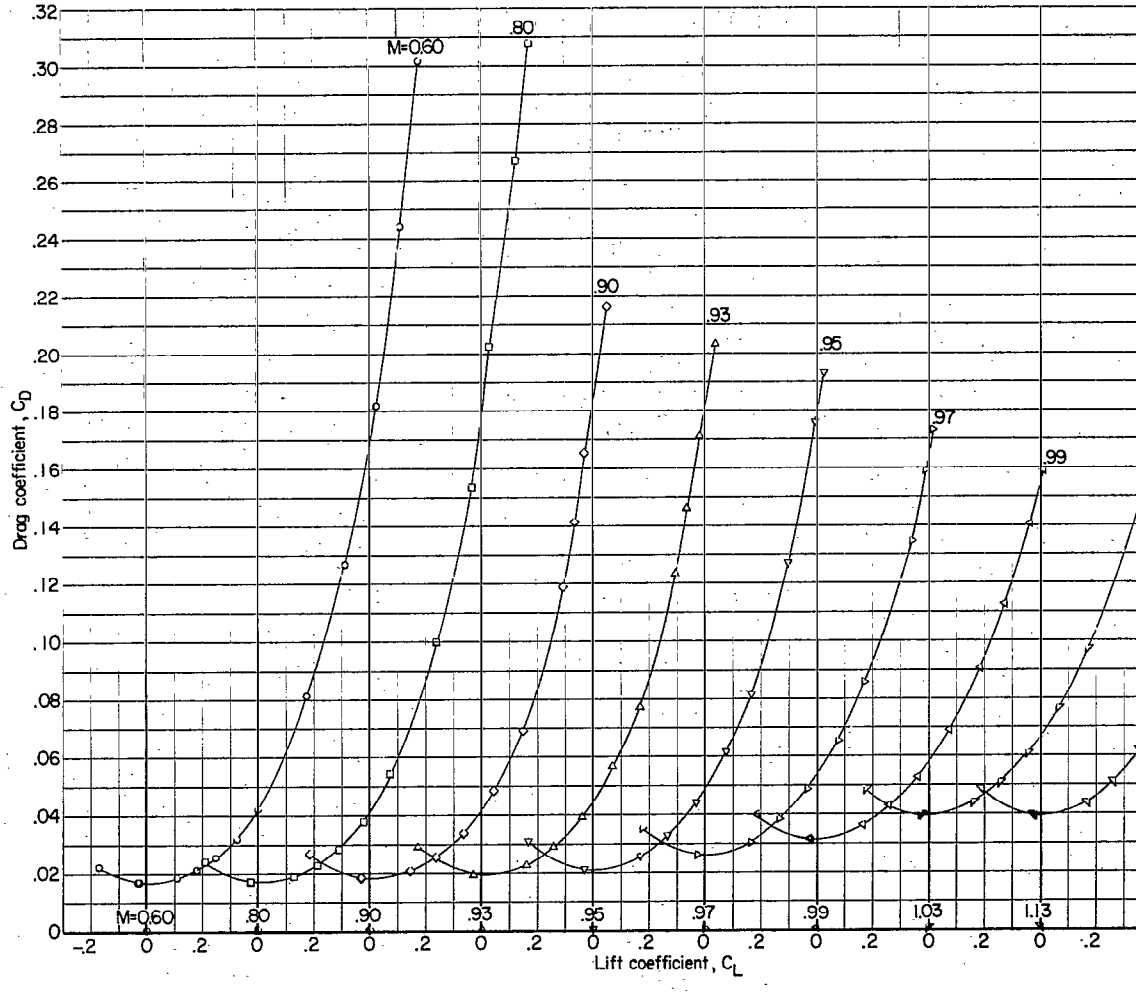

(b) Drag coefficient.

Figure 20.- Concluded.

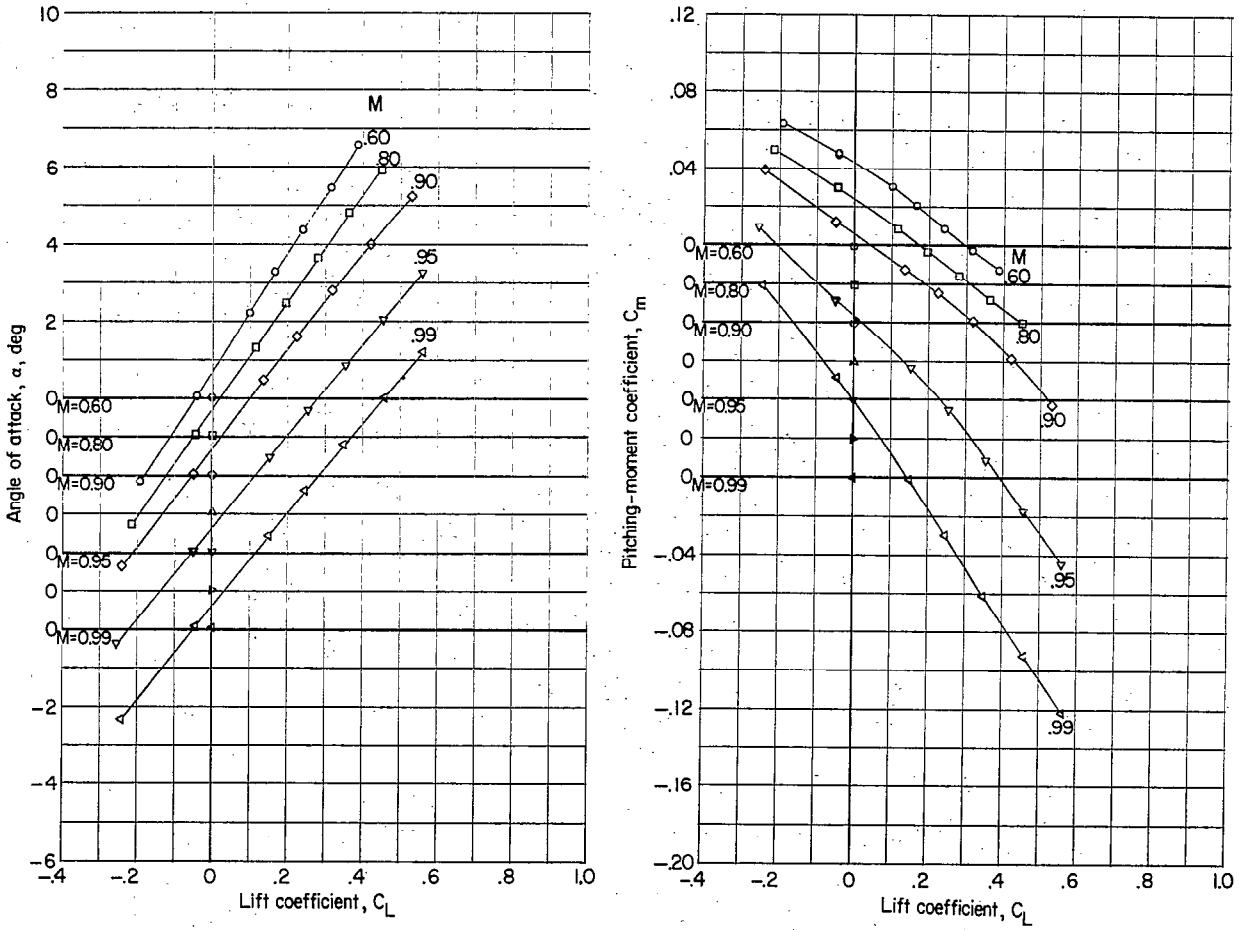

(a) Angle of attack and pitching-moment coefficient.

Figure 21.- Variation of aerodynamic characteristics with lift coefficient. Configuration 13; complete model; $i_t = -3^\circ$; $\delta_n = -15^\circ$; A = 3.18; supersonic inlet (cruise condition).

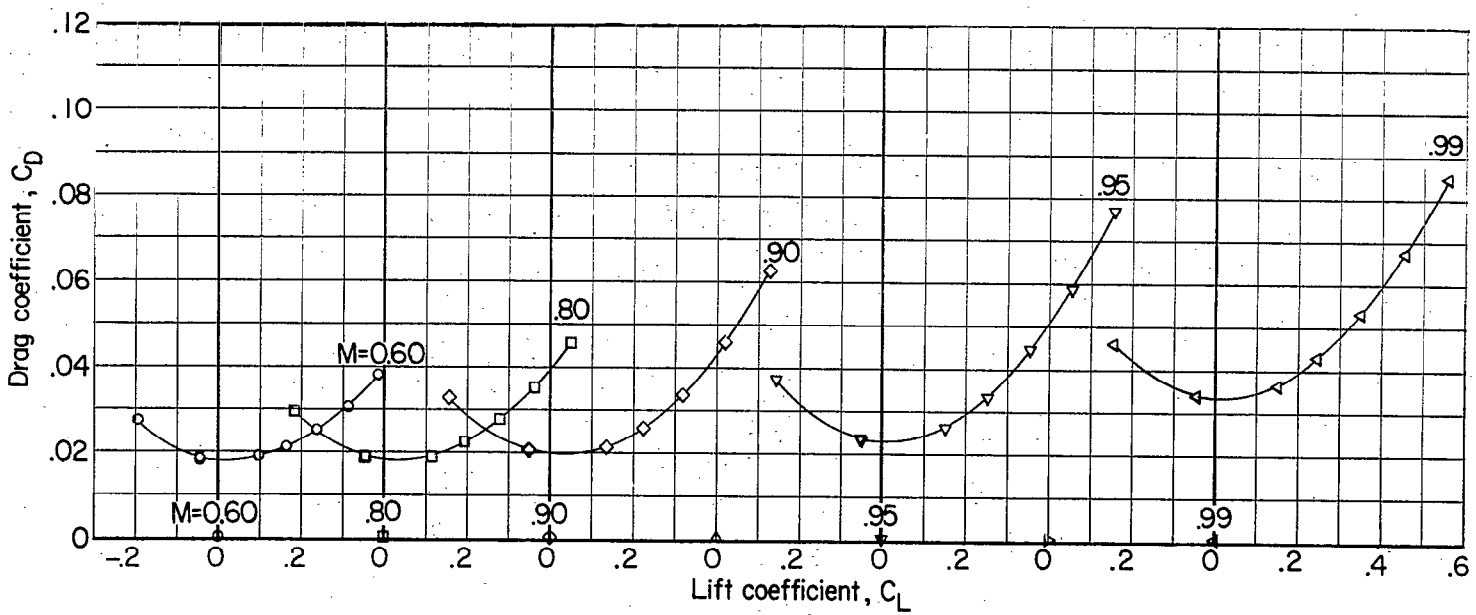

(b) Drag coefficient.

Figure 21.- Concluded.

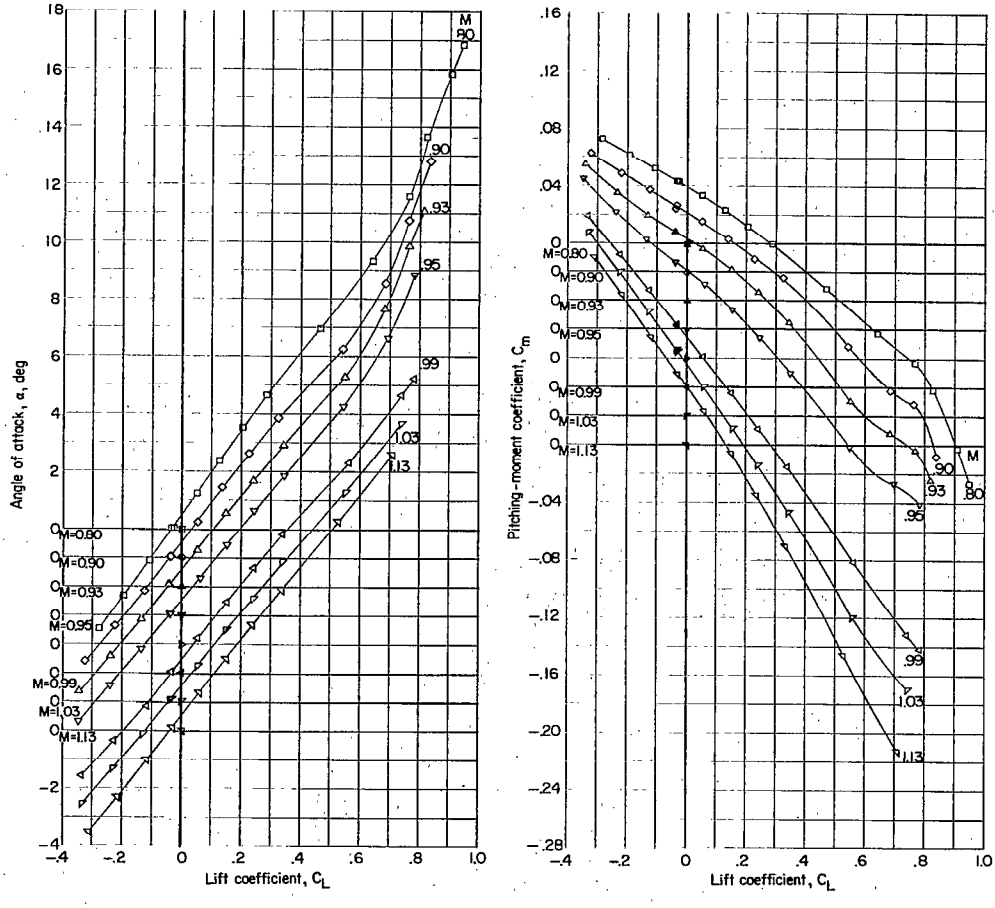

(a) Angle of attack and pitching-moment coefficient.

Figure 22.- Variation of aerodynamic characteristics with lift coefficient. Configuration 14; complete model; $i_t = -3^\circ$; $\delta_n = -7.5^\circ$; A = 3.18; drooped supersonic inlet (cruise condition).

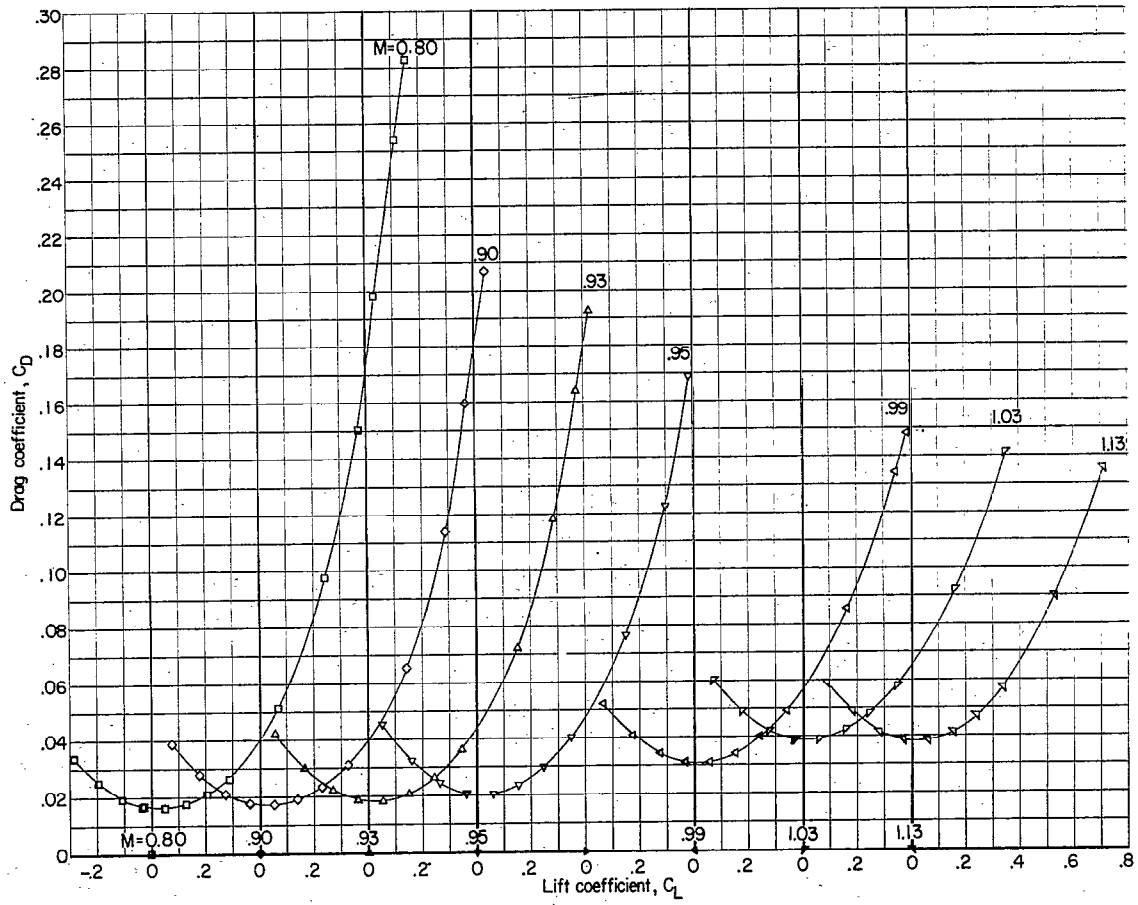

(b) Drag coefficient.

Figure 22.- Concluded.

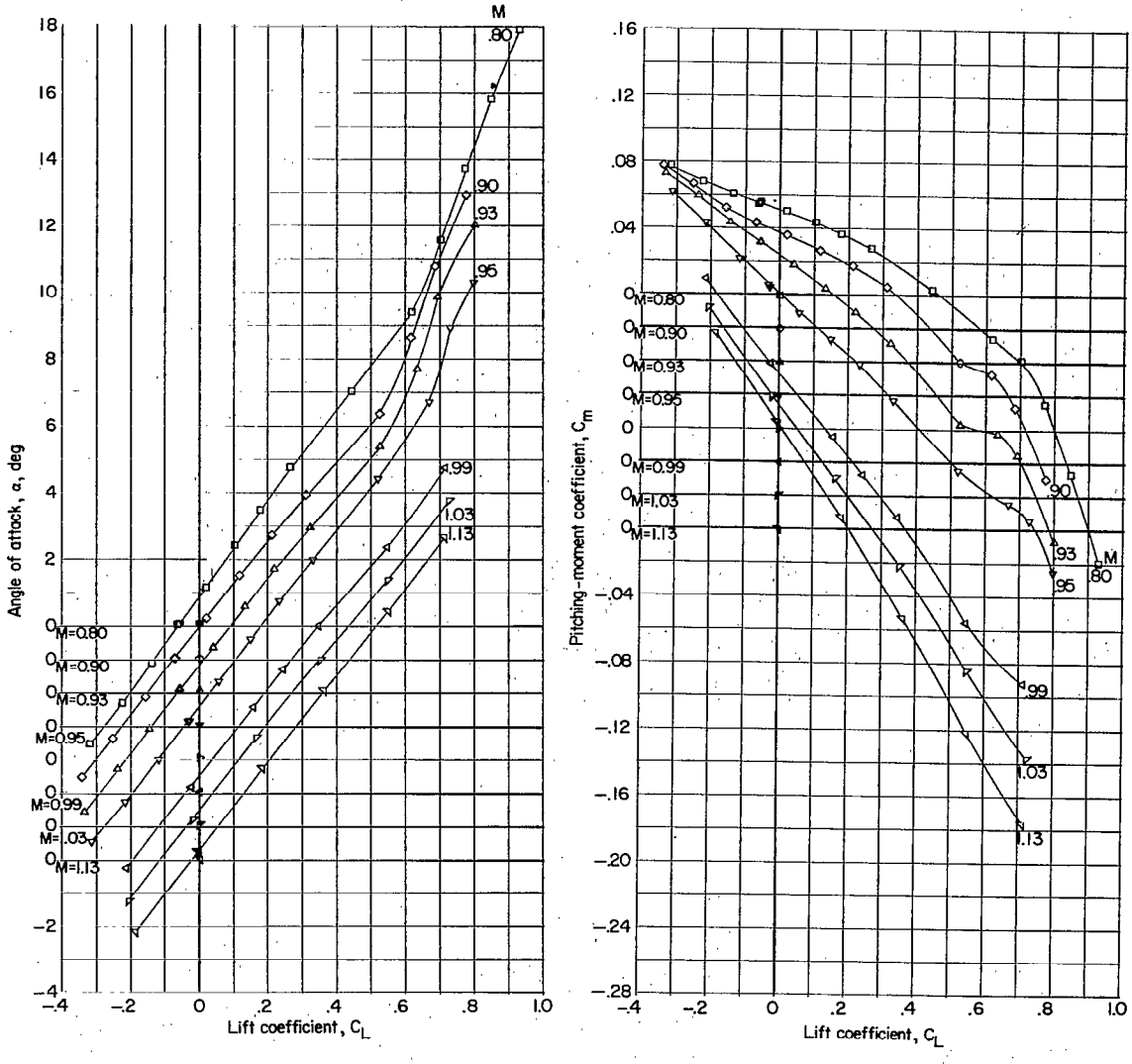

(a) Angle of attack and pitching-moment coefficient.

Figure 23.- Variation of aerodynamic characteristics with lift coefficient. Configuration 15; complete model plus wing pylon stores; $i_t = -3^\circ$; $\delta_n = -7.5^\circ$; A = 3.18; drooped supersonic inlet (cruise condition).

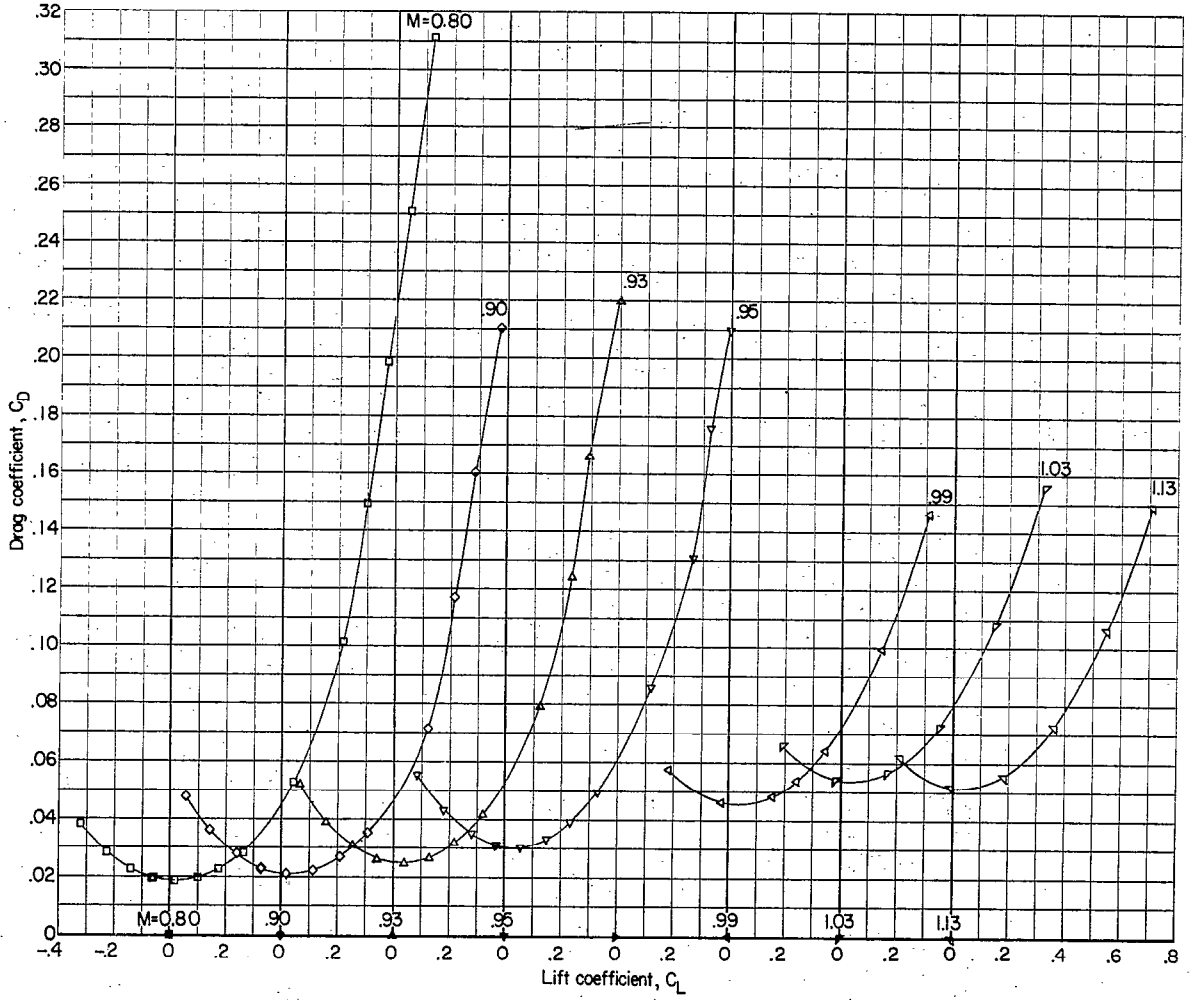

(b) Drag coefficient.

Figure 23.- Concluded.

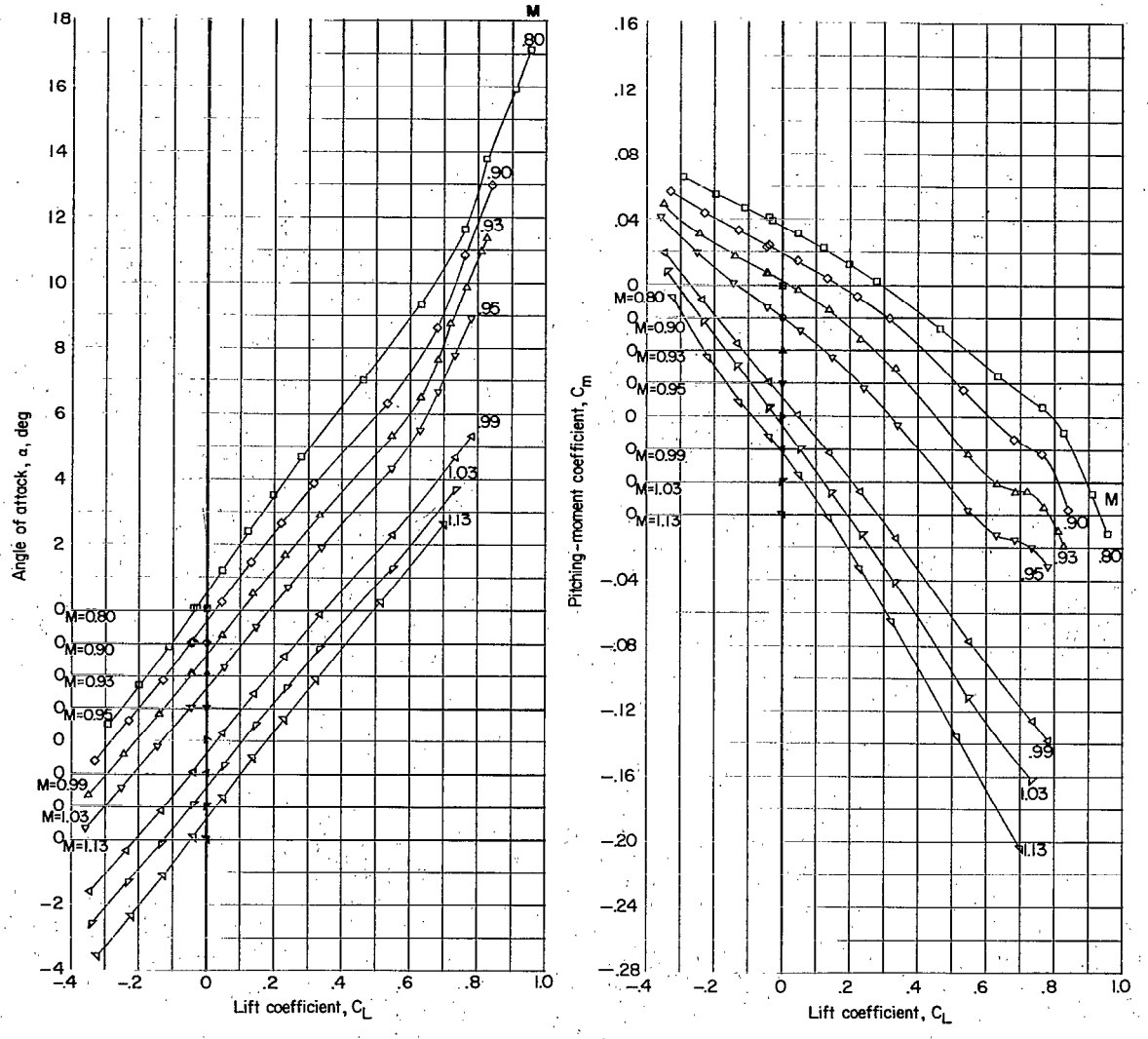

(a) Angle of attack and pitching-moment coefficient.

Figure 24.- Variation of aerodynamic characteristics with lift coefficient. Configuration 16; complete model; $i_t = -3^\circ$; $\delta_n = 7.5^\circ$; body with long nose; A = 3.18; drooped supersonic inlet (cruise condition).

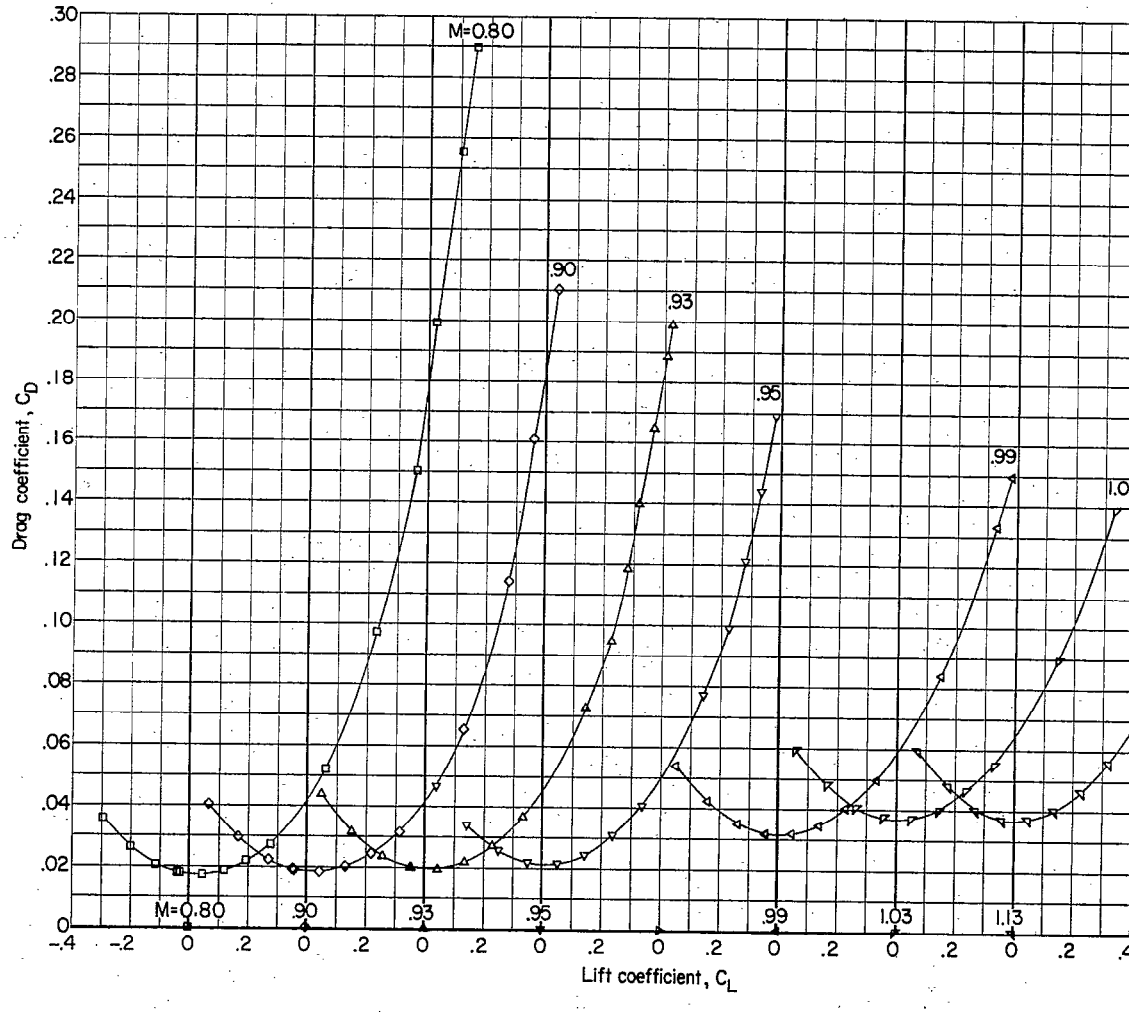

(b) Drag coefficient.

Figure 24.- Concluded.

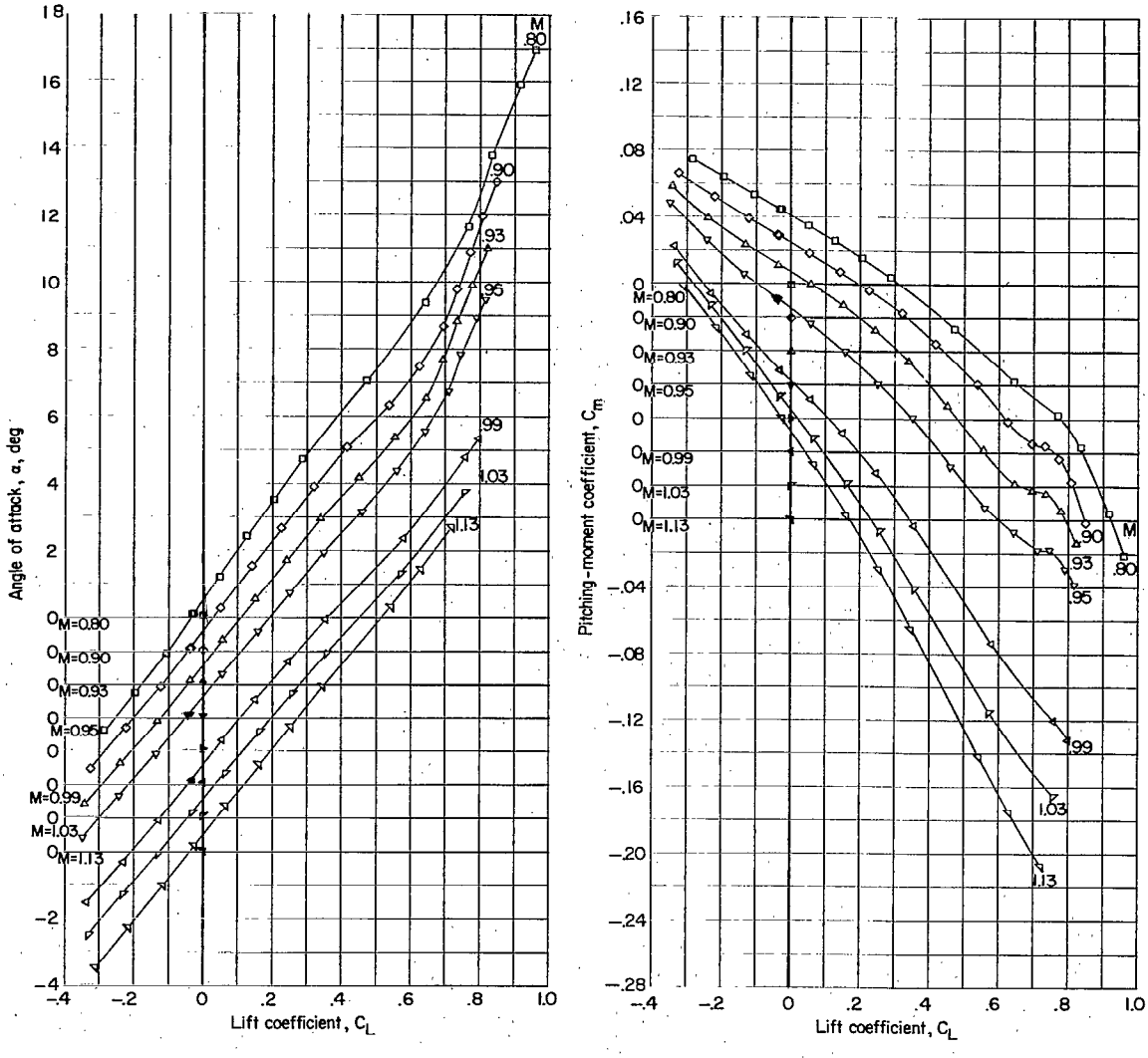

(a) Angle of attack and pitching-moment coefficient.

Figure 25.- Variation of aerodynamic characteristics with lift coefficient. Configuration 17; complete model; $i_t = -3^\circ$; $\delta_n = -7.5^\circ$; body with modified canopy; A = 3.18; drooped supersonic inlet (cruise condition).

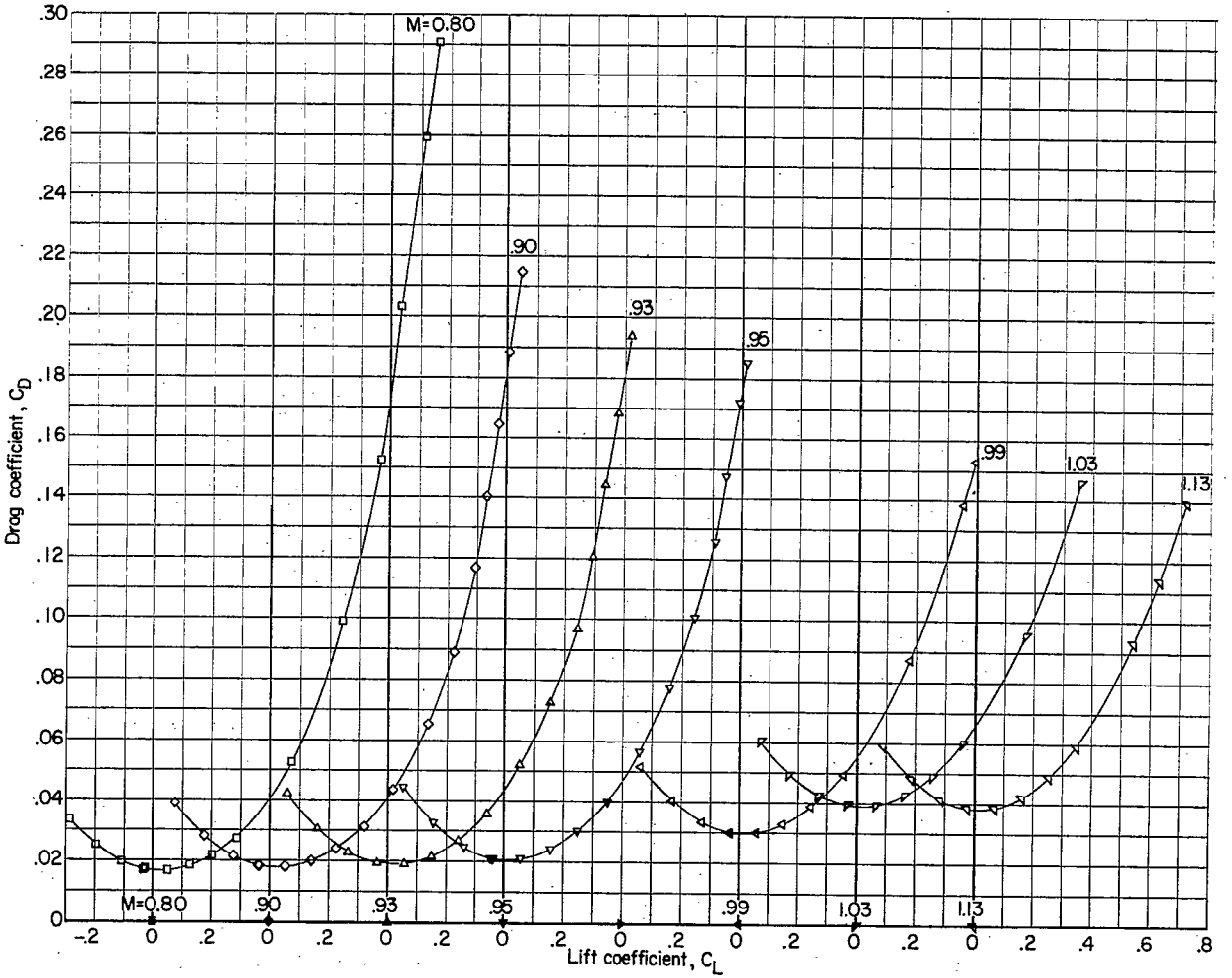

(b) Drag coefficient.

Figure 25.- Concluded.

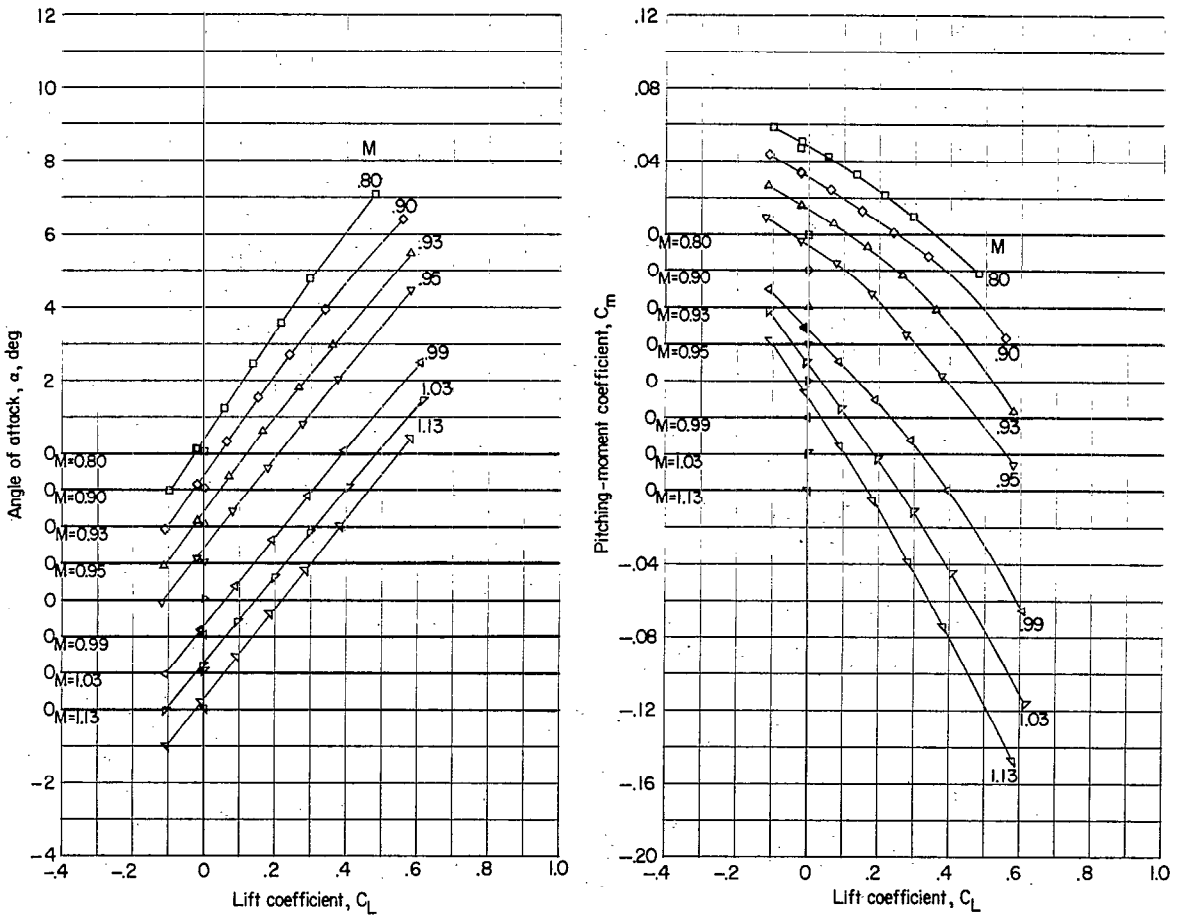

(a) Angle of attack and pitching-moment coefficient.

Figure 26.- Variation of aerodynamic characteristics with lift coefficient. Configuration 18; complete model; $i_t = -3^\circ$; $\delta_n = -7.5^\circ$; body with modified canopy and M = 1 bump; A = 3.18; drooped supersonic inlet (cruise condition).

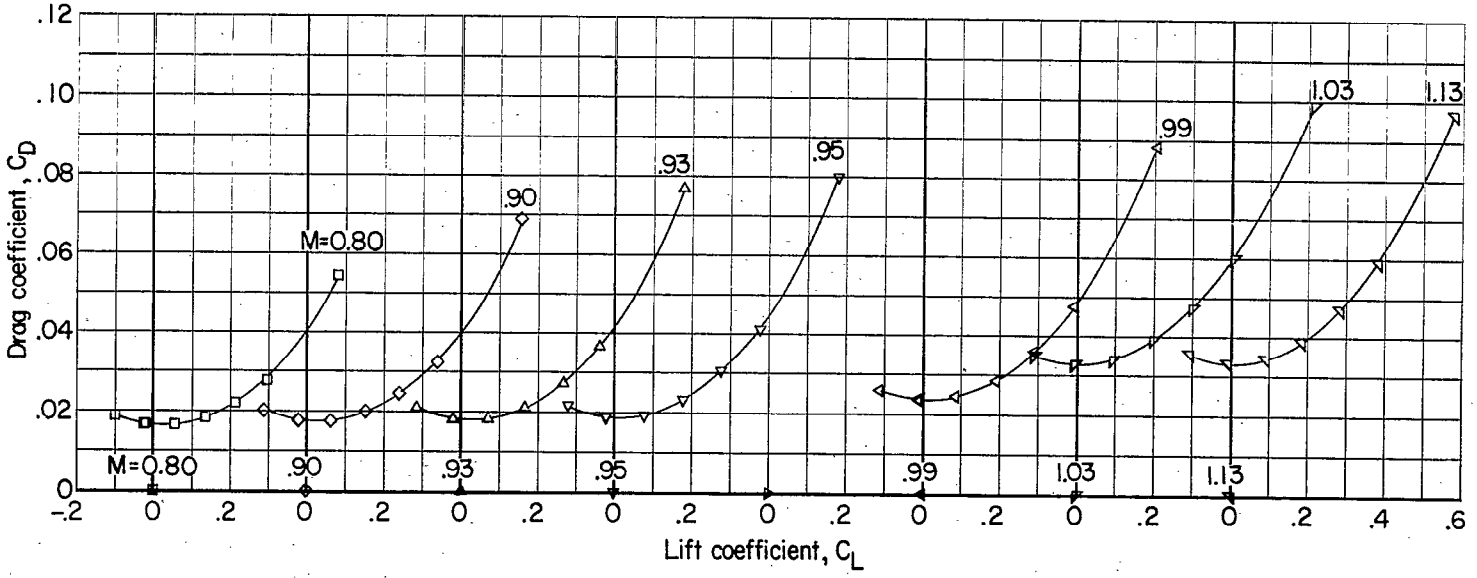

(b) Drag coefficient.

Figure 26.- Concluded.

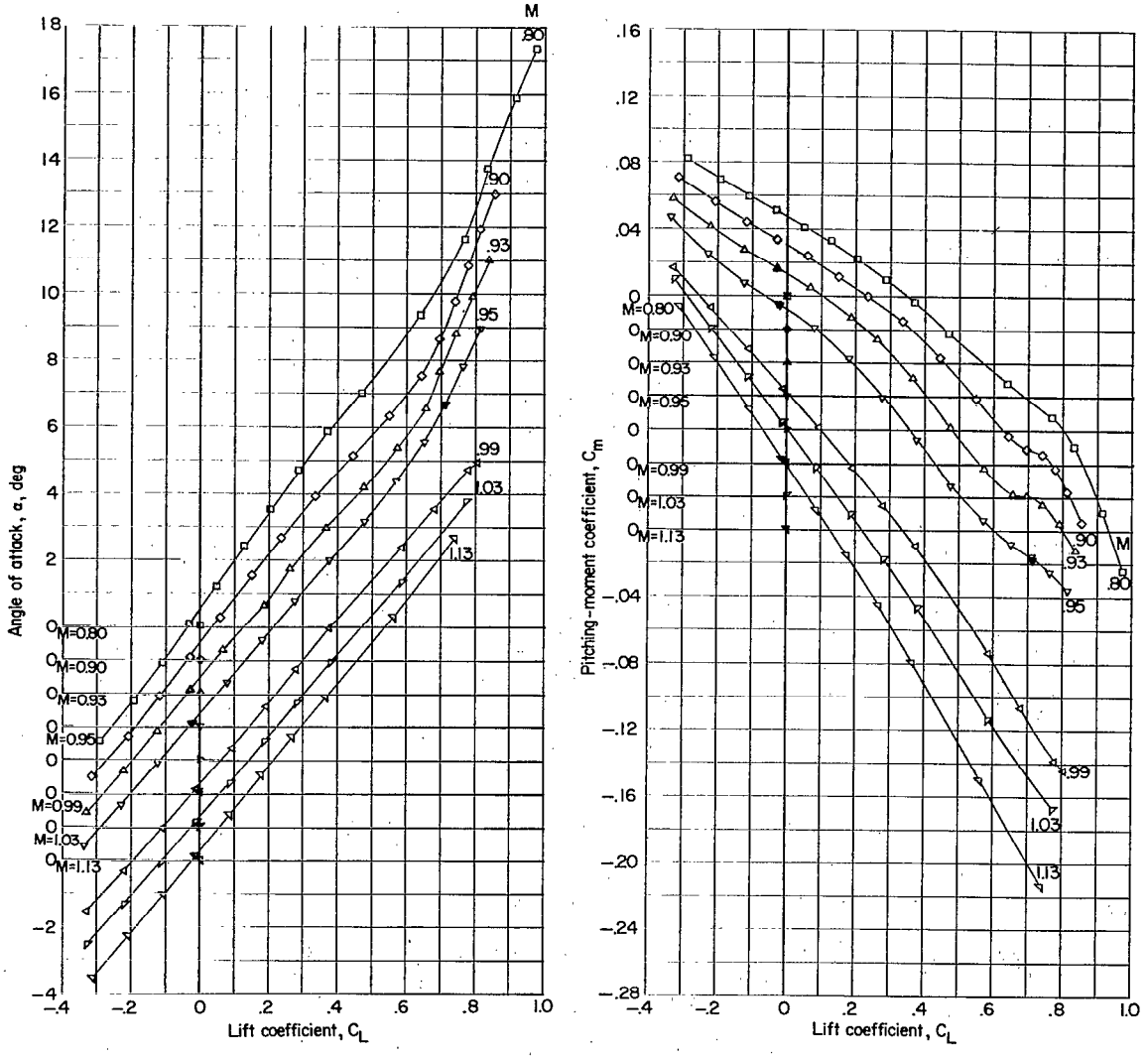

(a) Angle of attack and pitching-moment coefficient.

Figure 27.- Variation of aerodynamic characteristics with lift coefficient. Configuration 19; complete model; $i_t = -3^\circ$; $\delta_n = -7.5^\circ$; body with M = 1 bump; A = 3.18; drooped supersonic inlet (cruise condition).

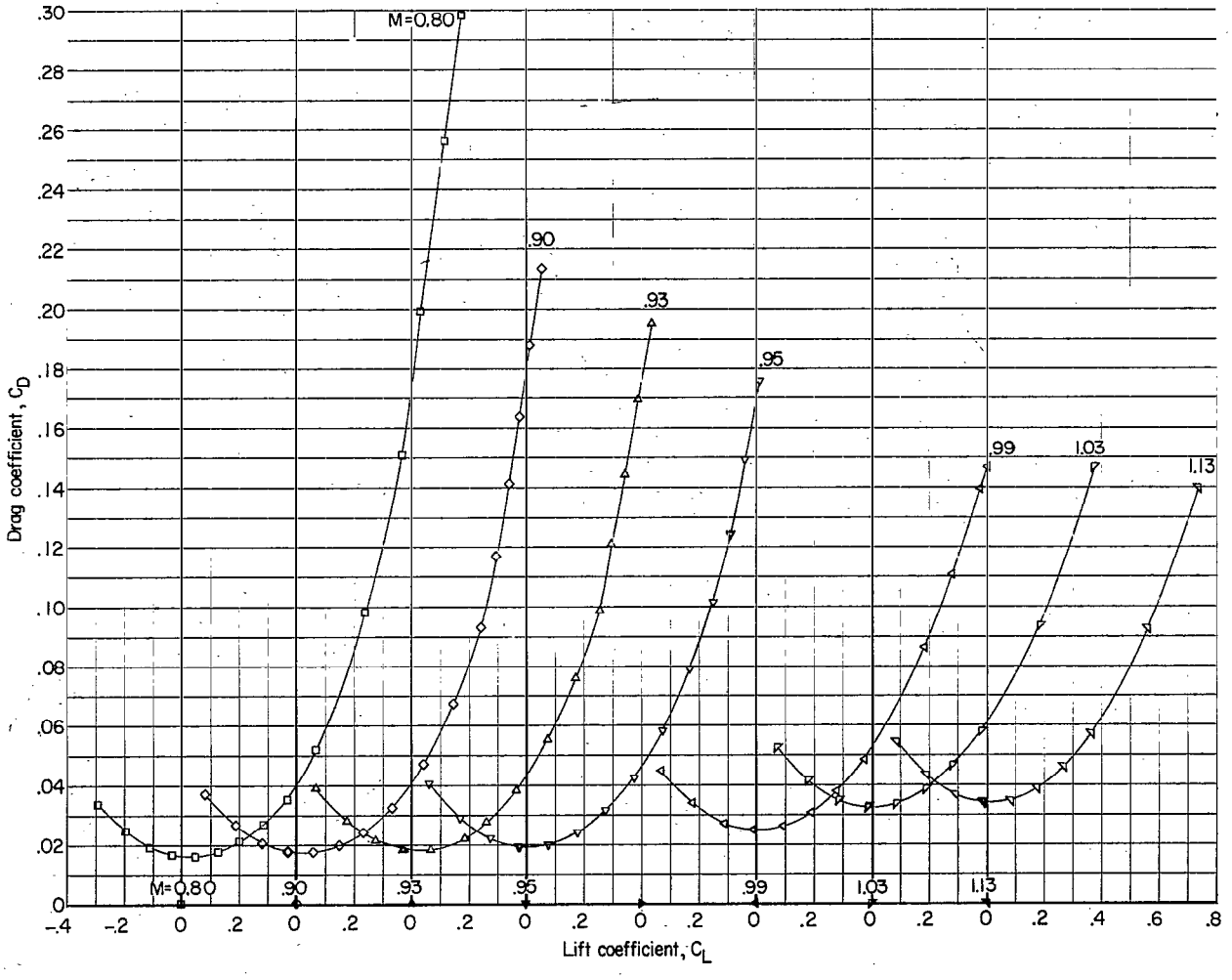

(b) Drag coefficient.

Figure 27.- Concluded.

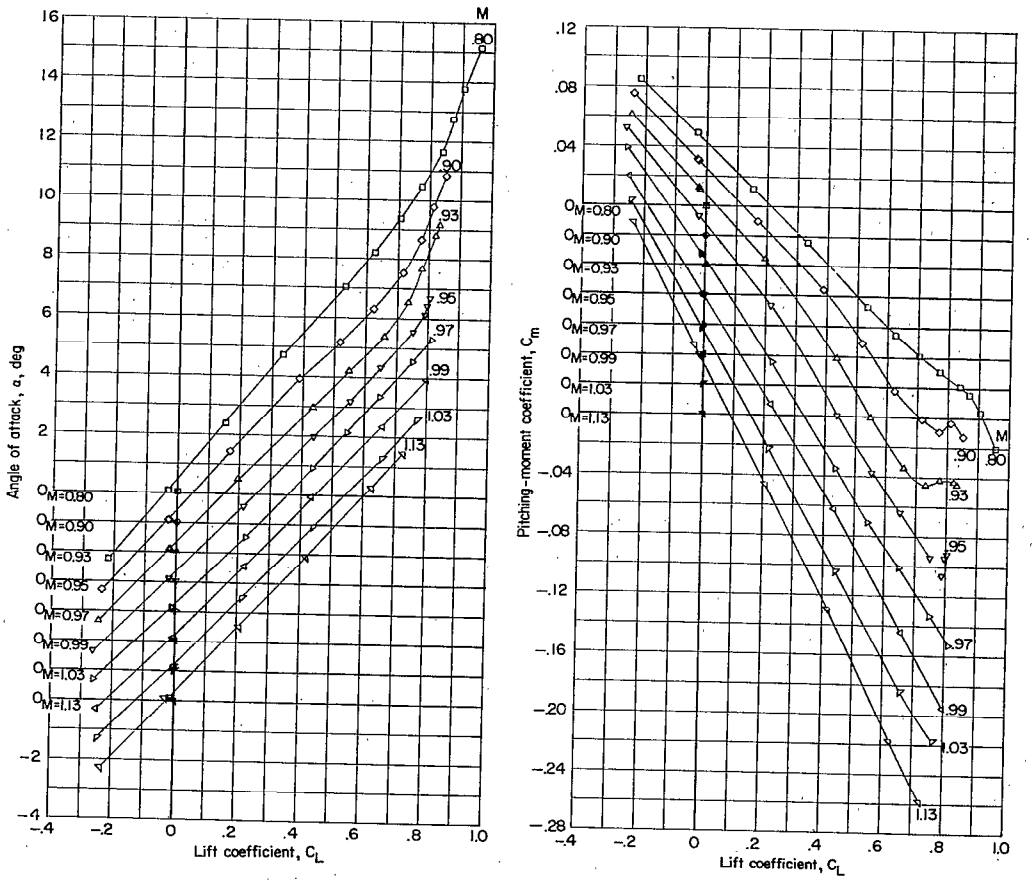

(a) Angle of attack and pitching-moment coefficient.

Figure 28.- Variation of aerodynamic characteristics with lift coefficient. Configuration 20; complete model; $i_t = -3^\circ$; $\delta_n = -7.5^\circ$; body with M = 1 bump; A = 3.69; drooped supersonic inlet (cruise condition).

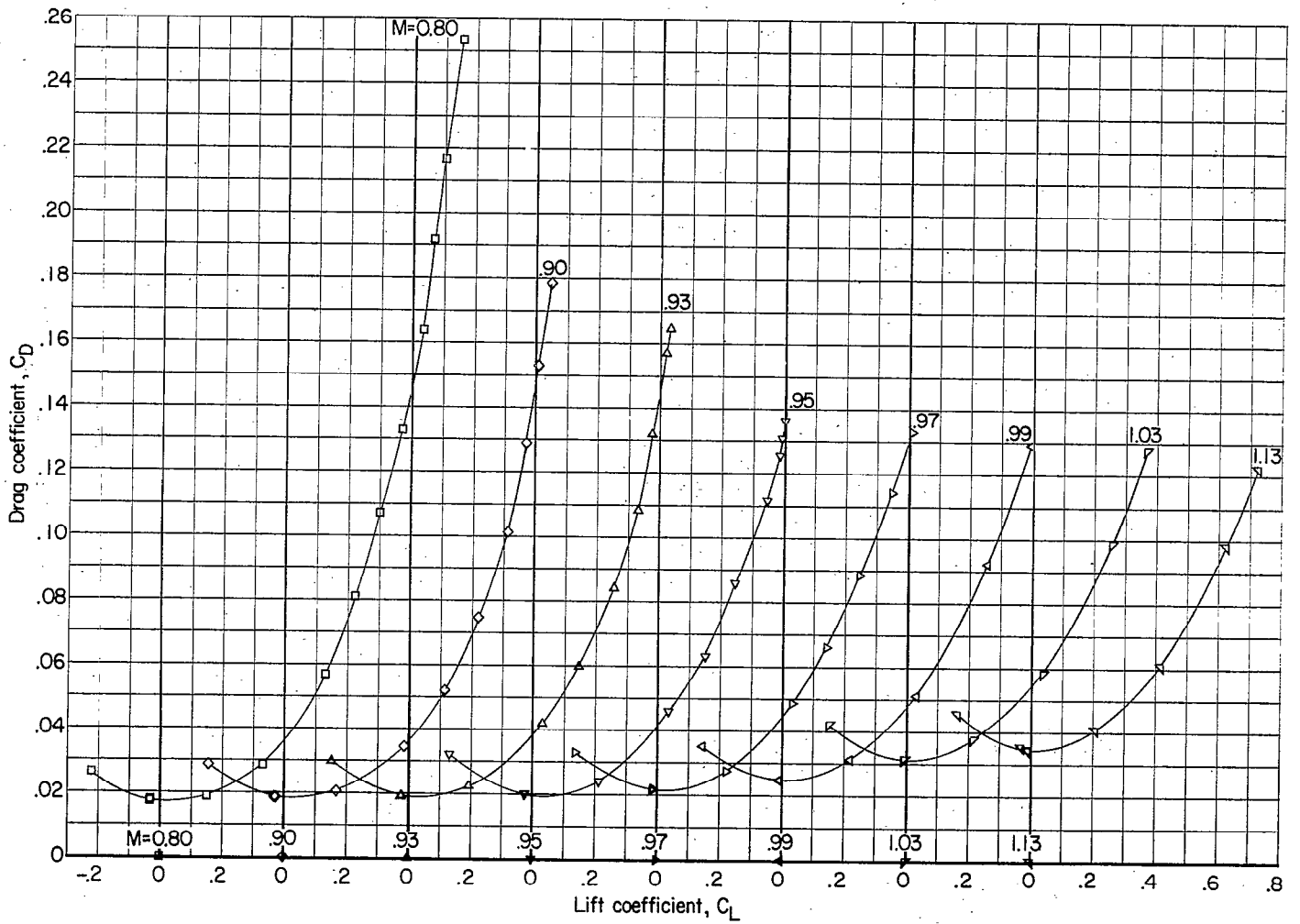

(b) Drag coefficient.

Figure 28.- Concluded.

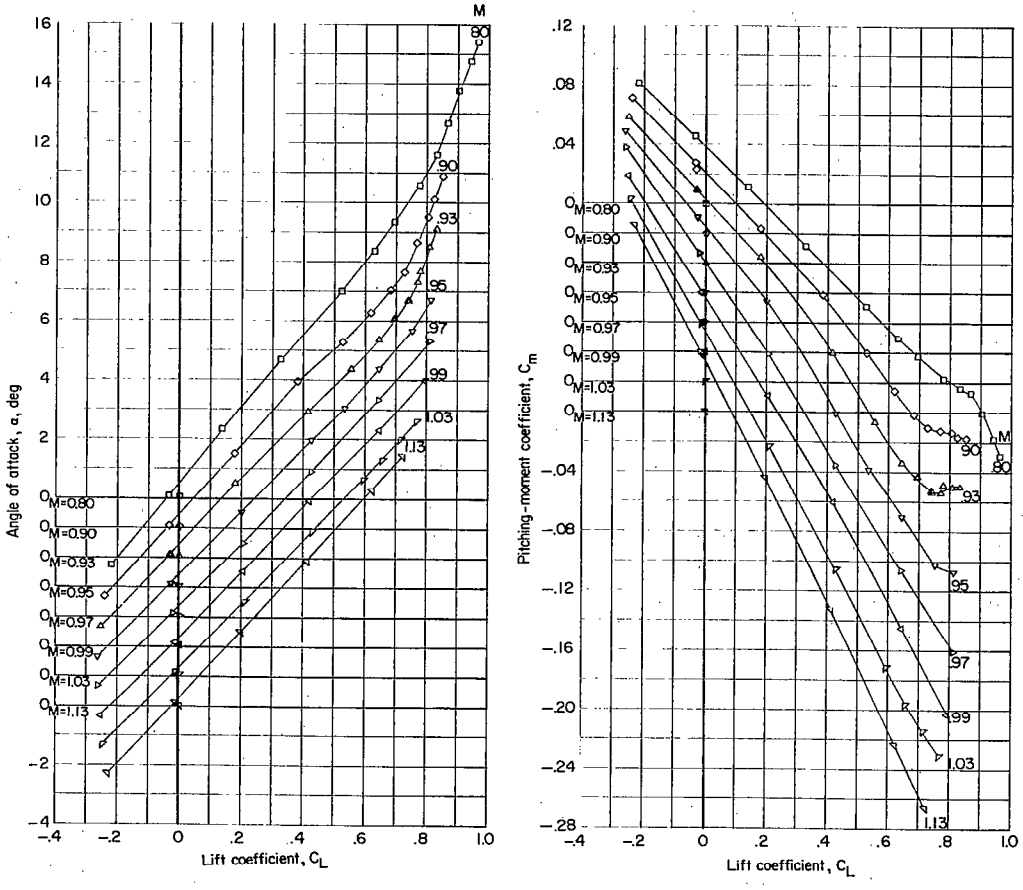

(a) Angle of attack and pitching-moment coefficient.

Figure 29.- Variation of aerodynamic characteristics with lift coefficient. Configuration 21; complete model; $i_t = -3°$; $\delta_n = -7.5°$; body with modified M = 1 bump; A = 3.69; drooped supersonic inlet (cruise condition).

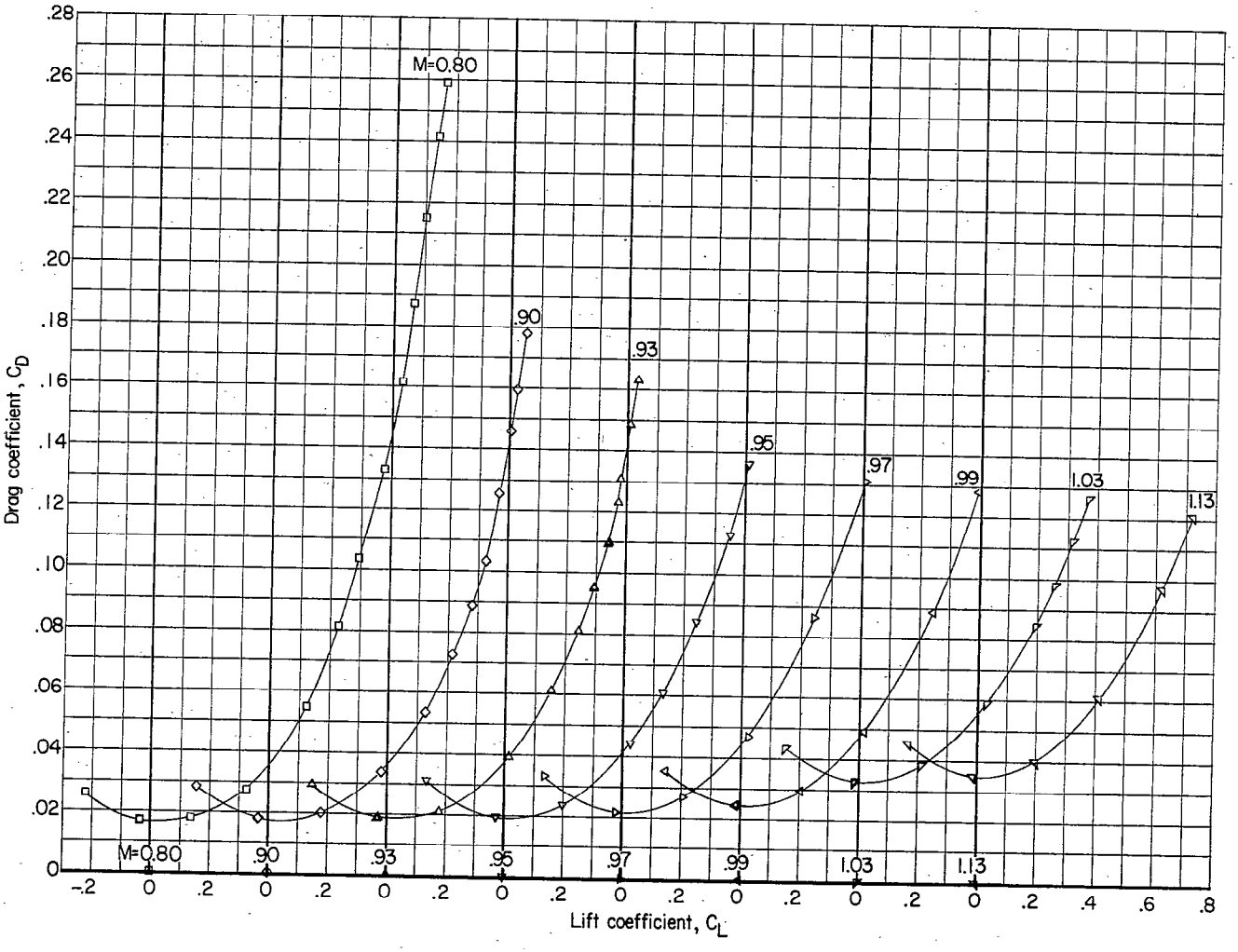

(b) Drag coefficient.

Figure 29.- Concluded.

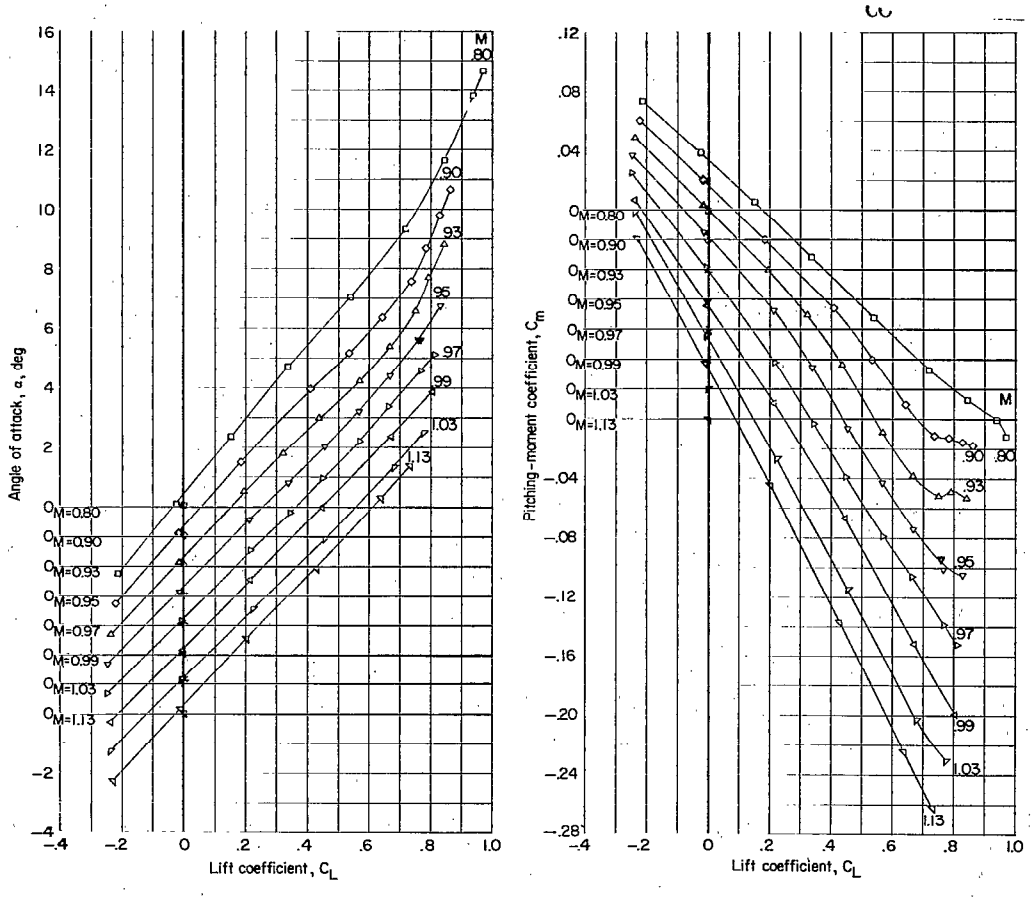

(a) Angle of attack and pitching-moment coefficient.

Figure 30.- Variation of aerodynamic characteristics with lift coefficient. Configuration 22; complete model; $i_t = -3^\circ$; $\delta_n = -7.5^\circ$; body with modified M = 1 bump; A = 3.69; wing modification 2; drooped supersonic inlet (cruise condition).

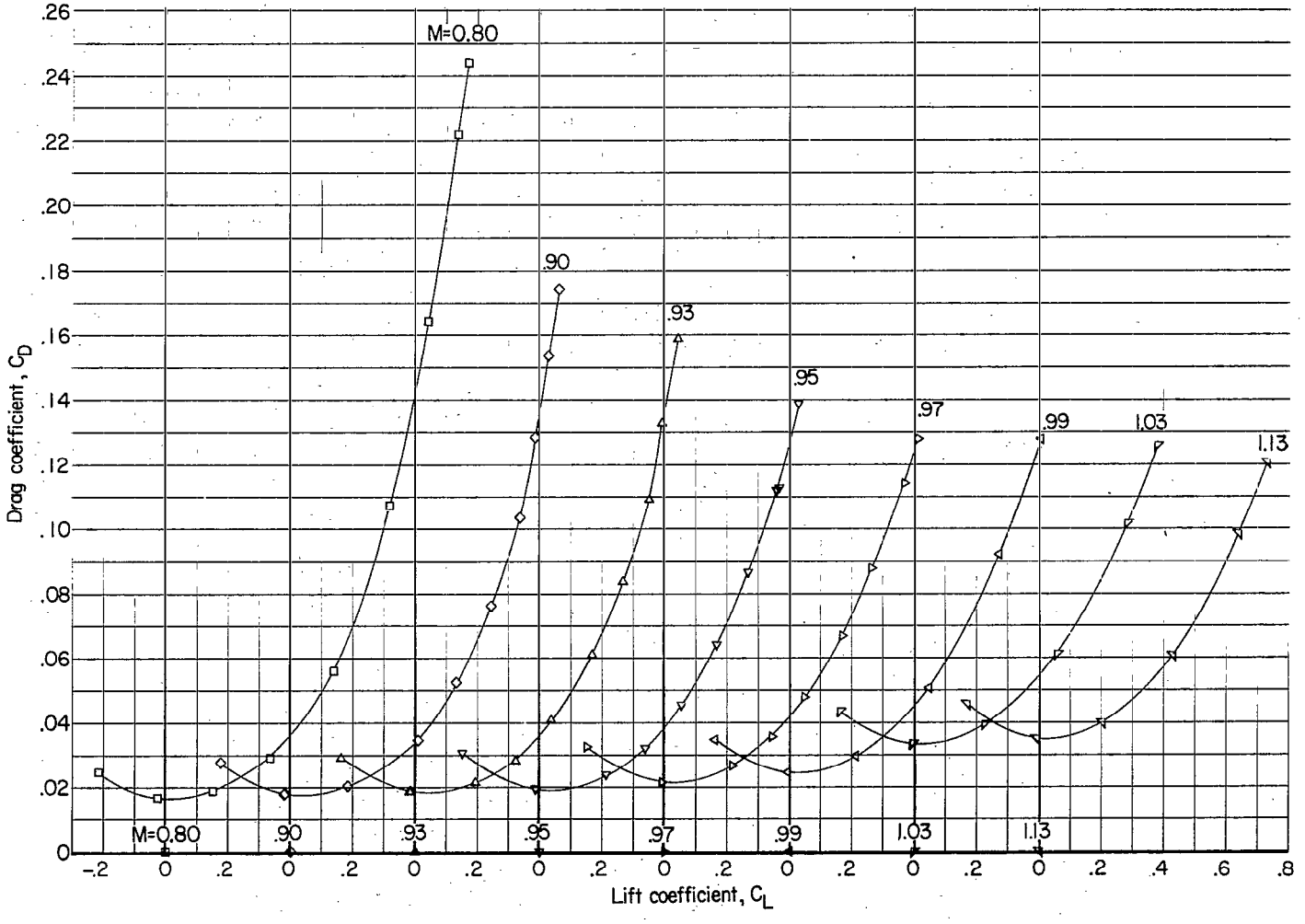

(b) Drag coefficient.

Figure 30.- Concluded.

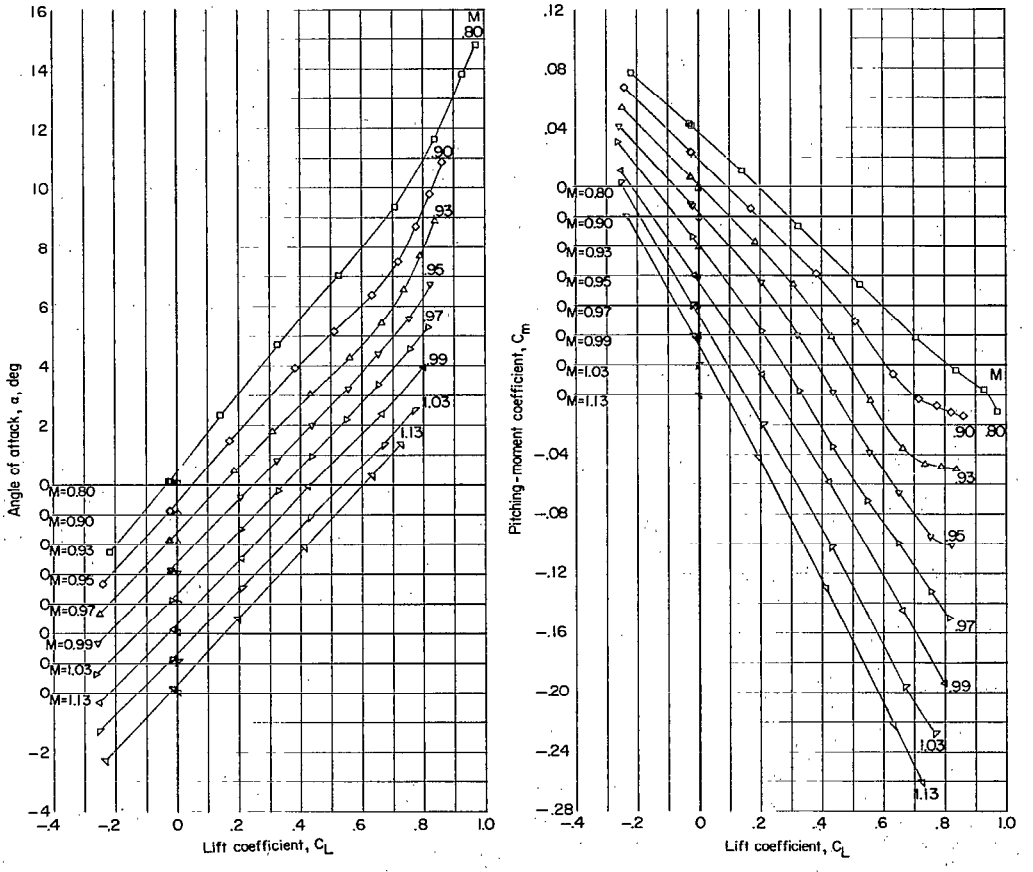

(a) Angle of attack and pitching-moment coefficient.

Figure 31.- Variation of aerodynamic characteristics with either lift coefficient or angle of attack. Configuration 23; complete model; $i_t = -3^\circ$; $\delta_n = -7.5^\circ$; body with modified M = 1 bump; A = 3.69; wing modification 2; drooped supersonic inlet (cruise condition) with inlet modification 1.

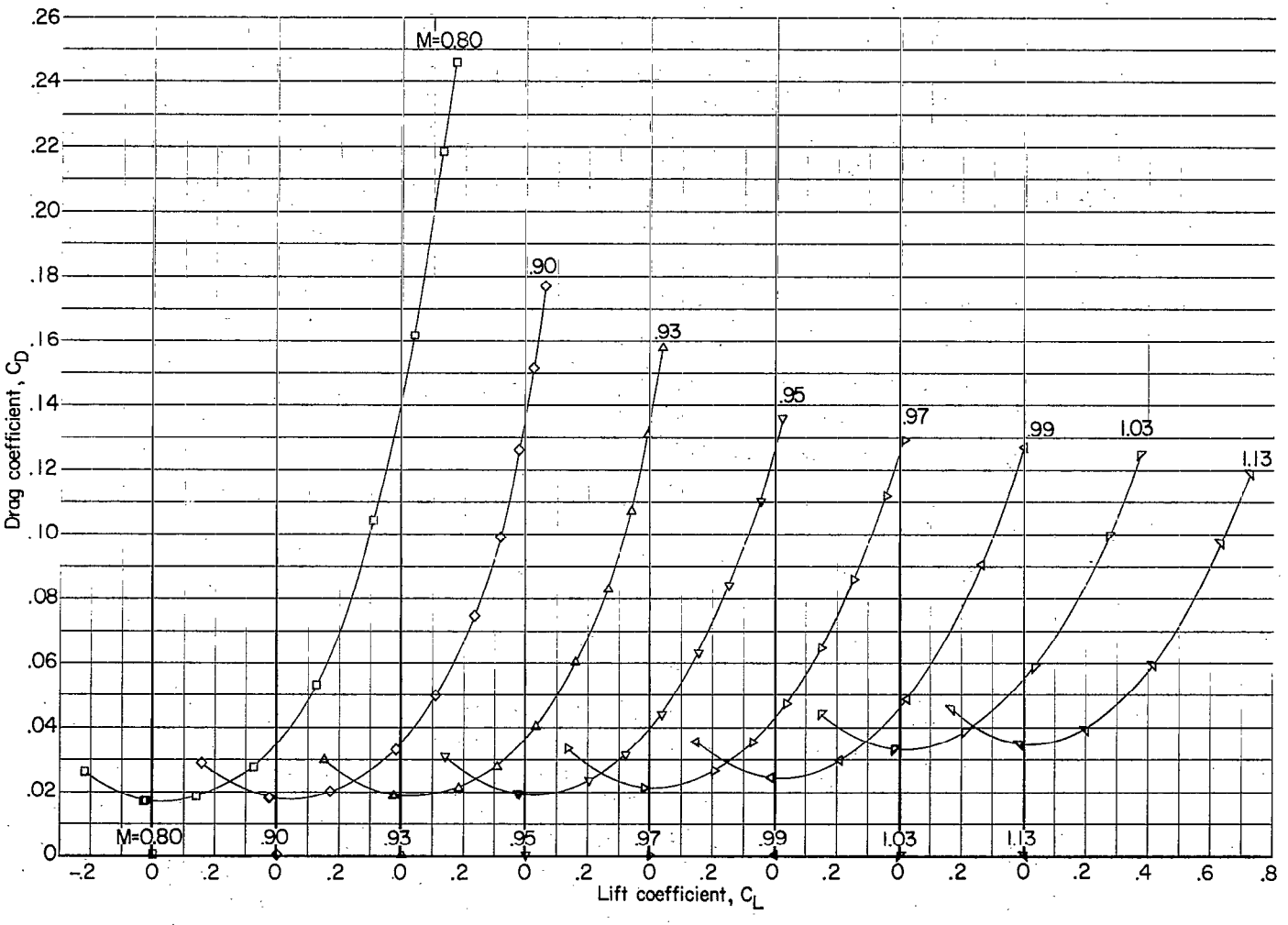

(b) Drag coefficient.

Figure 31.- Continued.

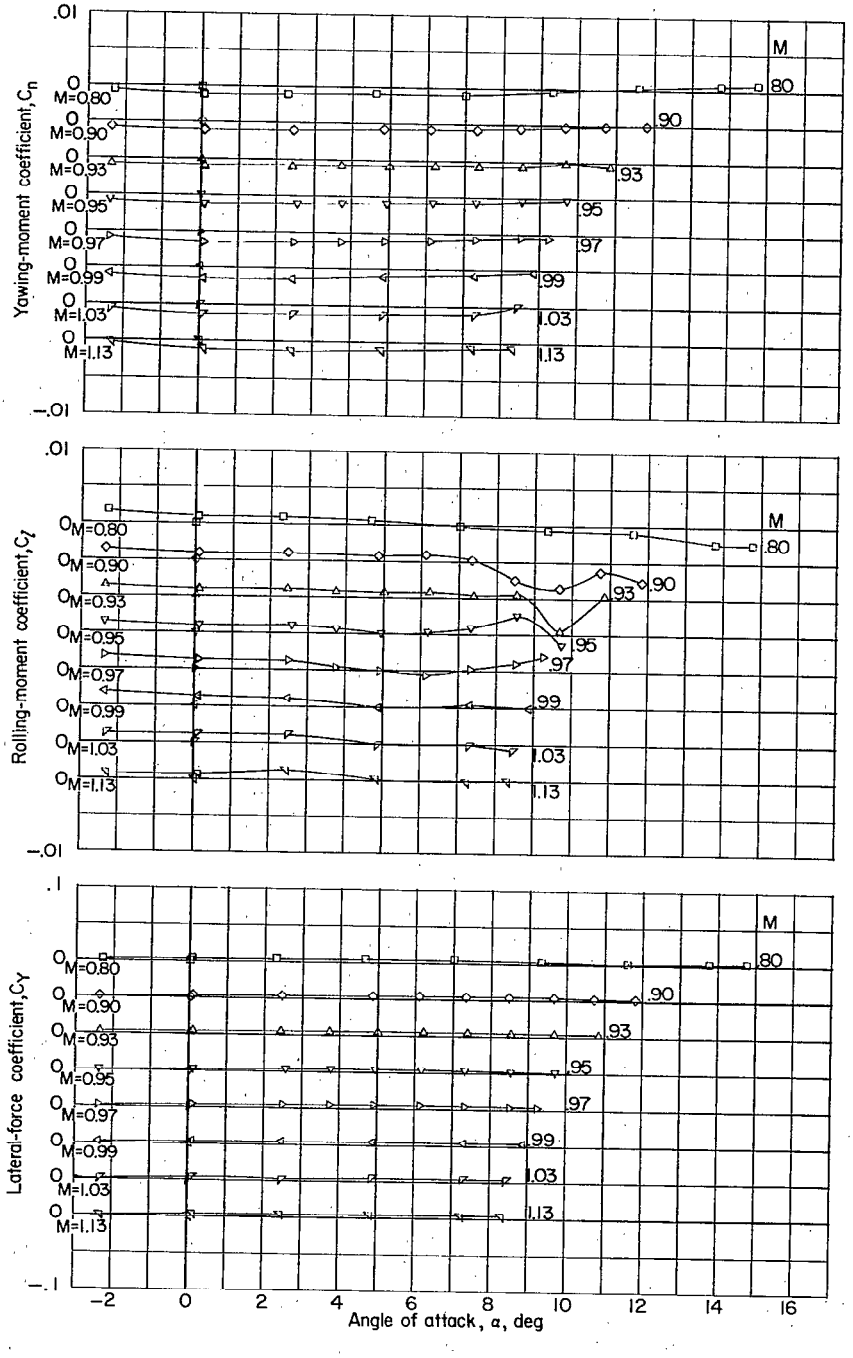

(c) Yawing-moment, rolling-moment, and lateral-force coefficients.

Figure 31.- Concluded.

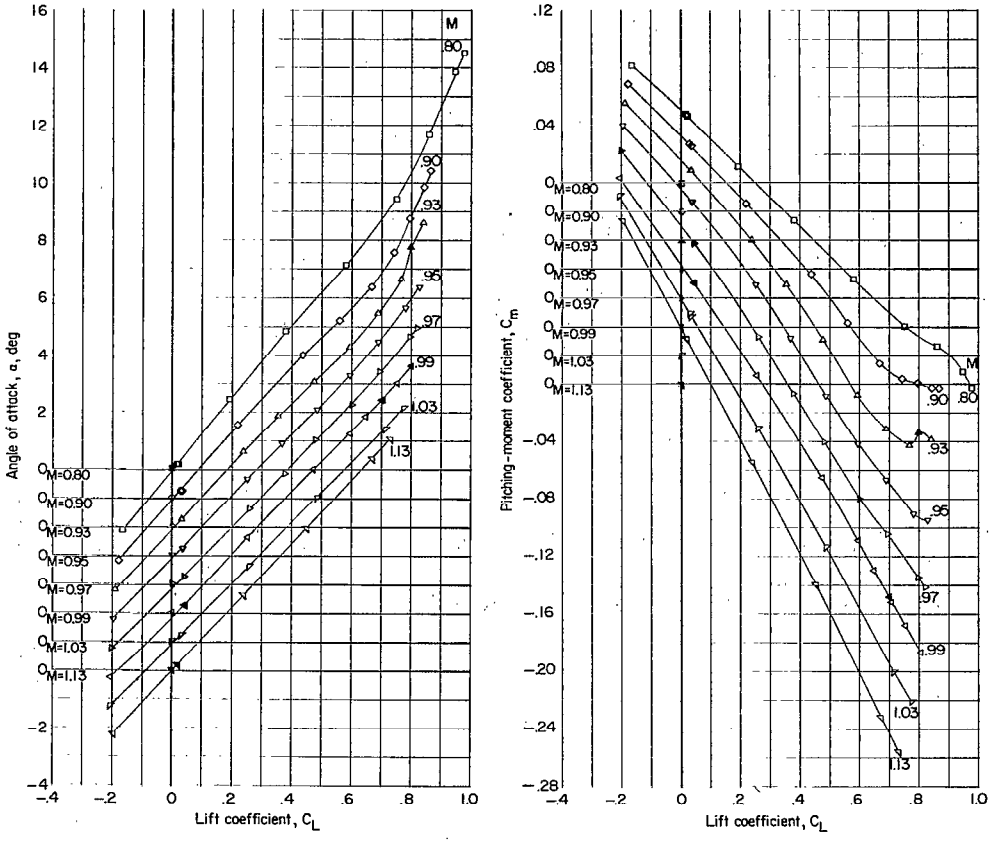

(a) Angle of attack and pitching-moment coefficient.

Figure 32.- Variation of aerodynamic characteristics with either lift coefficient or angle of attack. Configuration 24; complete model; $i_t = -3^\circ$; $\delta_n = -7.5^\circ$; $\delta_f = 5^\circ$; body with modified M = 1 bump; A = 3.69; wing modification 2; drooped supersonic inlet (cruise condition) with inlet modification 1.

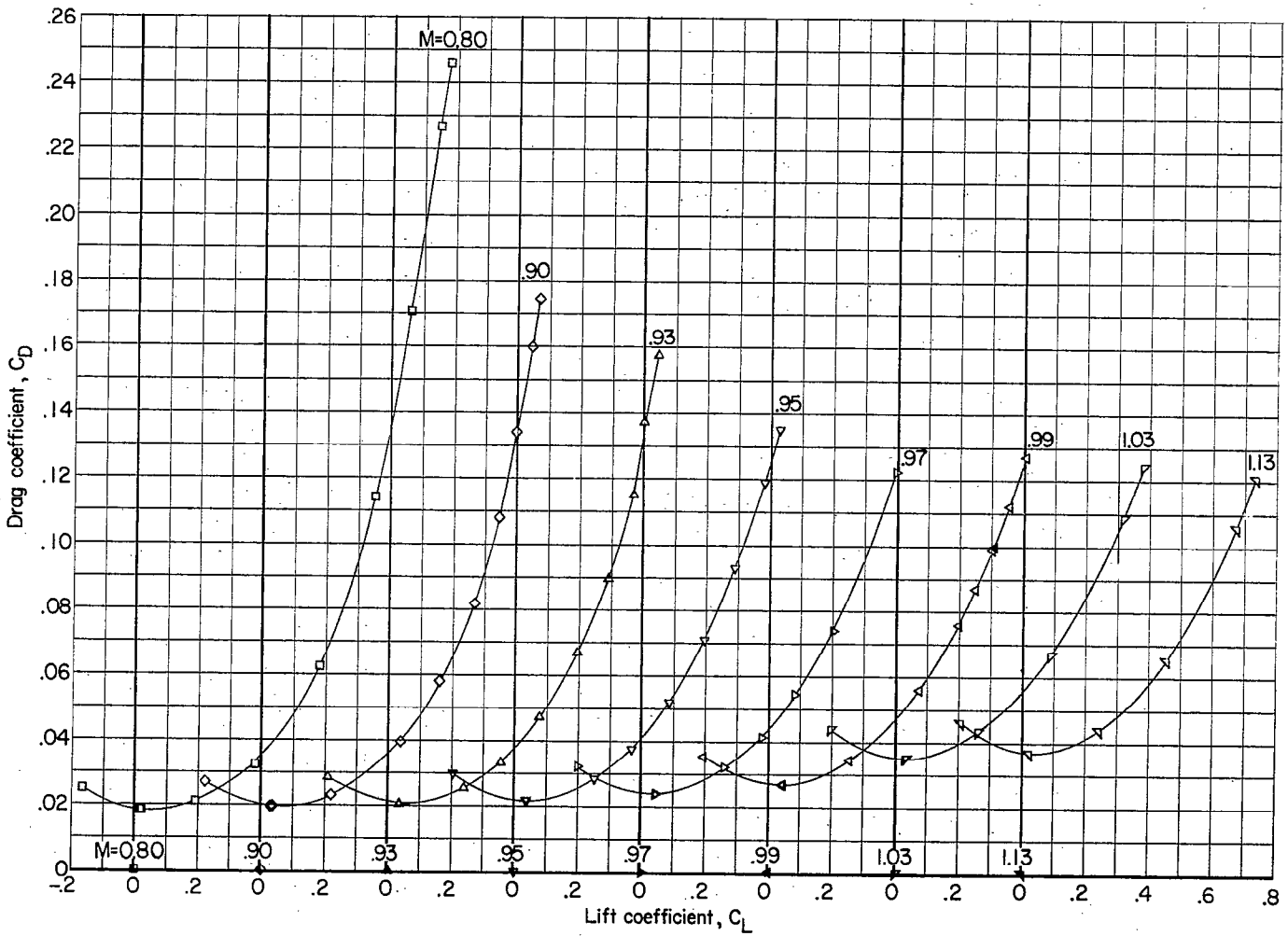

(b) Drag coefficient.

Figure 32.- Continued.

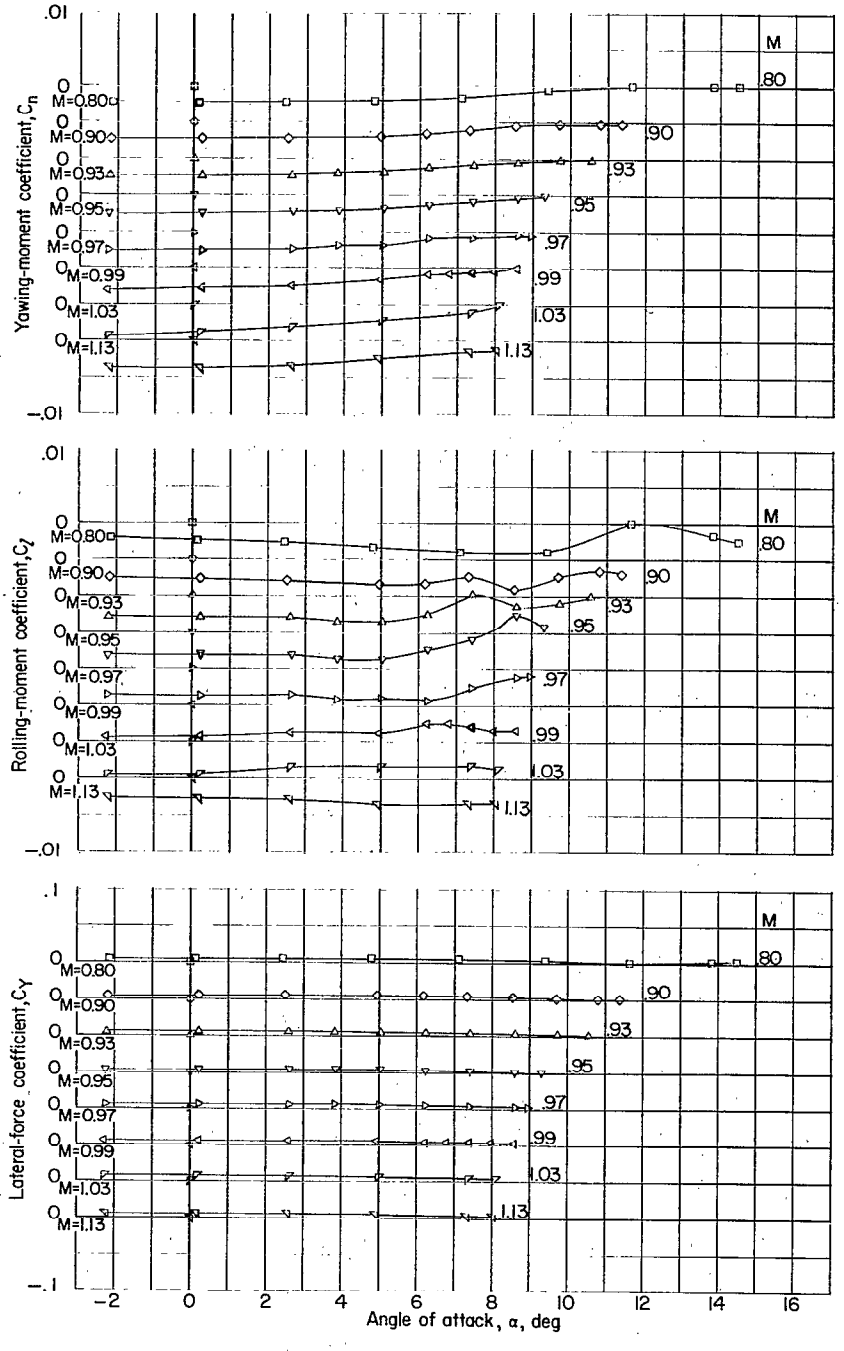

(c) Yawing-moment, rolling-moment, and lateral-force coefficients.

Figure 32.- Concluded.

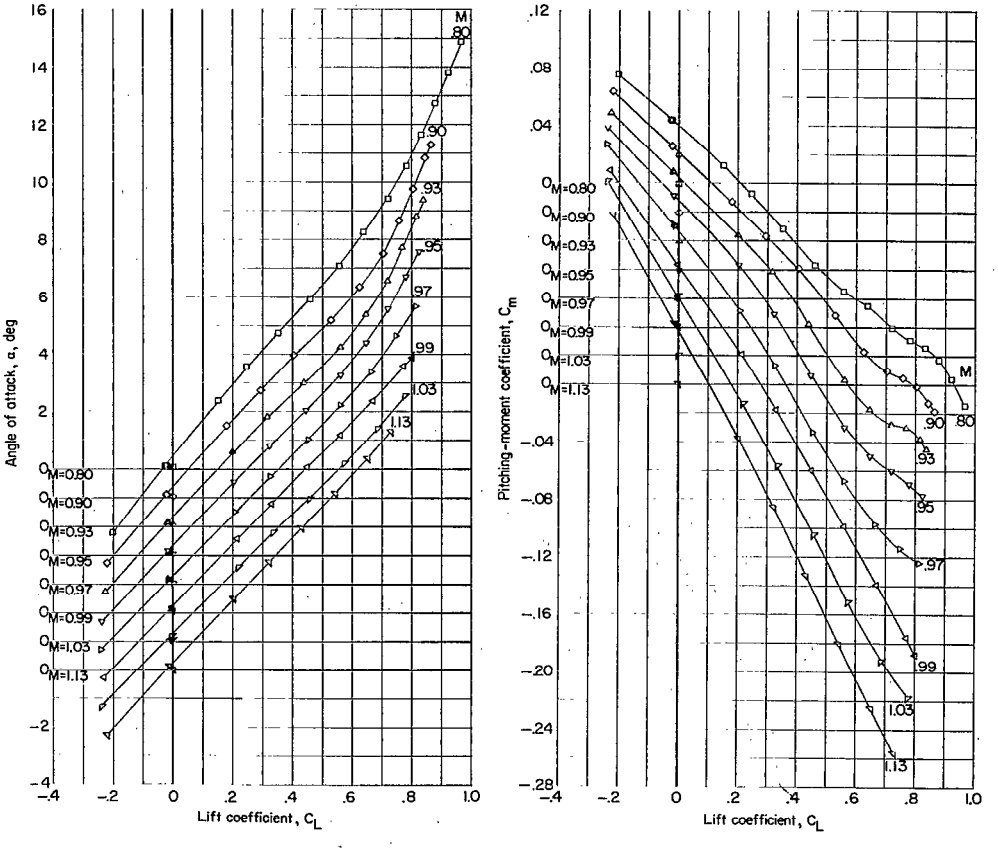

(a) Angle of attack and pitching-moment coefficient.

Figure 33.- Variation of aerodynamic characteristics with either lift coefficient or angle of attack. Configuration 25; complete model; $i_t = -3^\circ$; body with modified M = 1 bump; A = 3.69; wing modification 3; drooped supersonic inlet (cruise condition) with inlet modification 1.

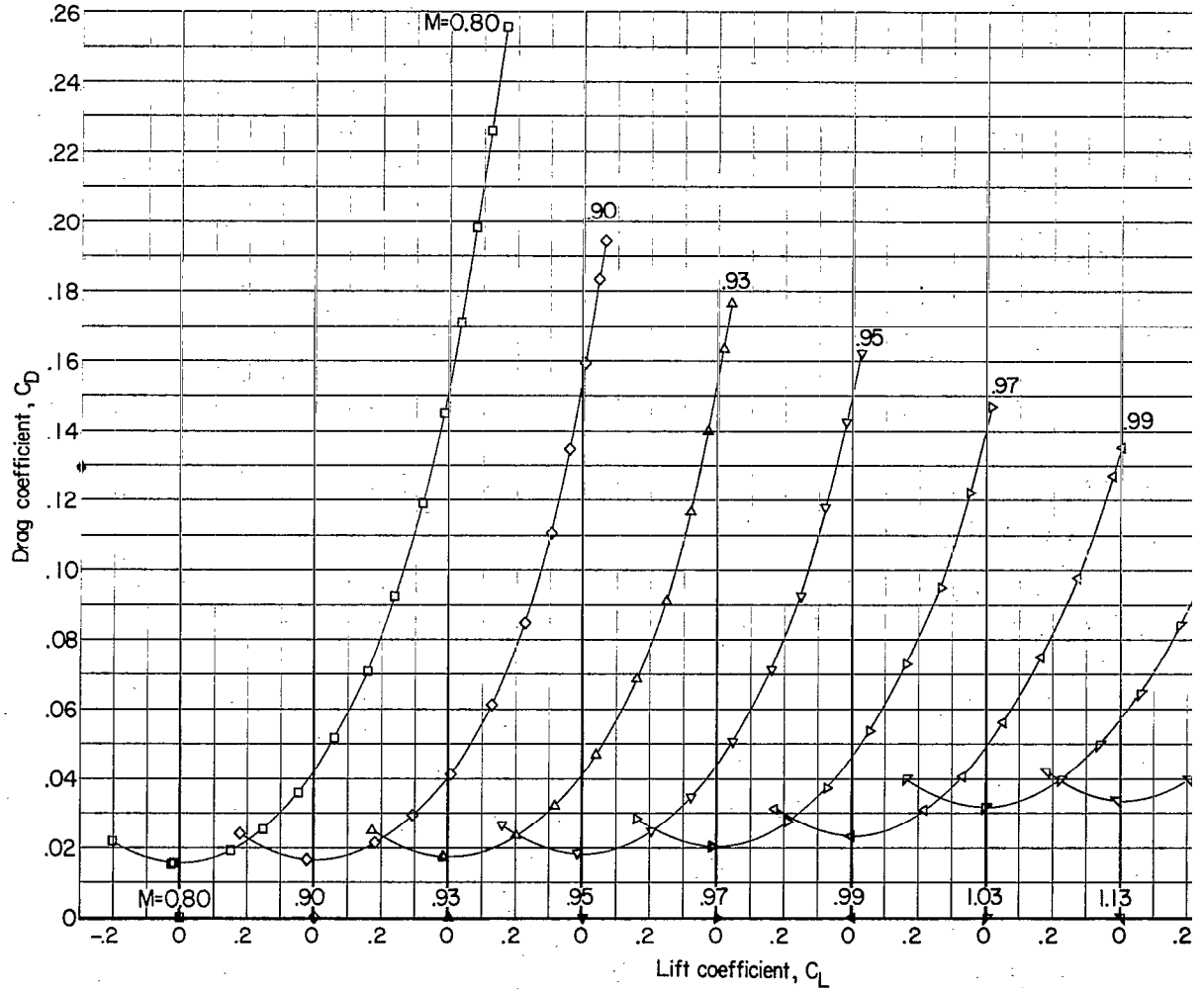

(b) Drag coefficient.

Figure 33.- Continued.

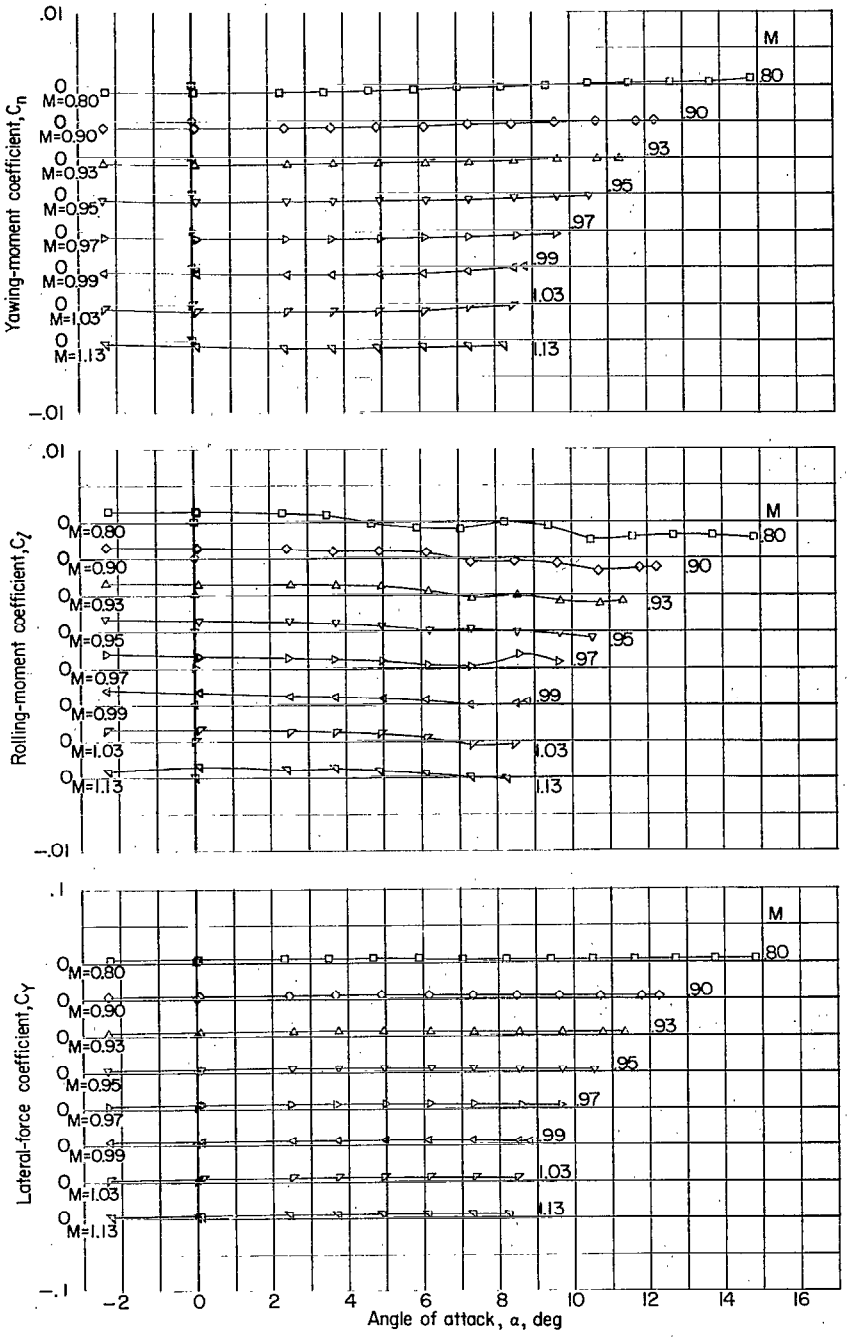

(c) Yawing-moment, rolling-moment, and lateral-force coefficients.

Figure 33.- Concluded.

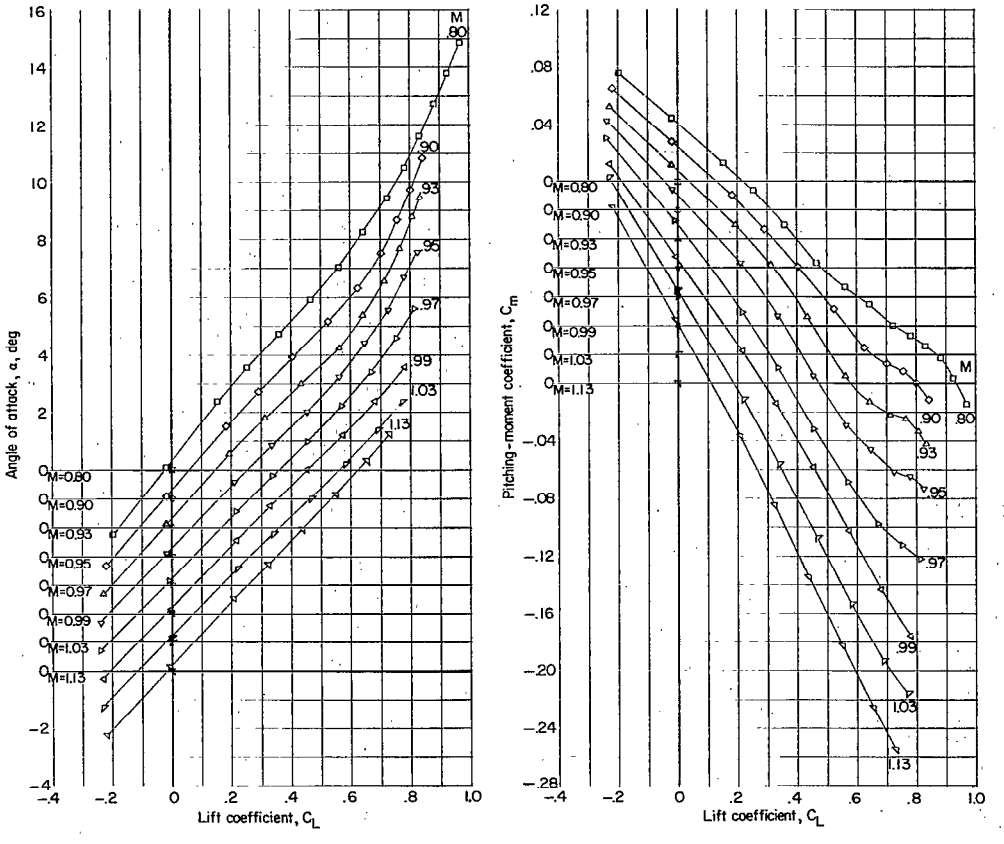

(a) Angle of attack and pitching-moment coefficient.

Figure 34.- Variation of aerodynamic characteristics with either lift coefficient or angle of attack. Configuration 26; complete model; $i_t = -3^\circ$; $\delta_r = 6^\circ$; body with modified M = 1 bump; A = 3.69; wing modification 3; drooped supersonic inlet (cruise condition) with inlet modification 1.

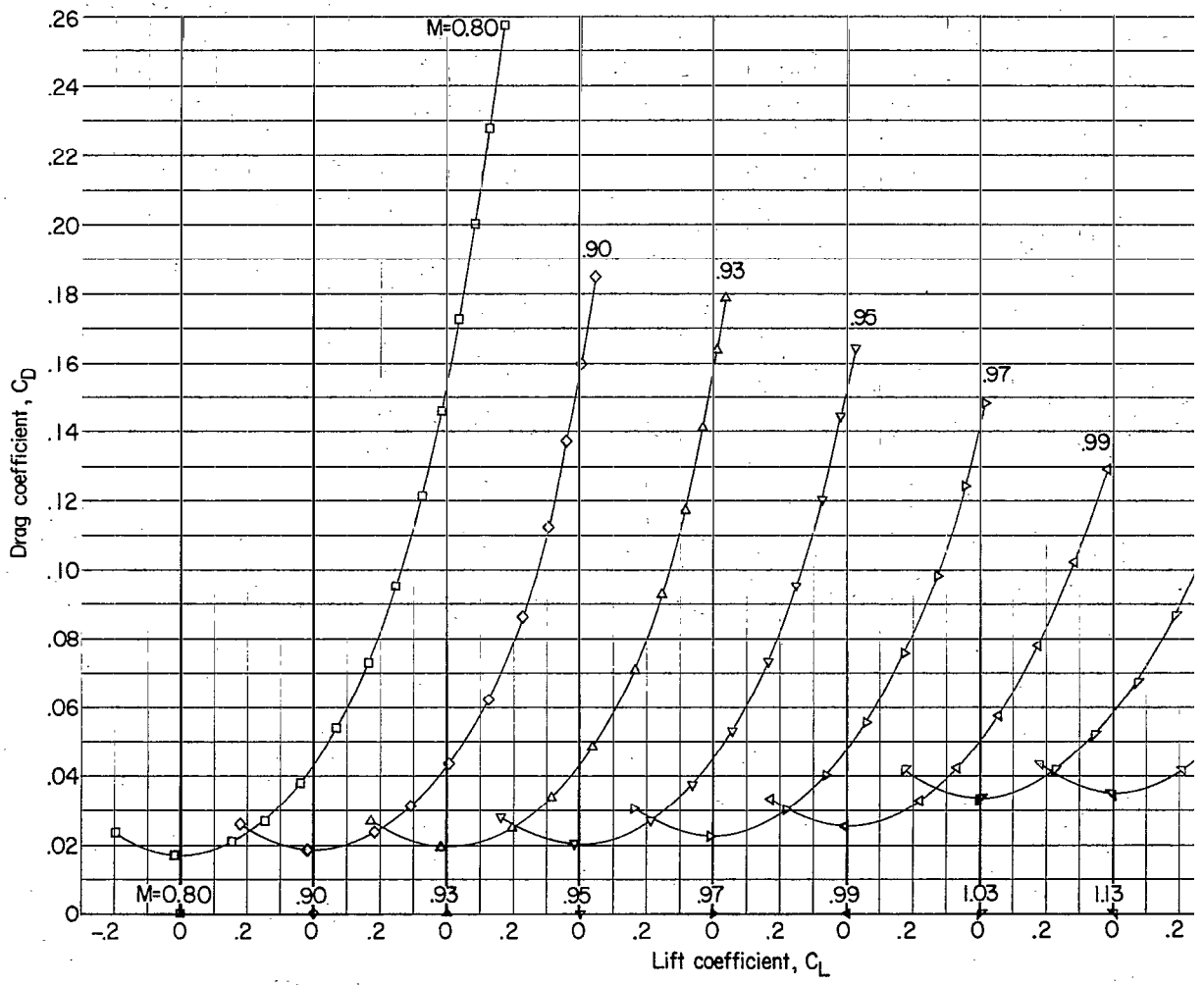

(b) Drag coefficient.

Figure 34.- Continued.

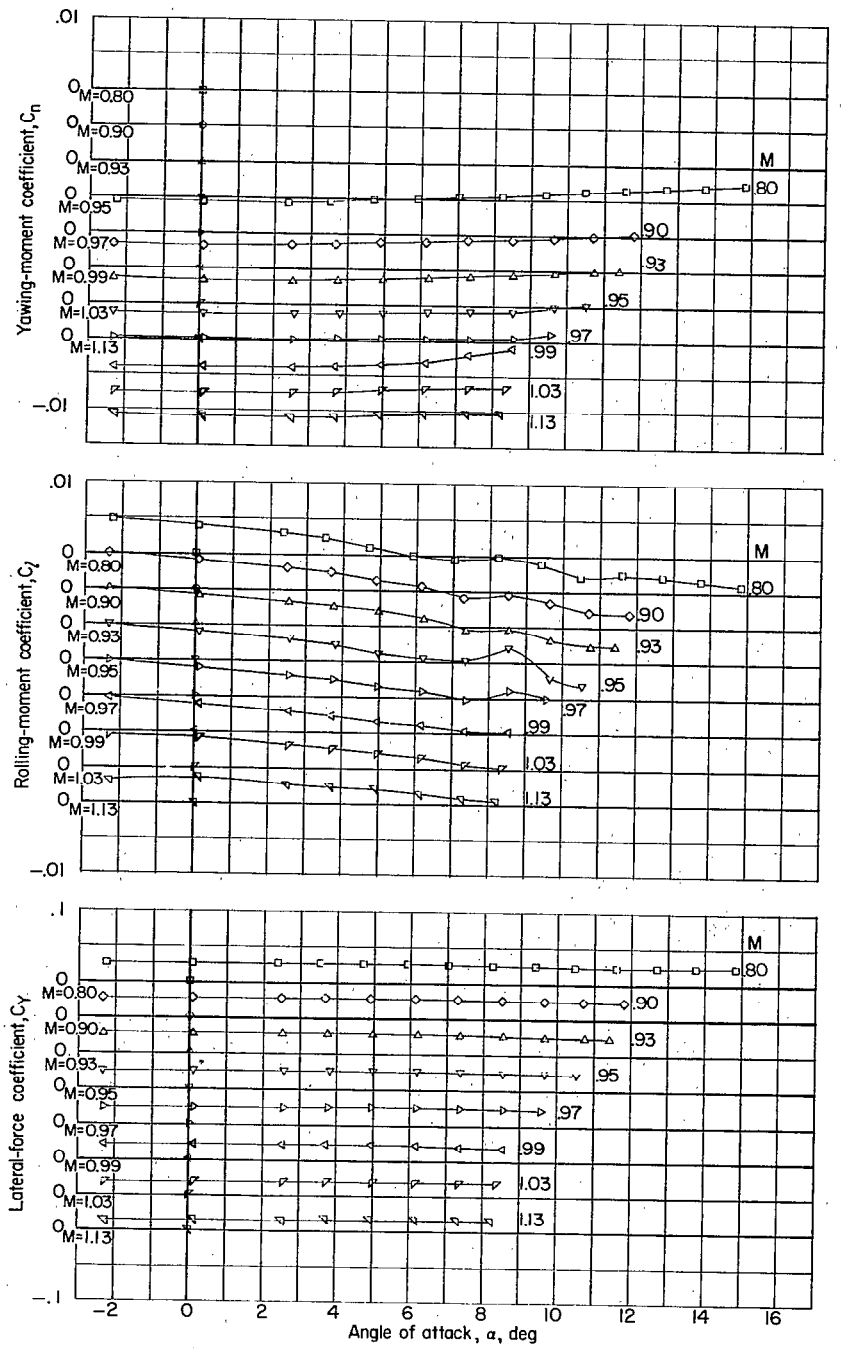

(c) Yawing-moment, rolling-moment, and lateral-force coefficients.

Figure 34.- Concluded.

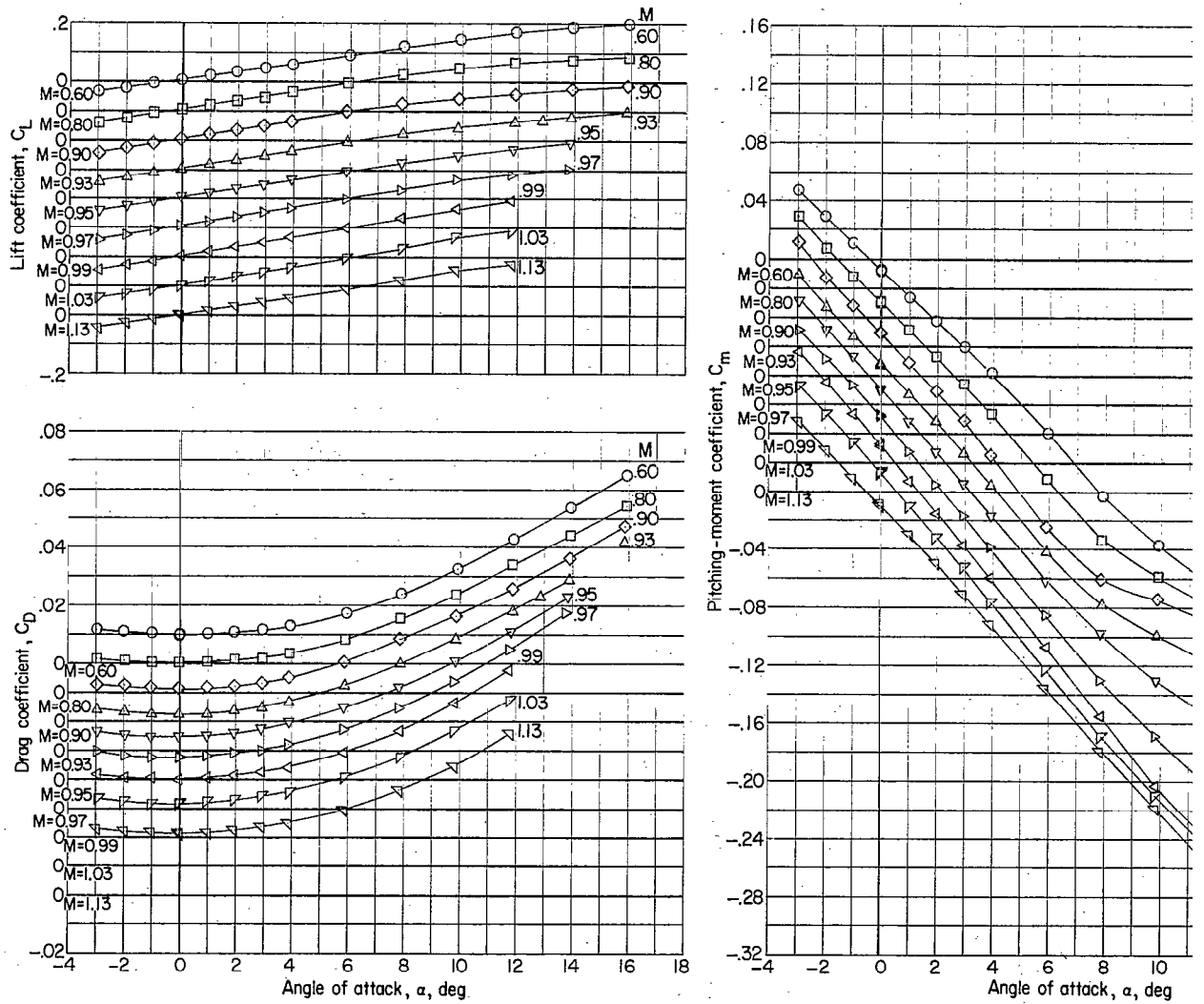

Figure 35.- Variation of aerodynamic characteristics with angle of at
Configuration 27; complete model less wing; $i_t = 0^o$.

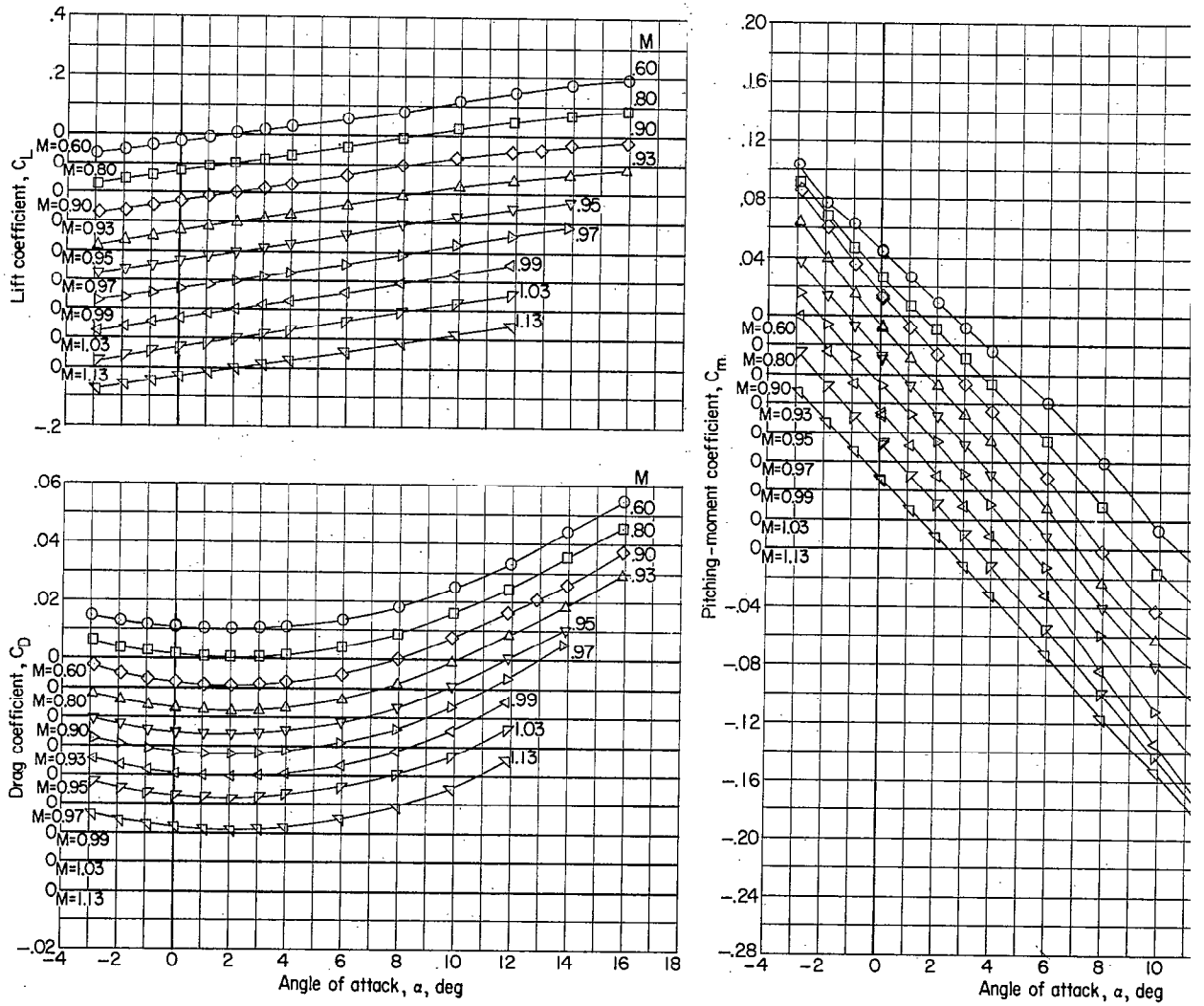

Figure 36.- Variation of aerodynamic characteristics with angle of atta
Configuration 28; complete model less wing; $i_t = -3^\circ$.

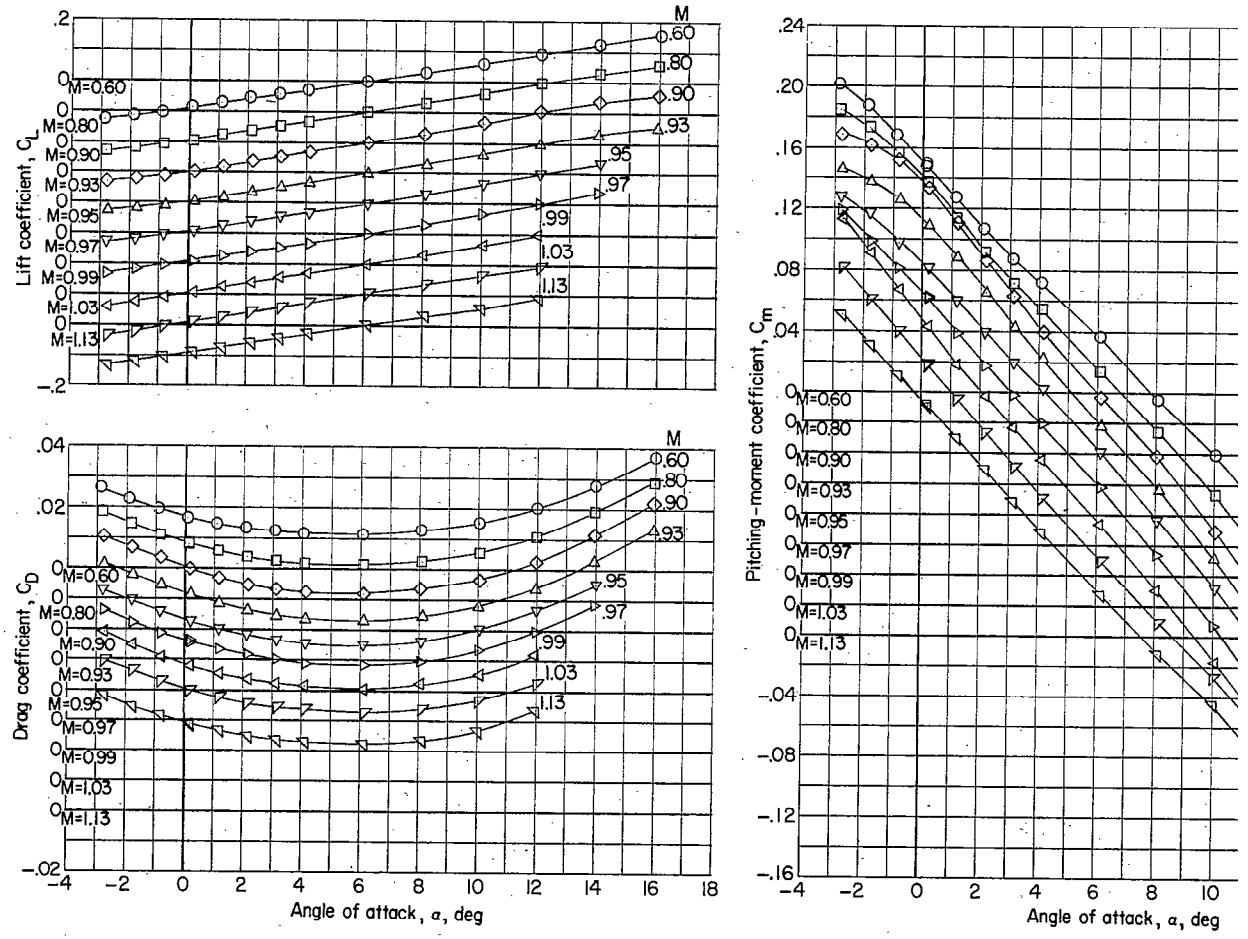

Figure 37.- Variation of aerodynamic characteristics with angle of att
Configuration 29; complete model less wing; $i_t = -8^o$.

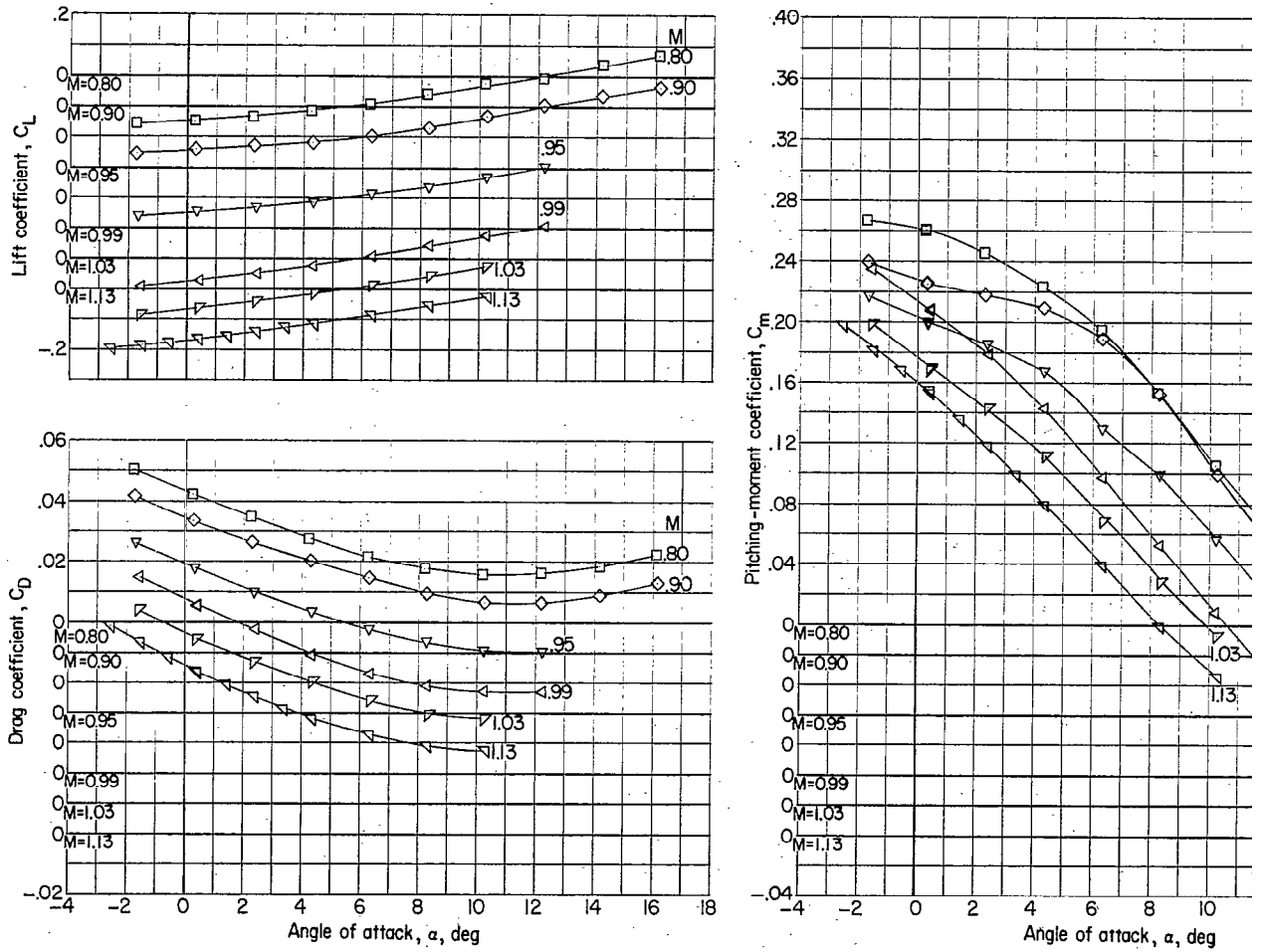

Figure 38.- Variation of aerodynamic characteristics with angle of atta
Configuration 30; complete model less wing; $i_t = -16^\circ$.

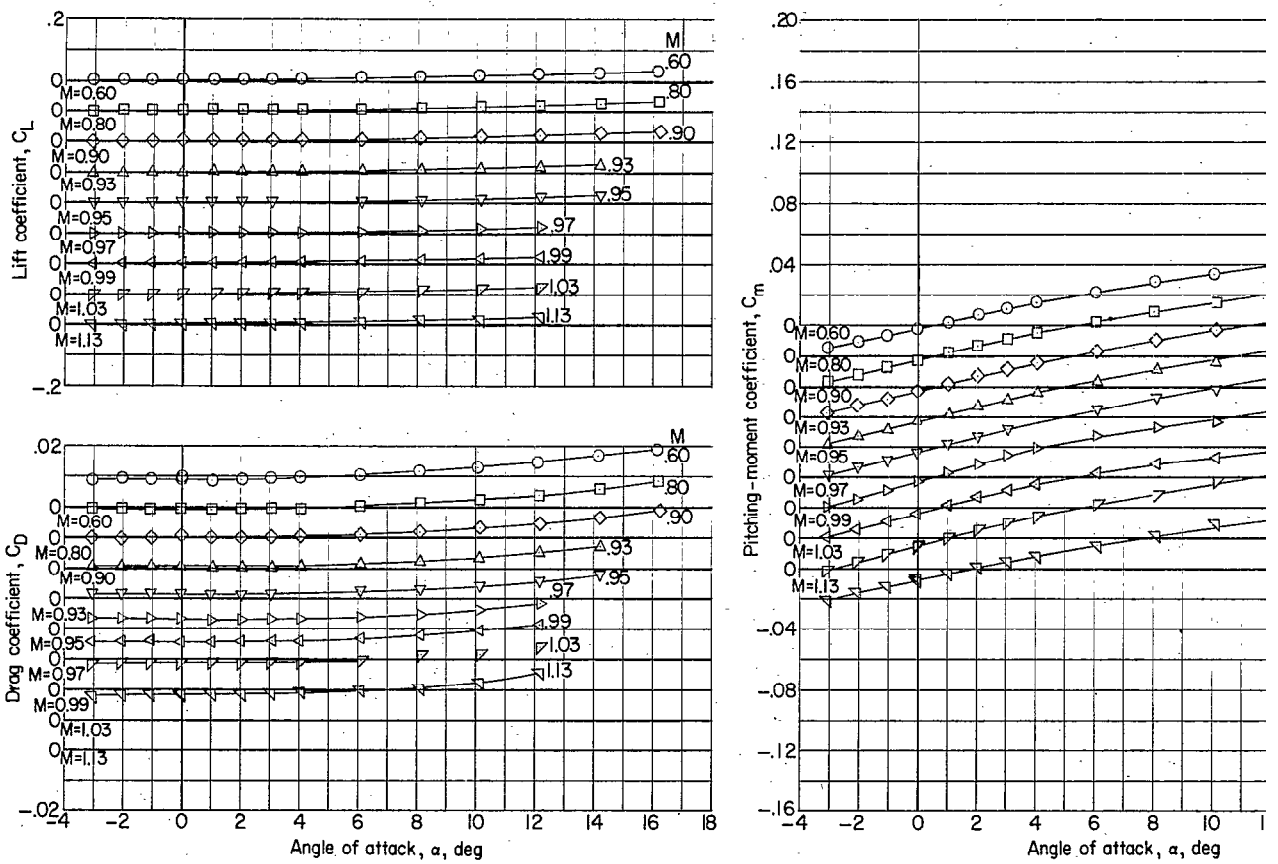

Figure 39.- Variation of aerodynamic characteristics with angle of attack Configuration 31; complete model less wing and less horizontal tail.

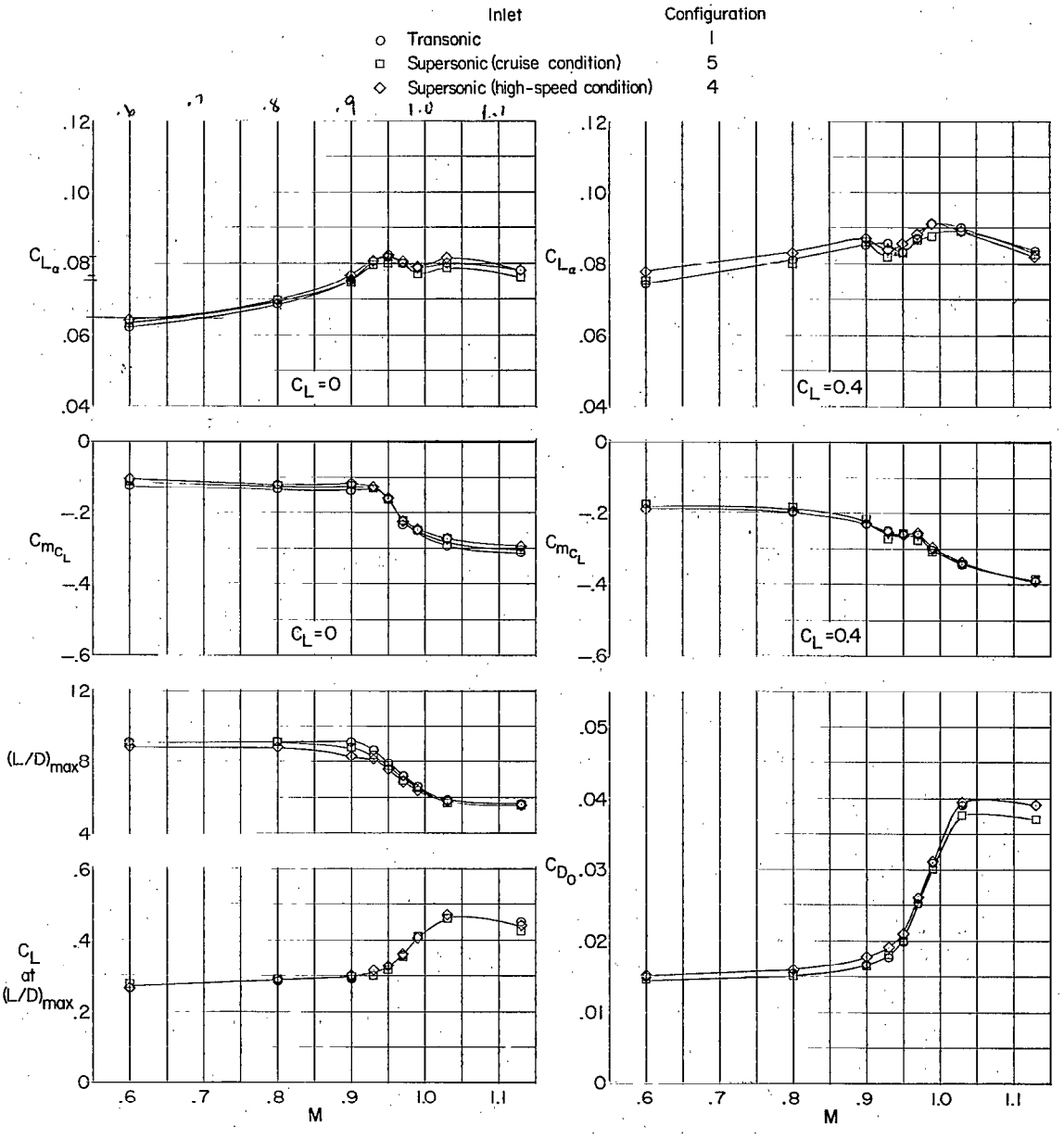

(a) Complete model; $i_t = -3^\circ$.

Figure 40.- Effect of inlet design on aerodynamic characteristics. Complete model and complete model less horizontal tail; A = 3.18.

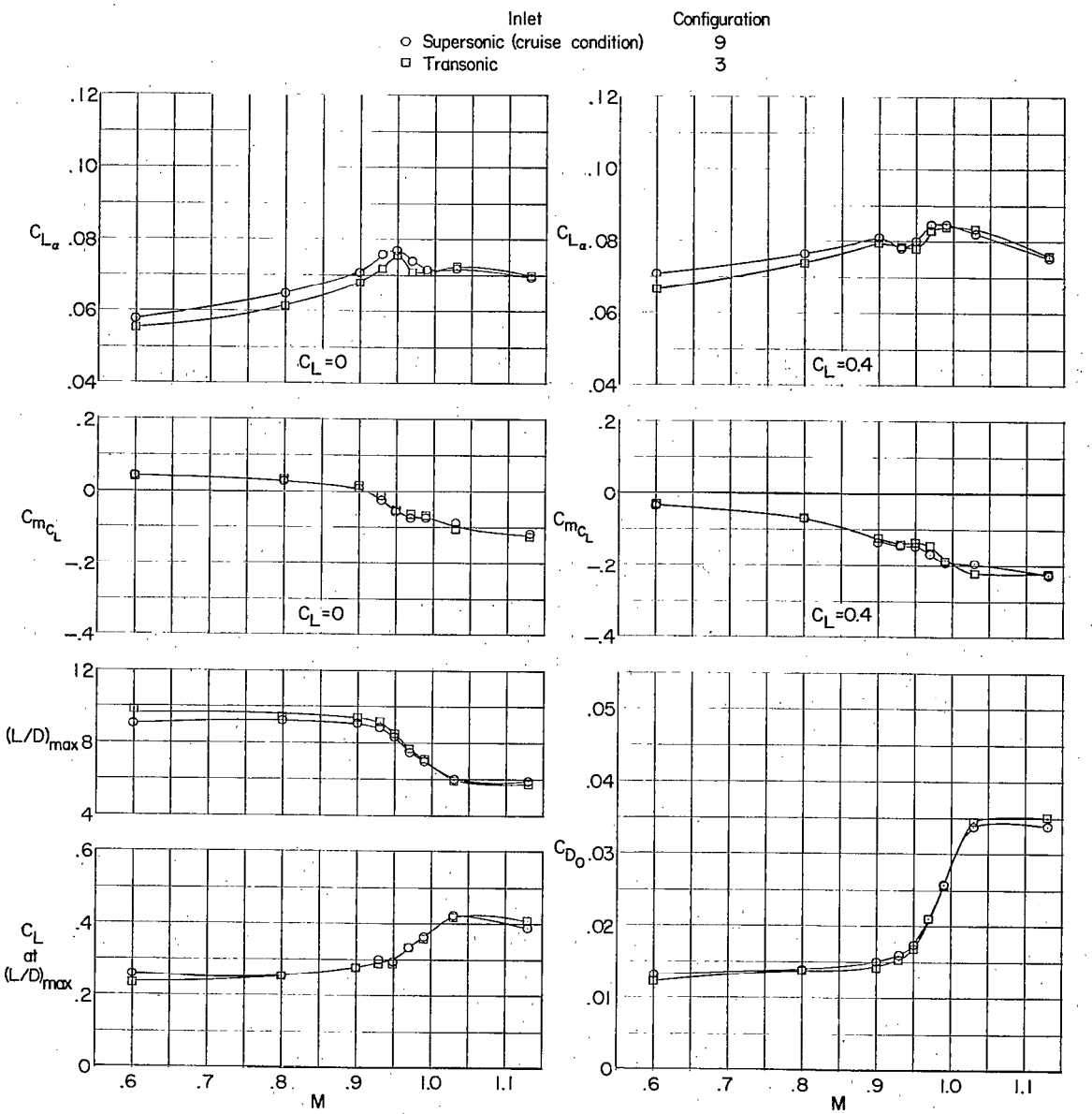

(b) Complete model less horizontal tail.

Figure 40.- Concluded.

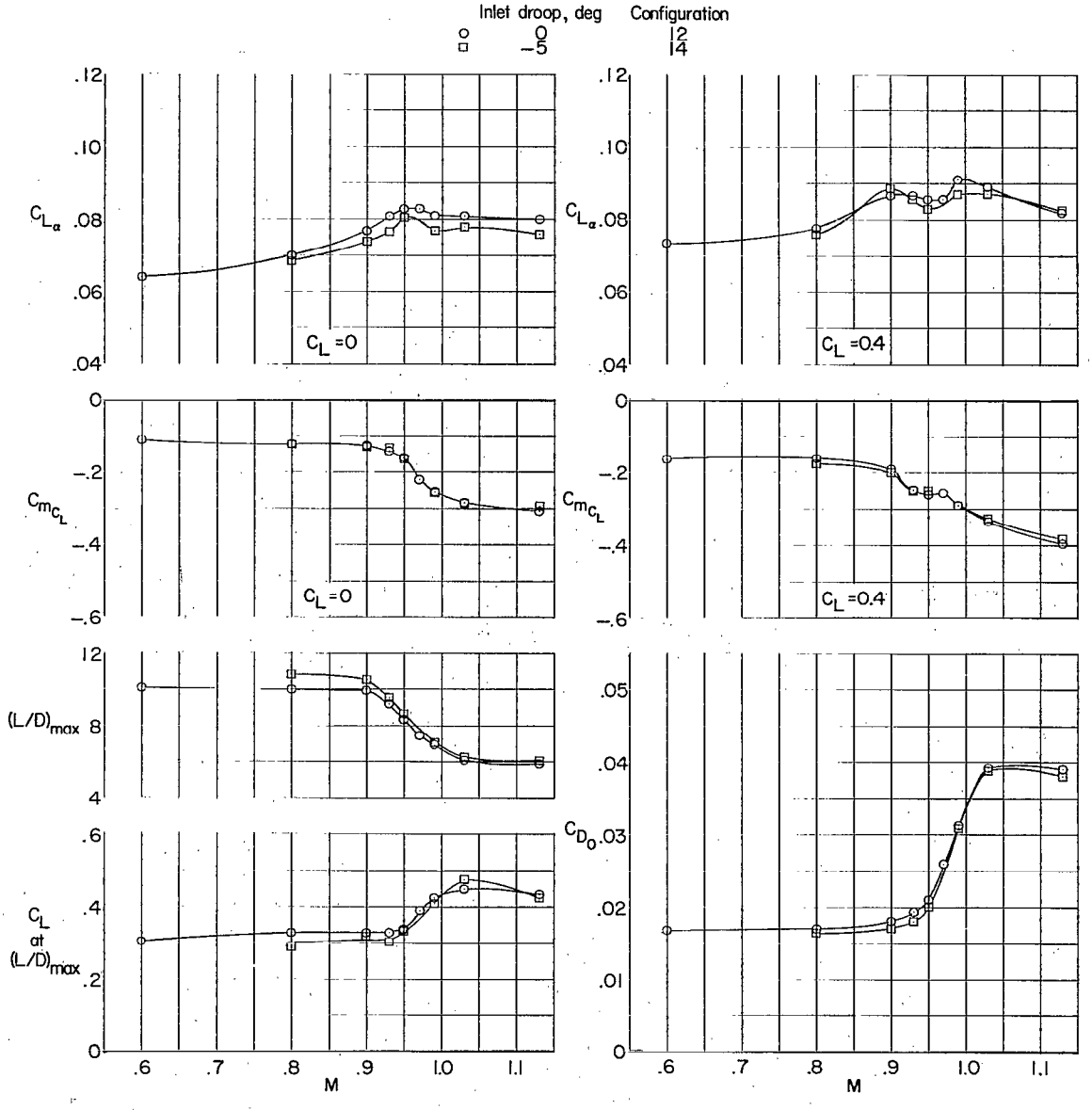

Figure 41.- Effect of inlet droop on aerodynamic characteristics. Complete model; $i_t = -3^\circ$; $\delta_n = -7.5^\circ$; A = 3.18; supersonic inlet (cruise condition).

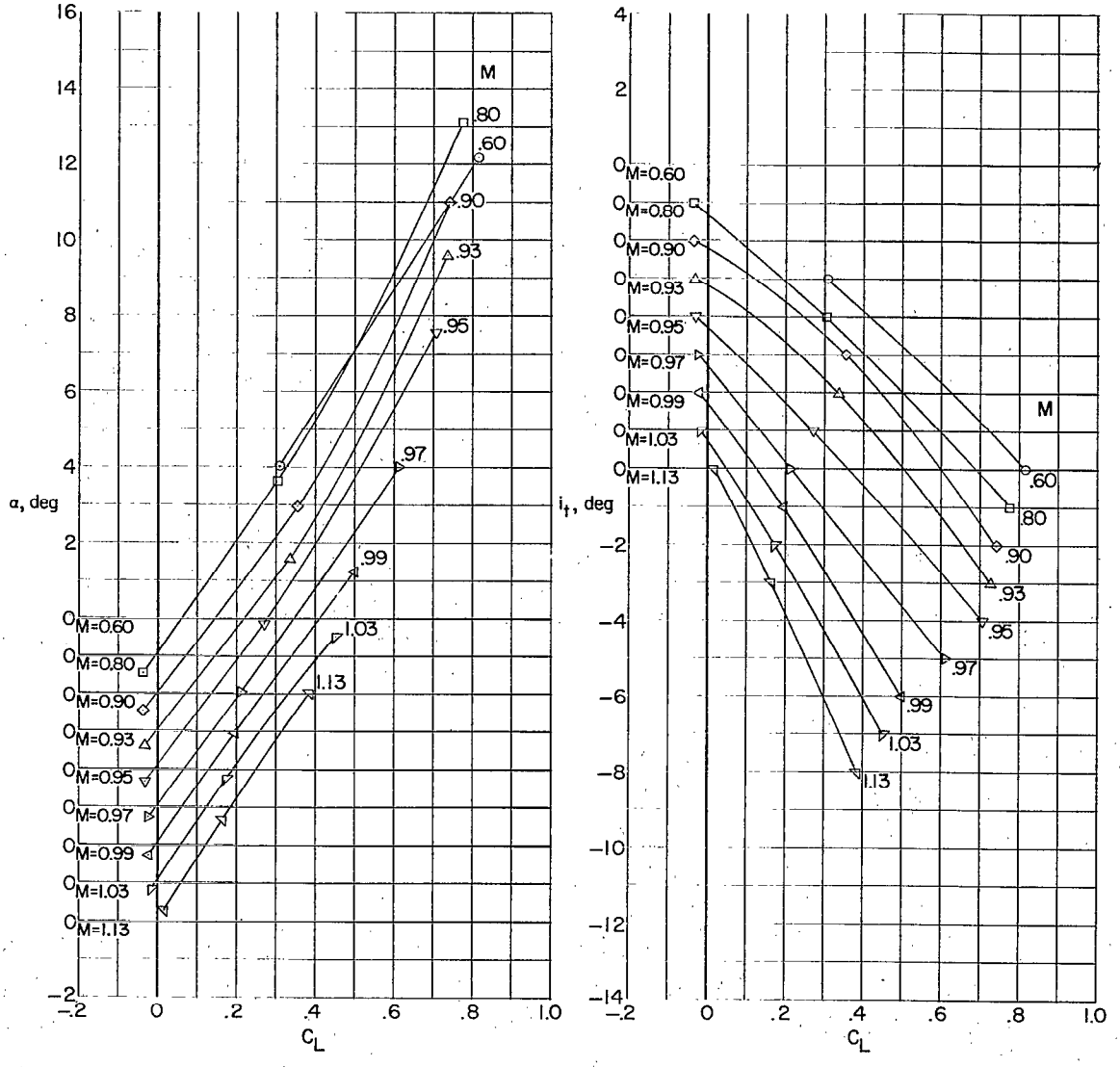

(a) Trim angle of attack and horizontal-tail incidence.

Figure 42.- Variation of aerodynamic characteristics with either lift coefficient or Mach number at trim conditions (C_m = 0). Complete model; A = 3.18; supersonic inlet (cruise condition).

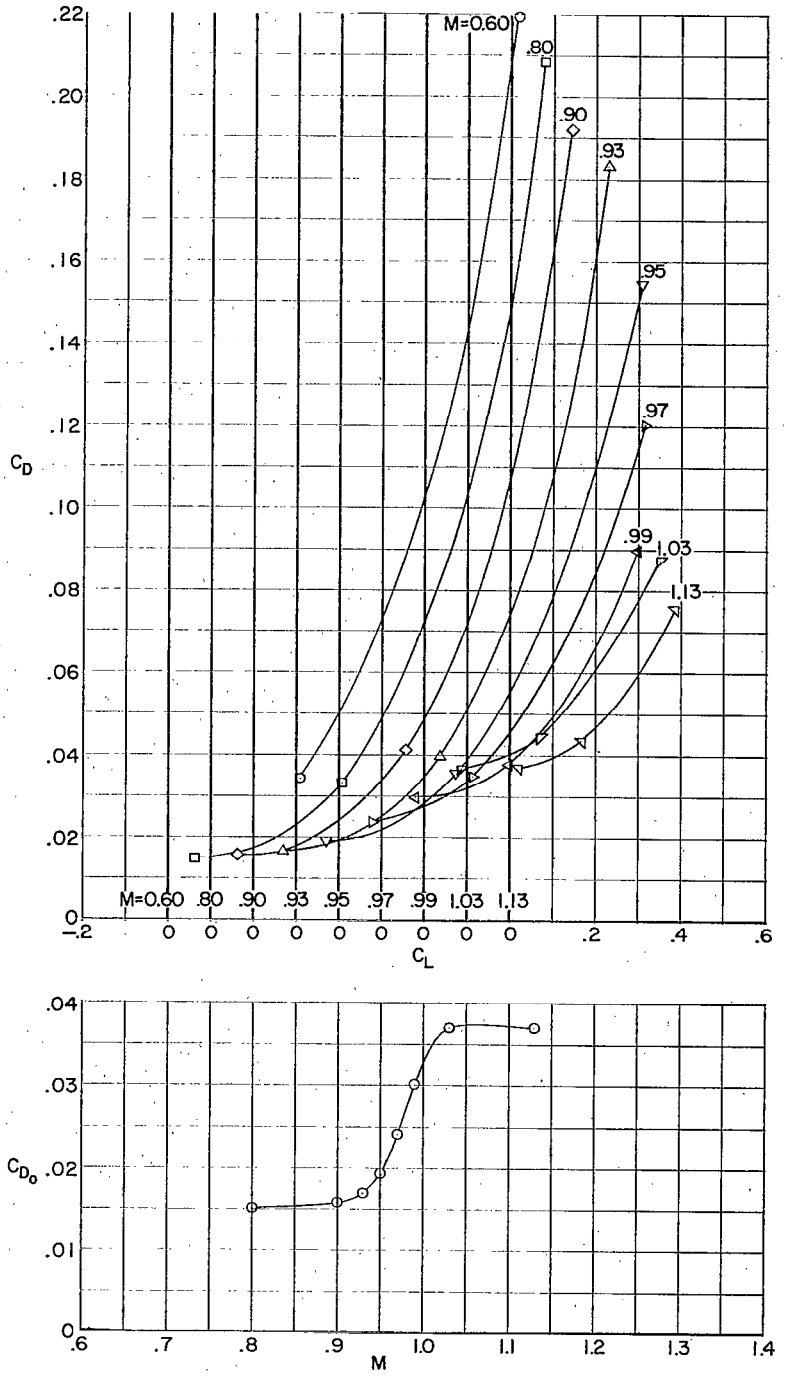

(b) Trim drag coefficient and zero-lift drag coefficient.

Figure 42.- Continued.

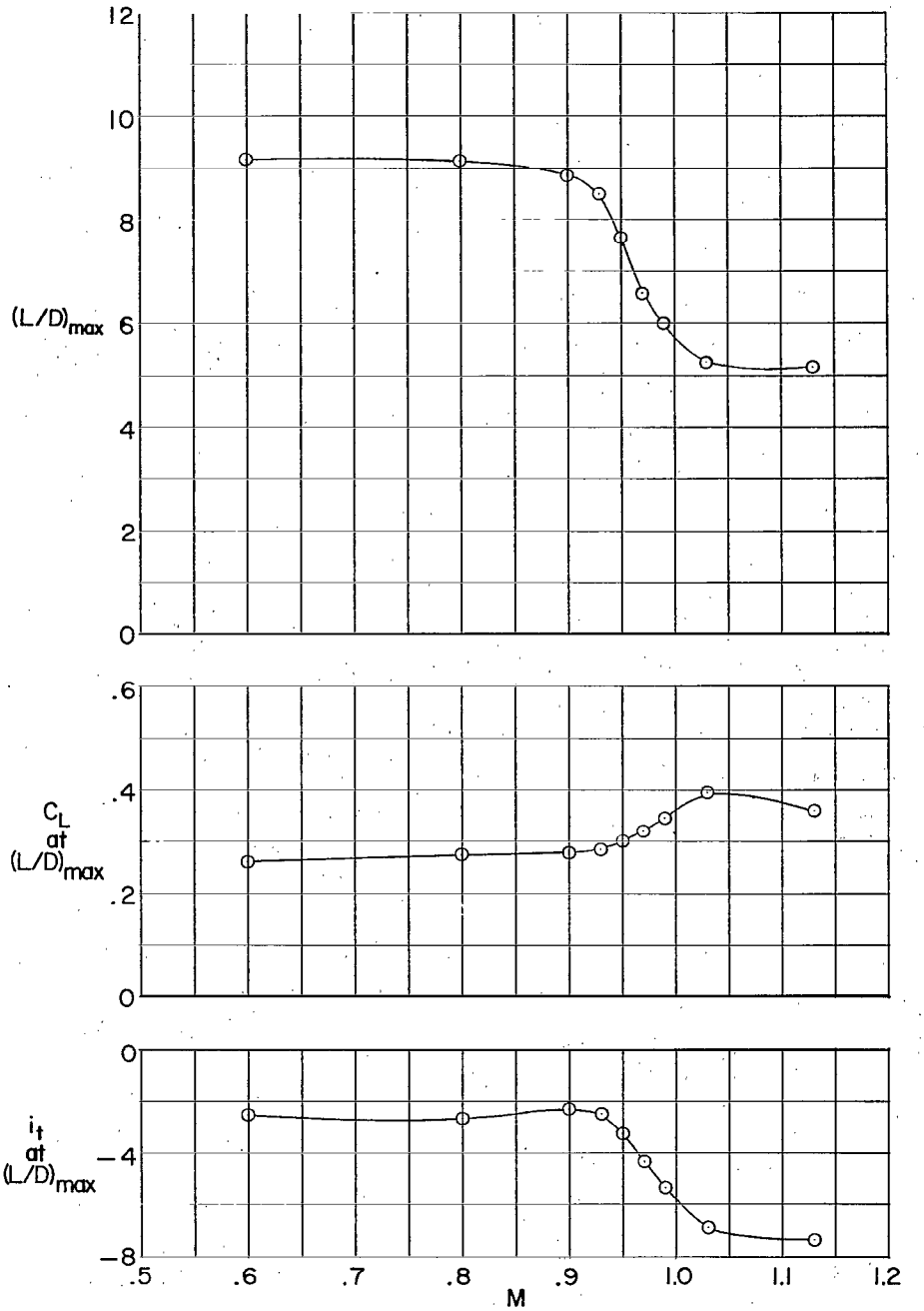

(c) Trim $(L/D)_{max}$, C_L at $(L/D)_{max}$, and i_t at $(L/D)_{max}$.

Figure 42.- Concluded.

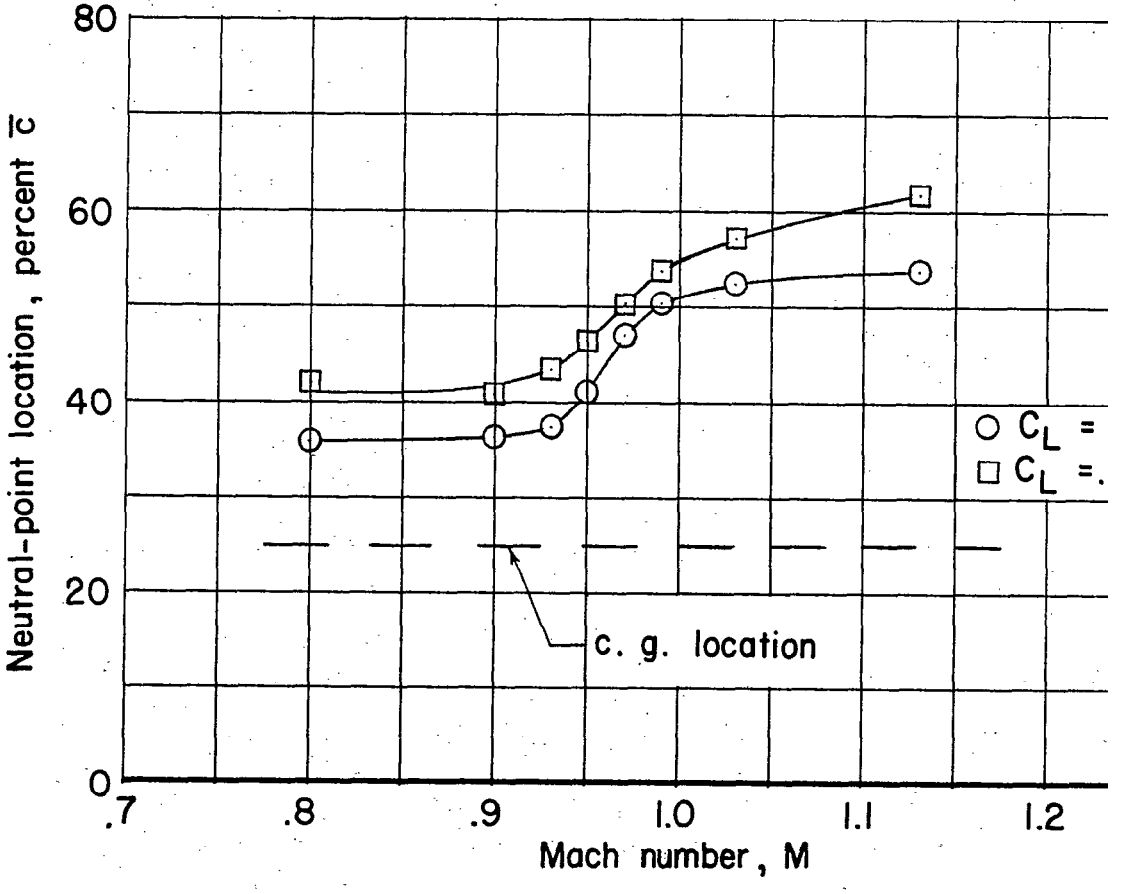

Figure 43.- Variation of neutral-point location with Mach number. plete model; A = 3.18; supersonic inlet (cruise condition).

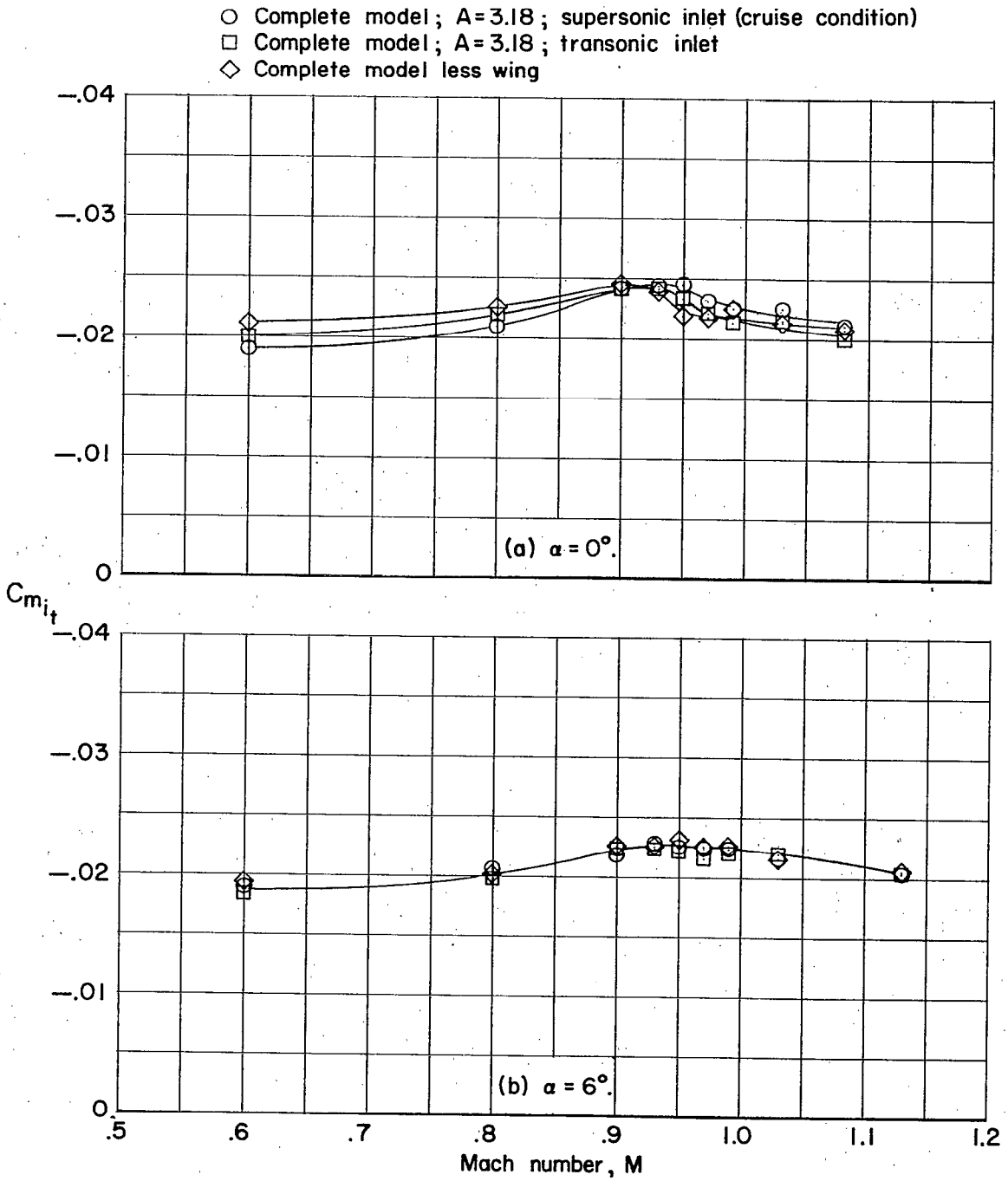

Figure 44.- Variation of horizontal-tail effectiveness with Mach number. Complete model, A = 3.18, and complete model less wing.

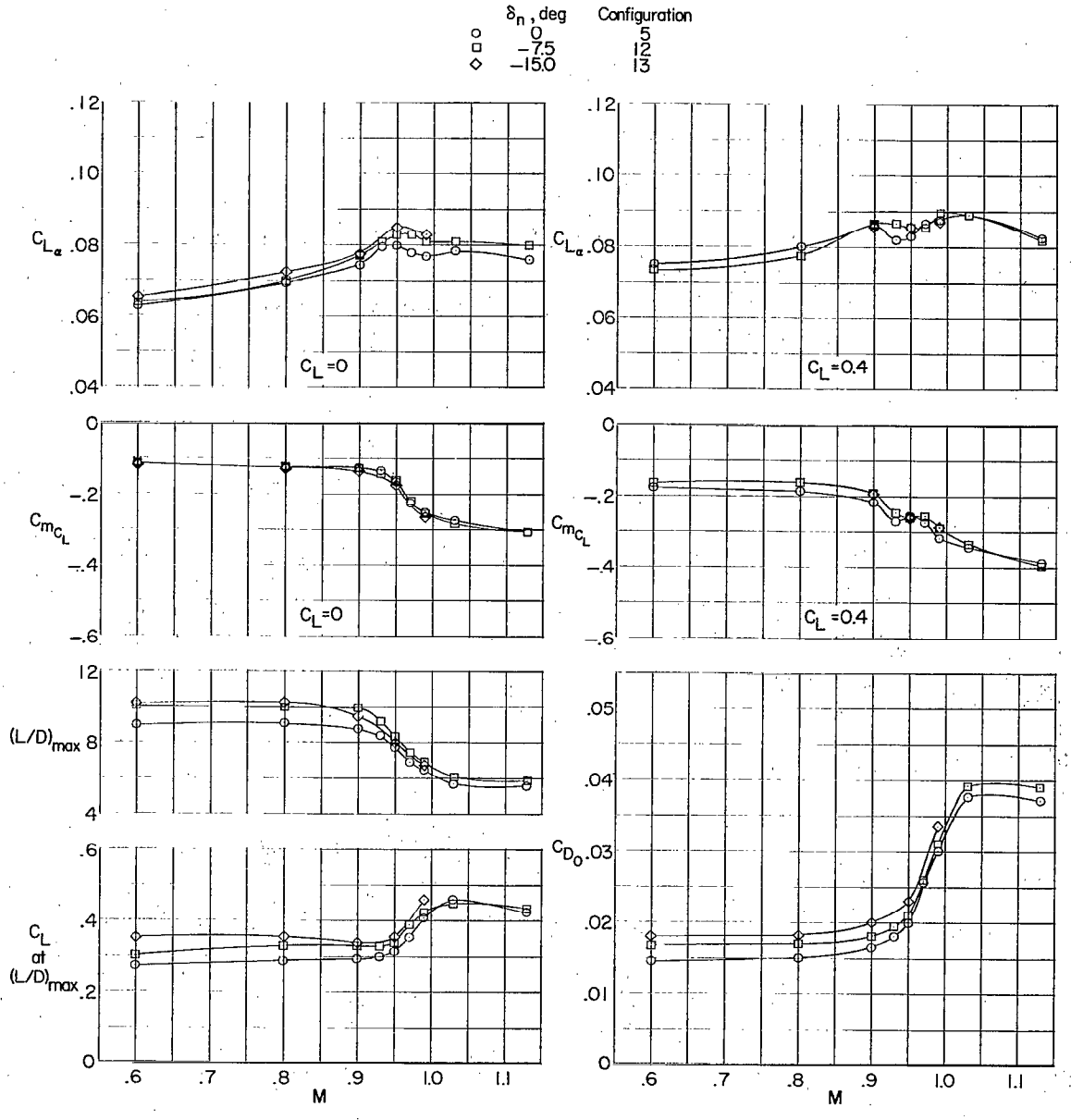

Figure 45.- Effect of wing leading-edge flap on aerodynamic characteristics. Complete model; $i_t = -3^\circ$; A = 3.18; supersonic inlet (cruise condition).

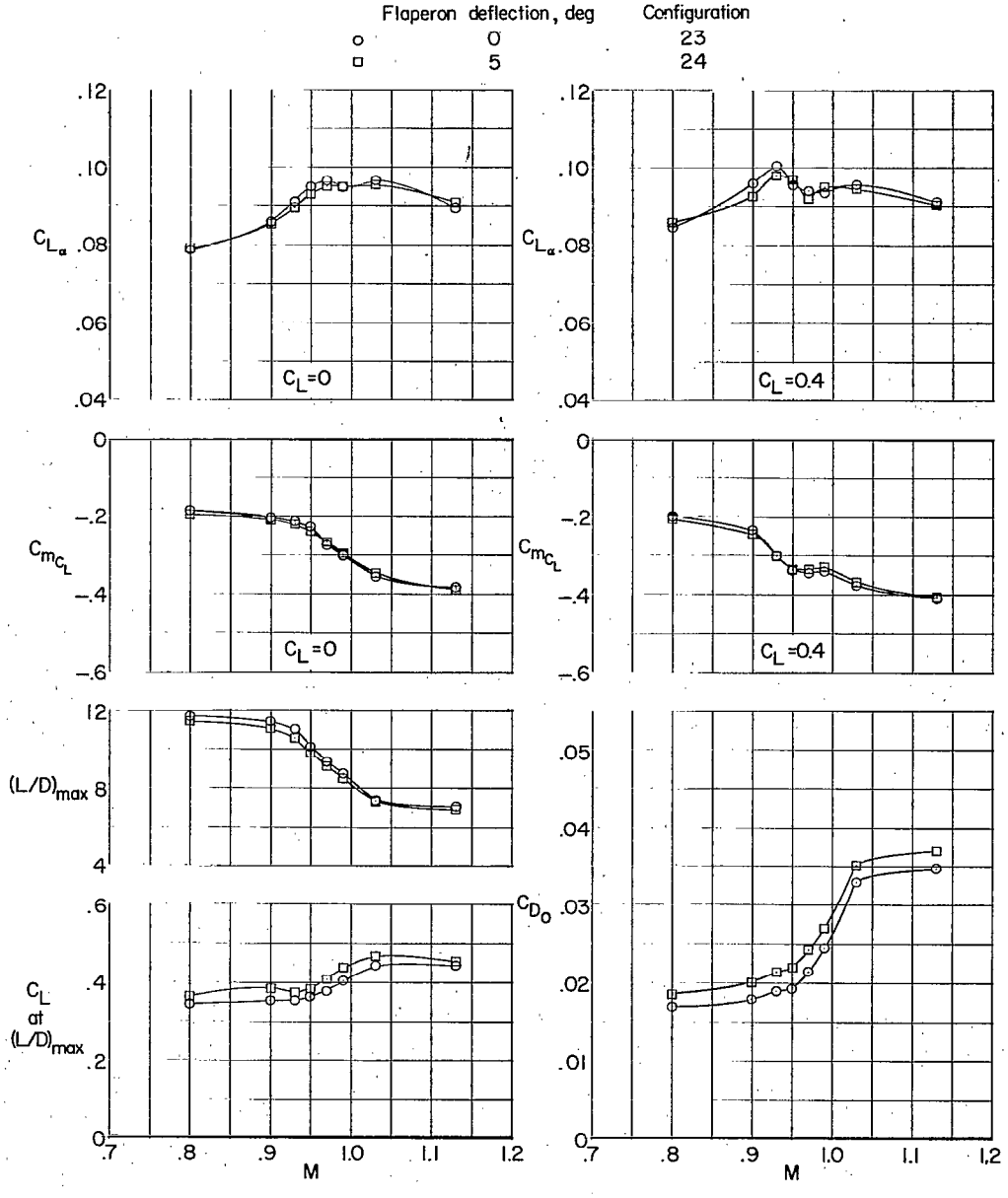

(a) C_{L_α}, $C_{m_{C_L}}$, $(L/D)_{max}$, and C_{D_o} characteristics.

Figure 46.- Effect of wing flaperon deflection on aerodynamic characteristics. Complete model; $i_t = -3^\circ$; $\delta_n = -7.5^\circ$; body with modified M = 1 bump; A = 3.69; wing modification 2; drooped supersonic inlet (cruise condition) with inlet modification 1.

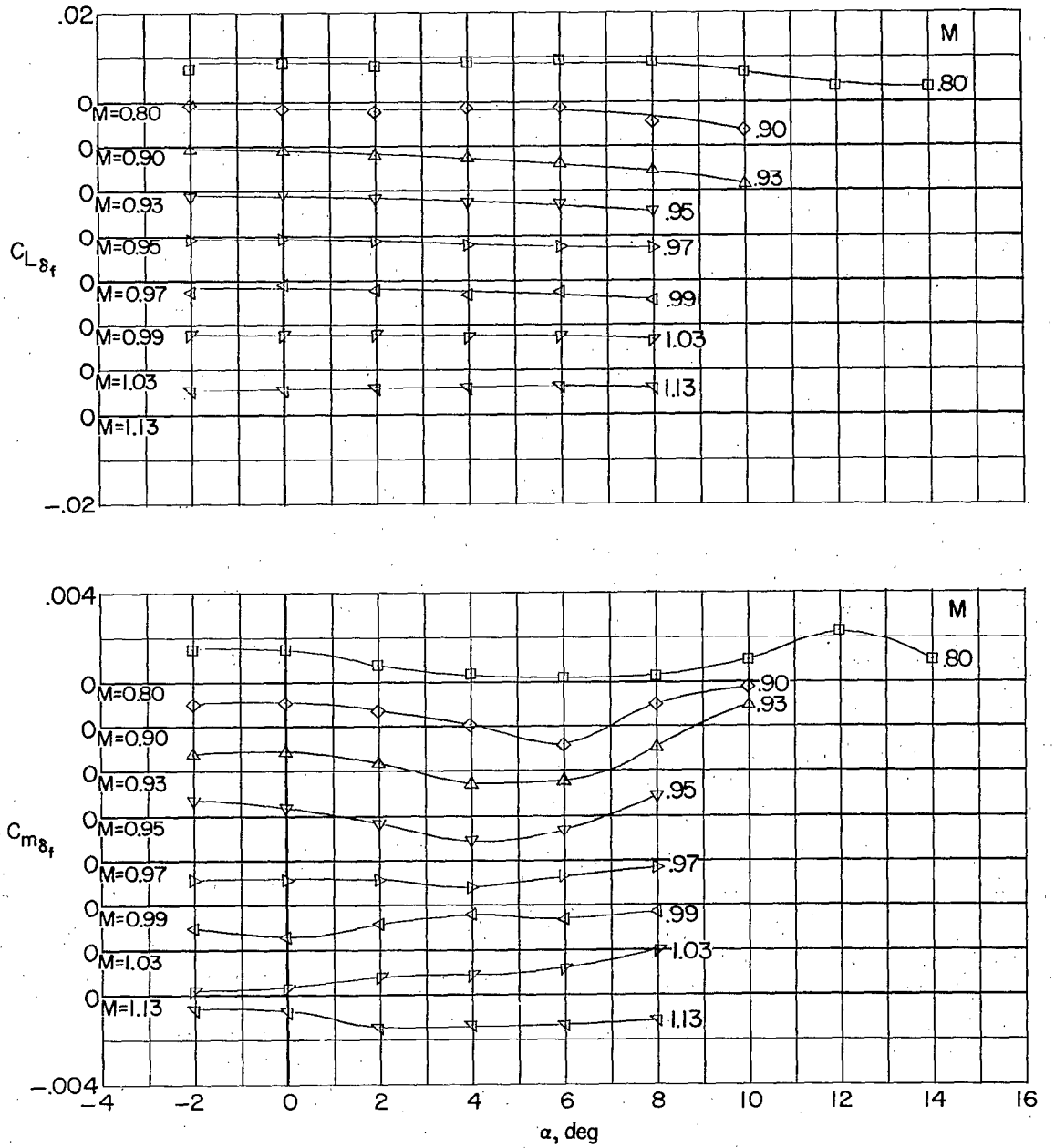

(b) $C_{L_{\delta_f}}$ and $C_{m_{\delta_f}}$.

Figure 46.- Continued.

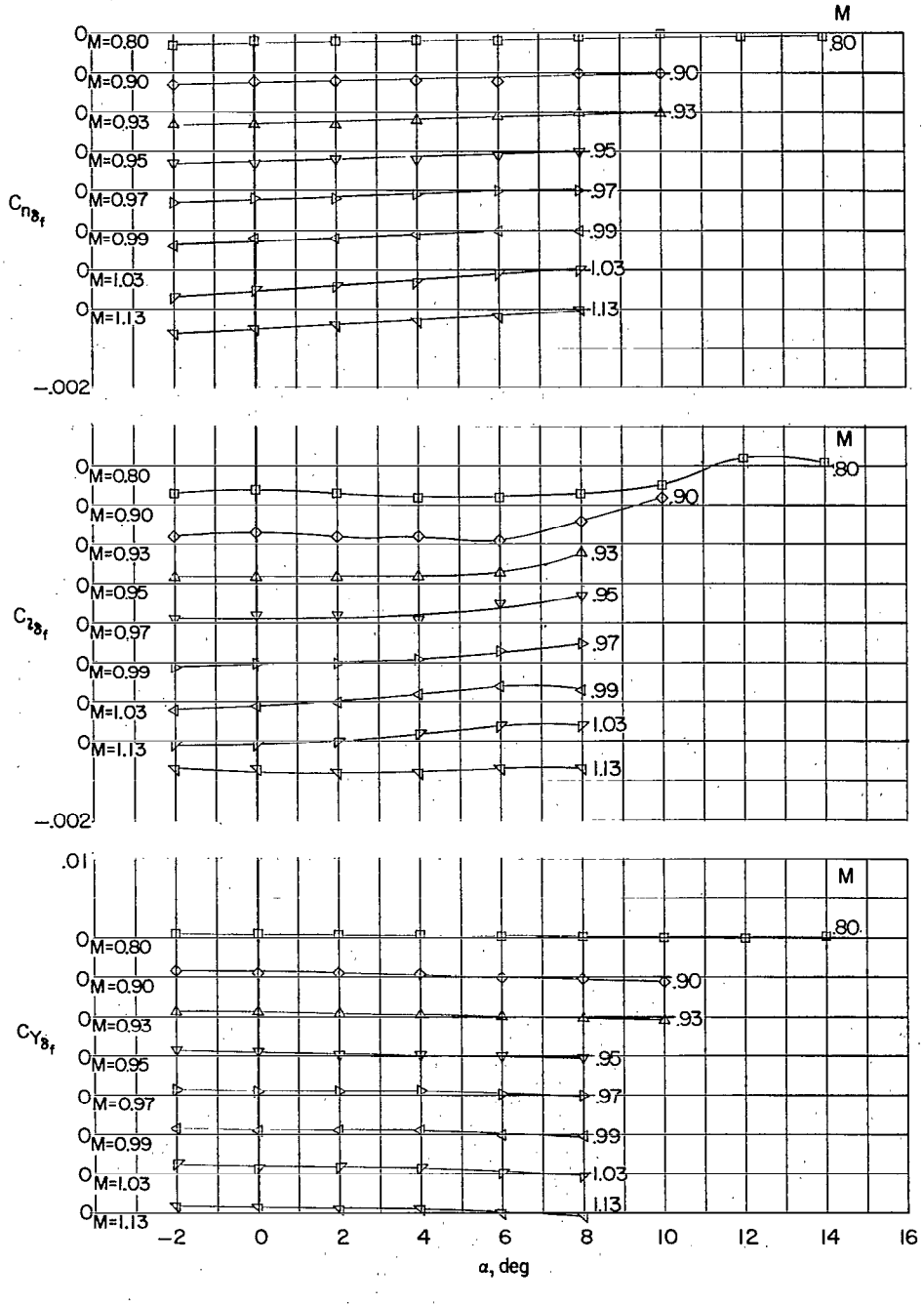

(c) $C_{n_{\delta_f}}$, $C_{l_{\delta_f}}$, and $C_{Y_{\delta_f}}$.

Figure 46.- Continued.

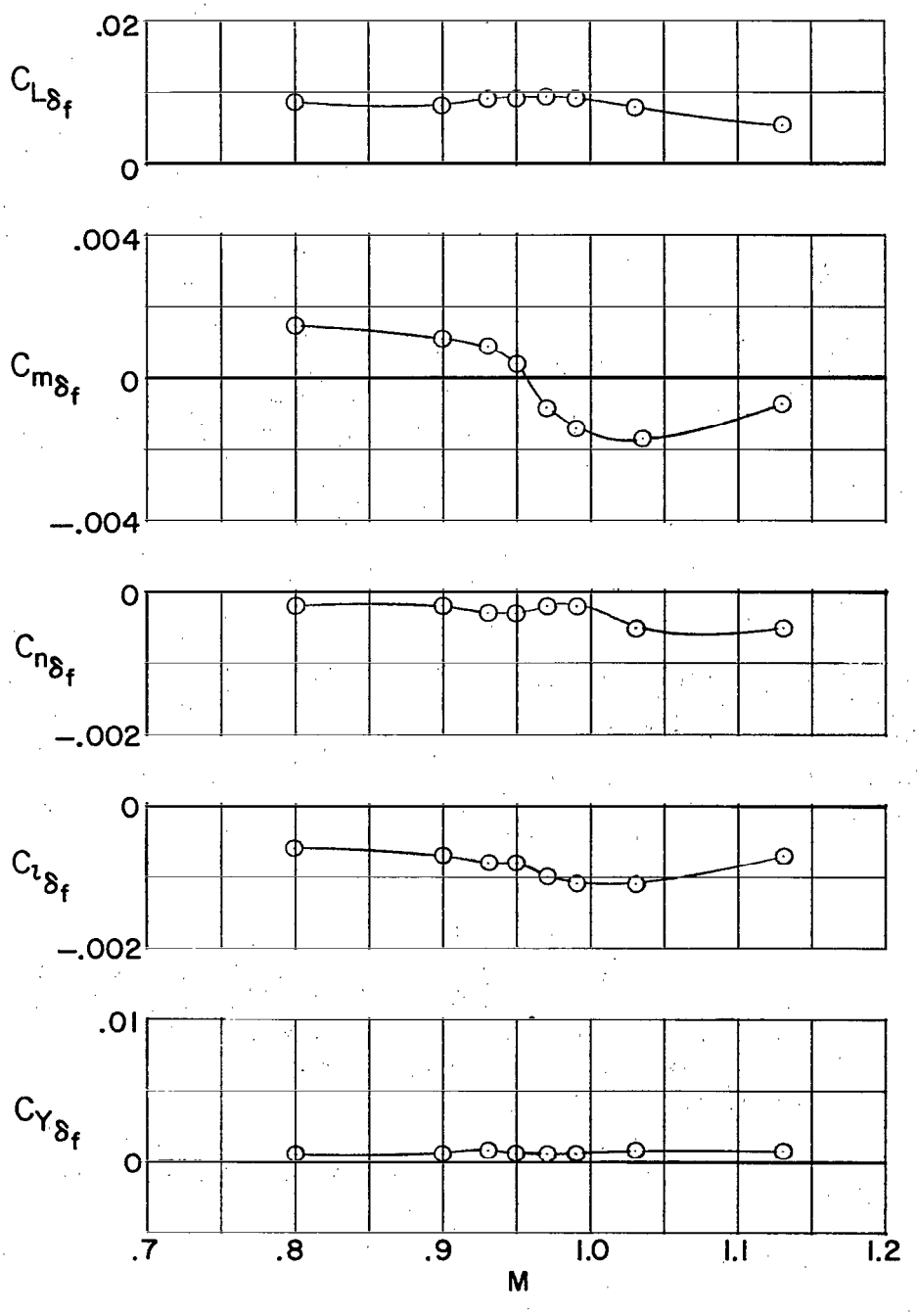

(d) $C_{L_{\delta_f}}$, $C_{m_{\delta_f}}$, $C_{n_{\delta_f}}$, $C_{l_{\delta_f}}$, and $C_{Y_{\delta_f}}$ at $\alpha = 0^\circ$.

Figure 46.- Concluded.

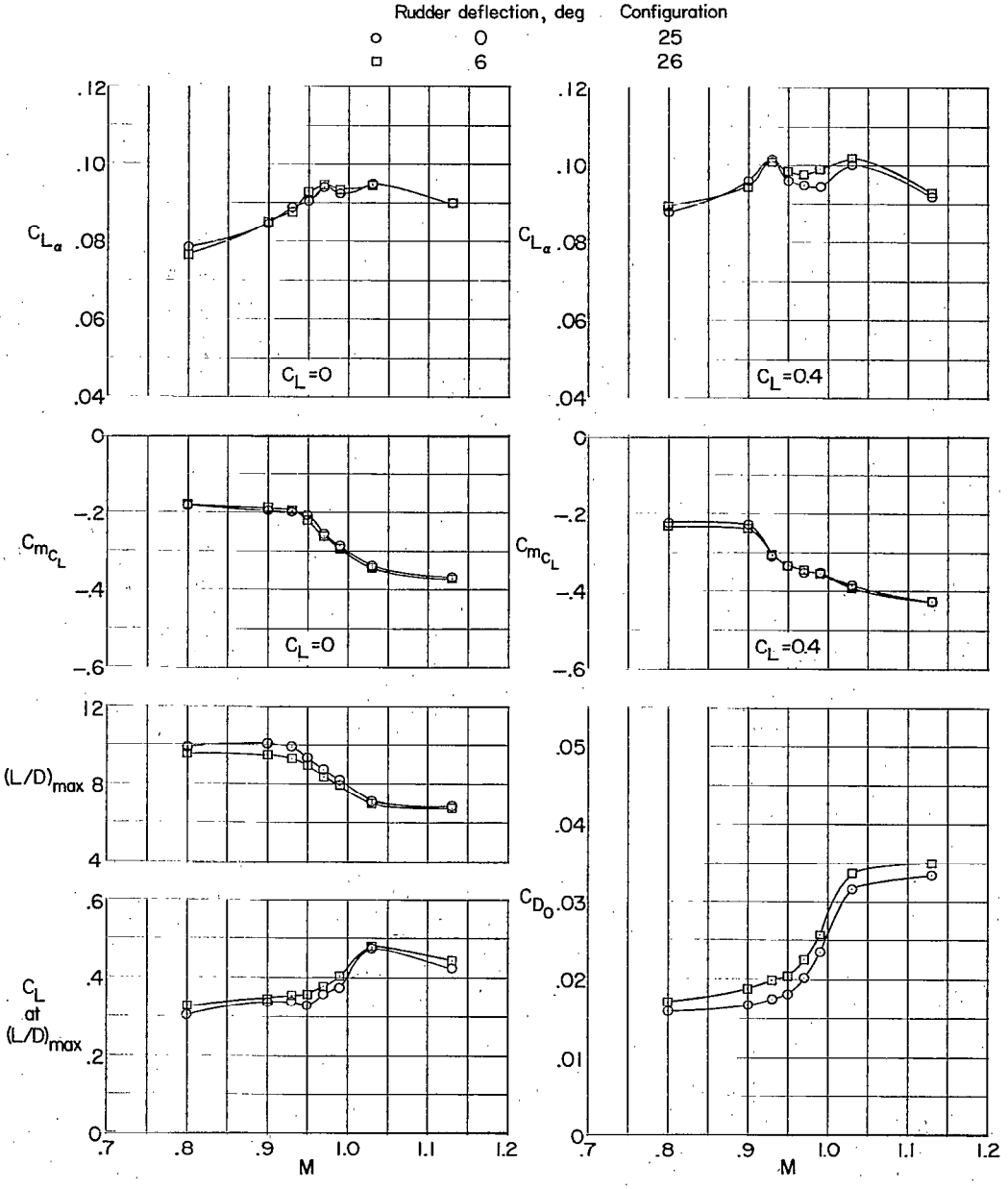

(a) C_{L_α}, $C_{m_{C_L}}$, $(L/D)_{max}$, and C_{D_o} characteristics.

Figure 47.- Effect of rudder deflection on aerodynamic characteristics. Complete model; $i_t = -3^o$; body with modified M = 1 bump; A = 3.69; wing modification 3; drooped supersonic inlet (cruise condition) with inlet modification 1.

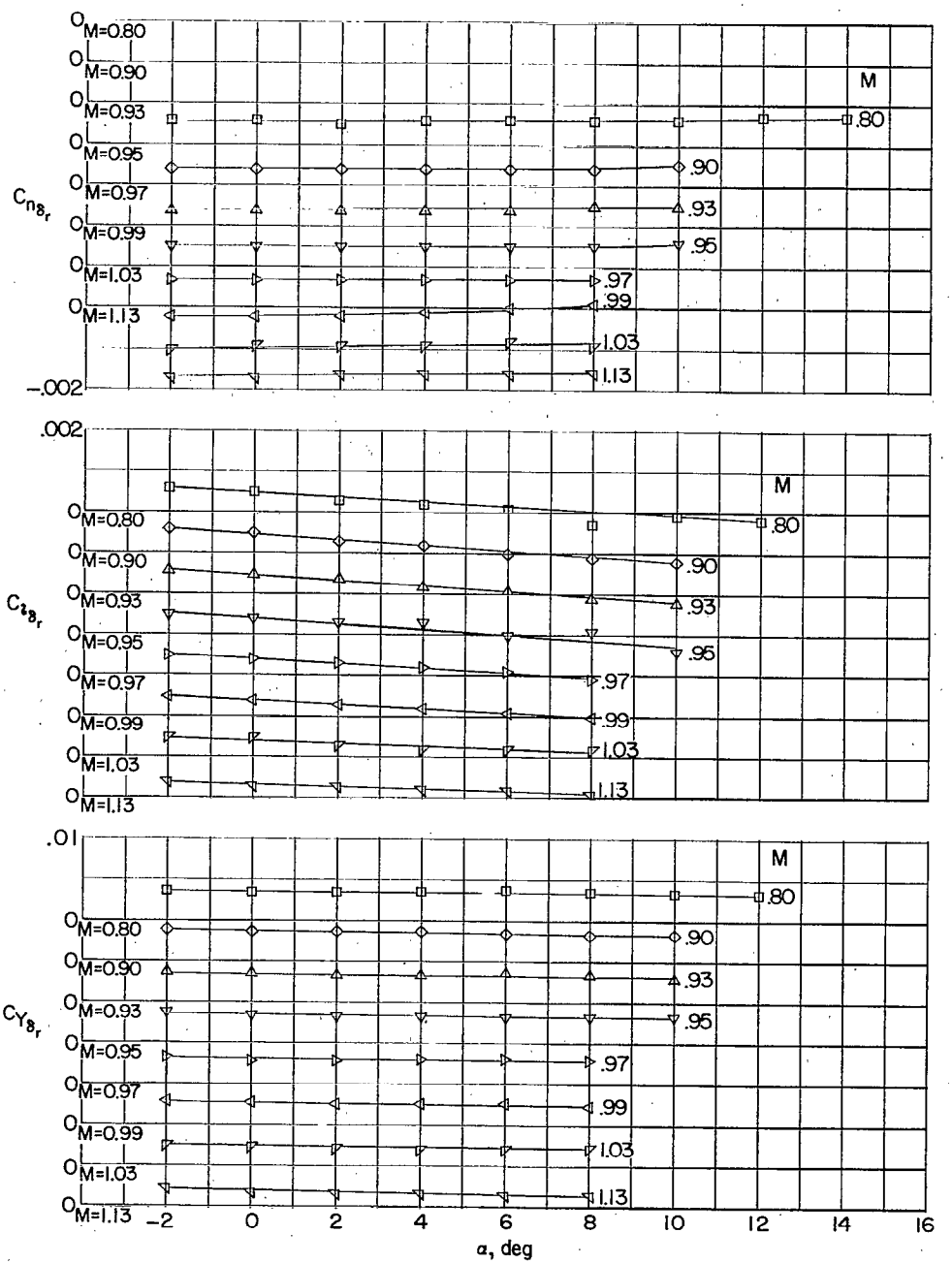

(b) $C_{n_{\delta_r}}$, $C_{l_{\delta_r}}$, and $C_{Y_{\delta_r}}$.

Figure 47.- Continued.

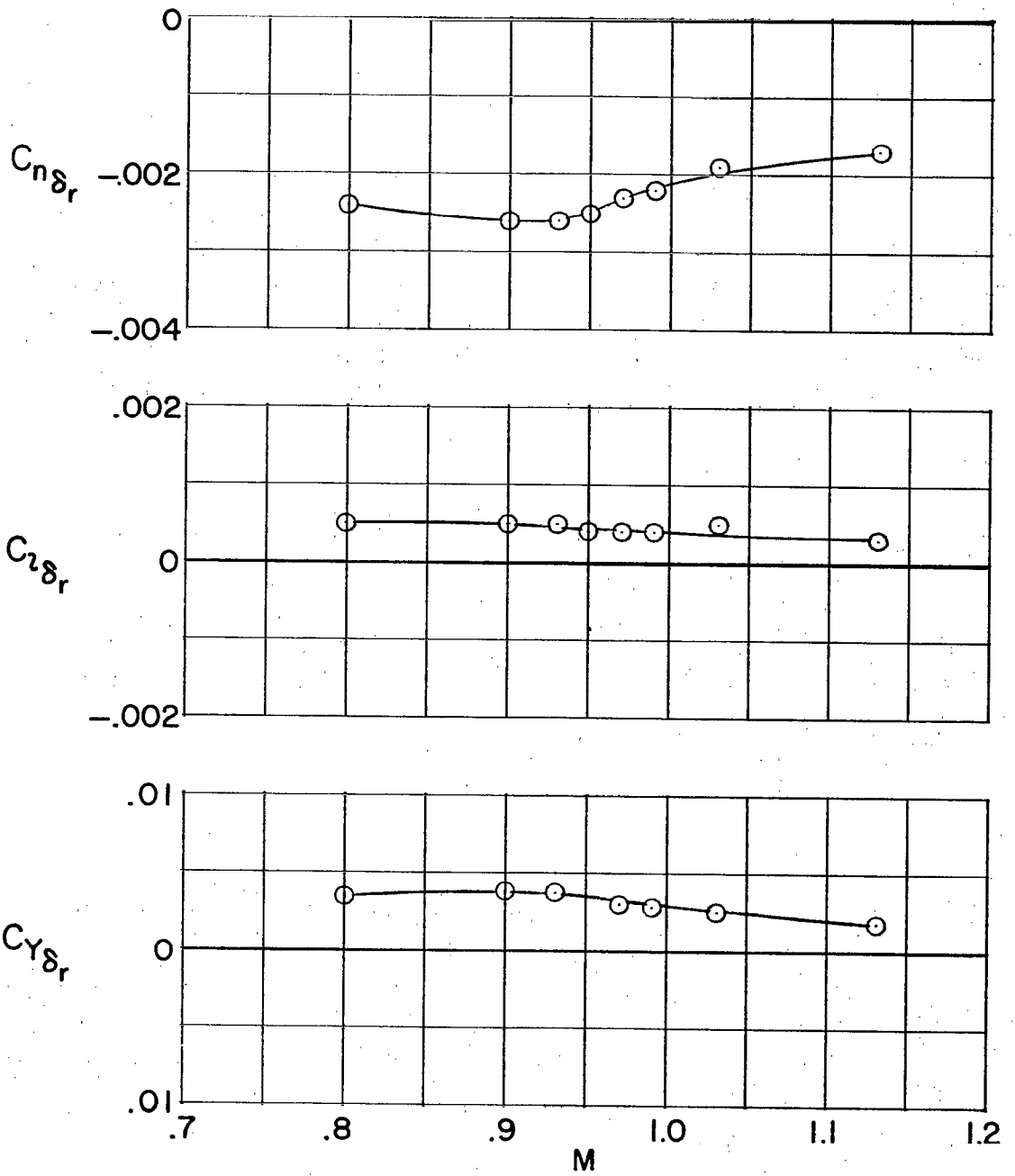

(c) $C_{n_{\delta_r}}$, $C_{l_{\delta_r}}$, and $C_{Y_{\delta_r}}$ at $\alpha = 0^\circ$.

Figure 47.- Concluded.

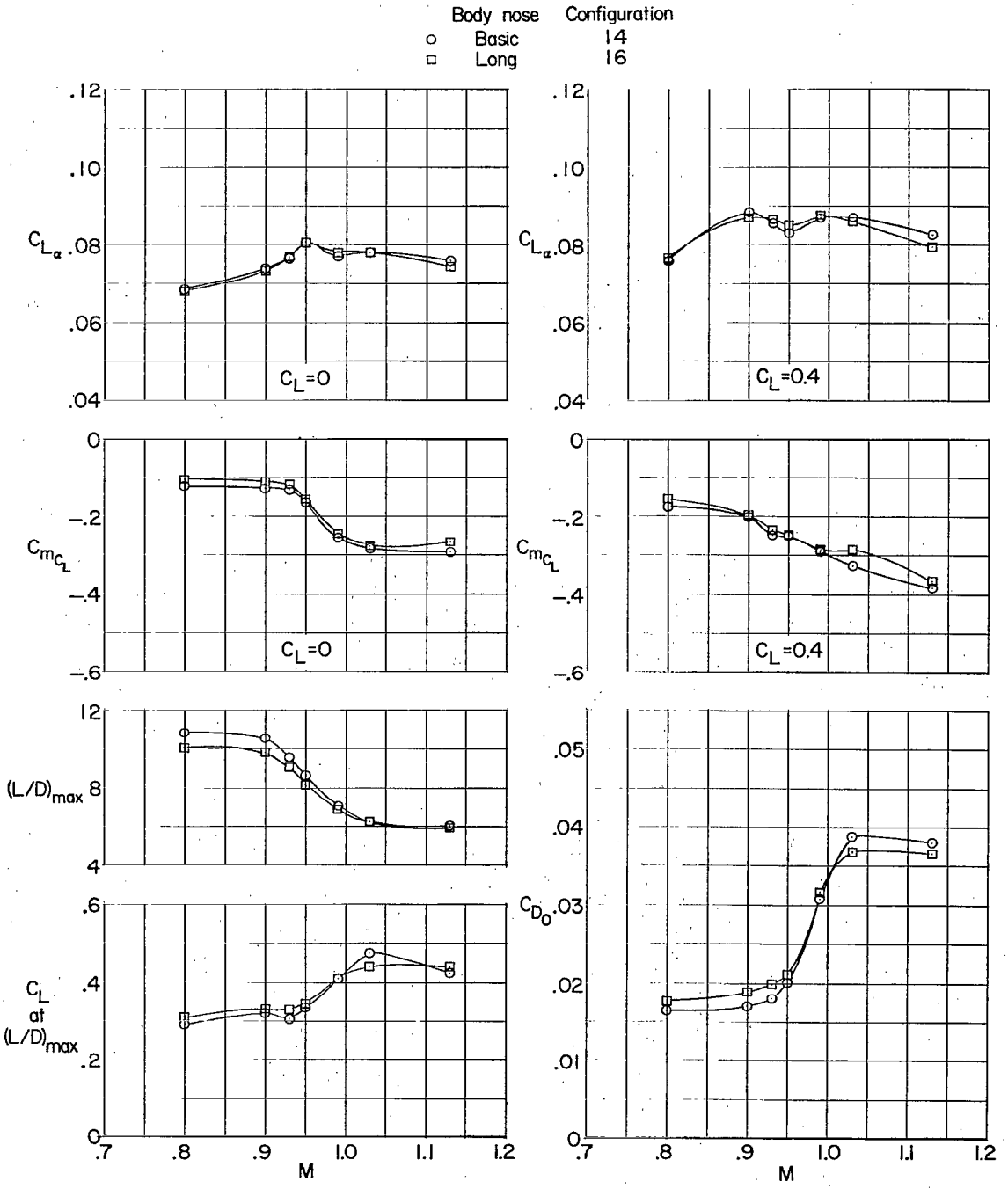

Figure 48.- Effect of body-nose extension on aerodynamic characteristics. Complete model; $i_t = -3^\circ$; $\delta_n = -7.5^\circ$; A = 3.18; drooped supersonic inlet (cruise condition).

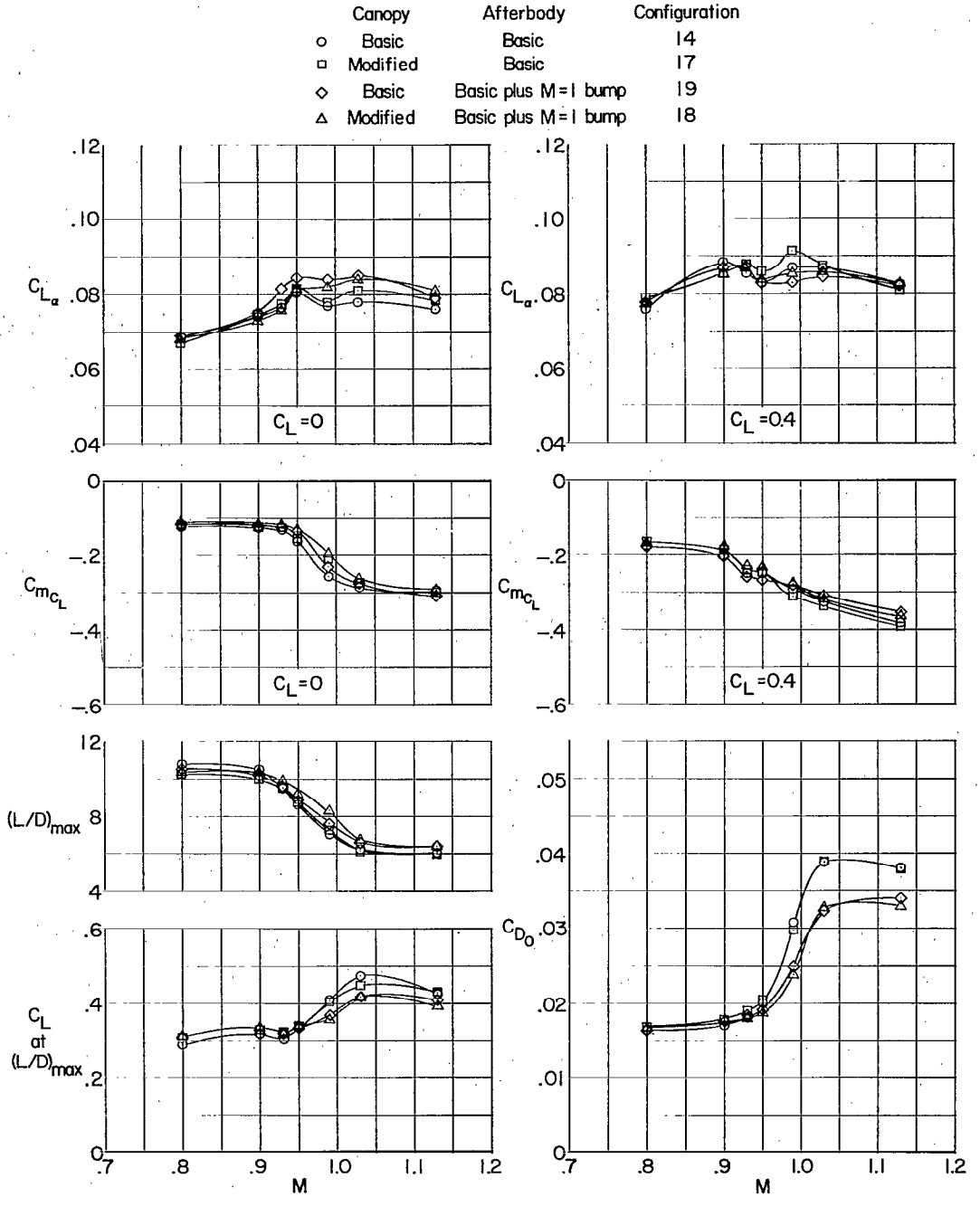

Figure 49.- Effect of canopy modification and M = 1 bump on aerodynamic characteristics. Complete model; $i_t = -3^\circ$; $\delta_n = -7.5^\circ$; A = 3.18; drooped supersonic inlet (cruise condition).

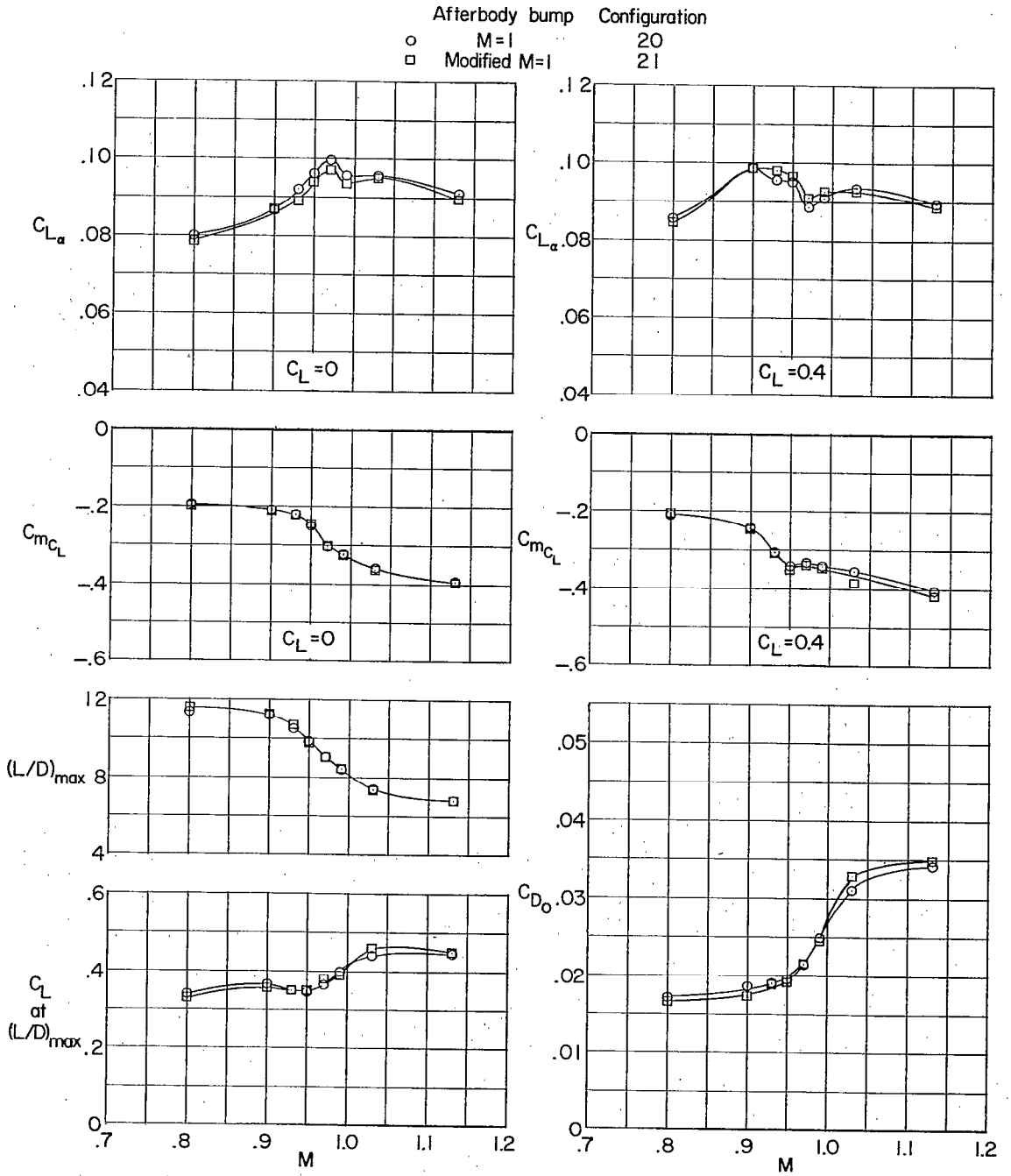

Figure 50.- Comparison of aerodynamic characteristics of afterbody bumps. Complete model; $i_t = -3^\circ$; $\delta_n = -7.5^\circ$; A = 3.69; drooped supersonic inlet (cruise condition).

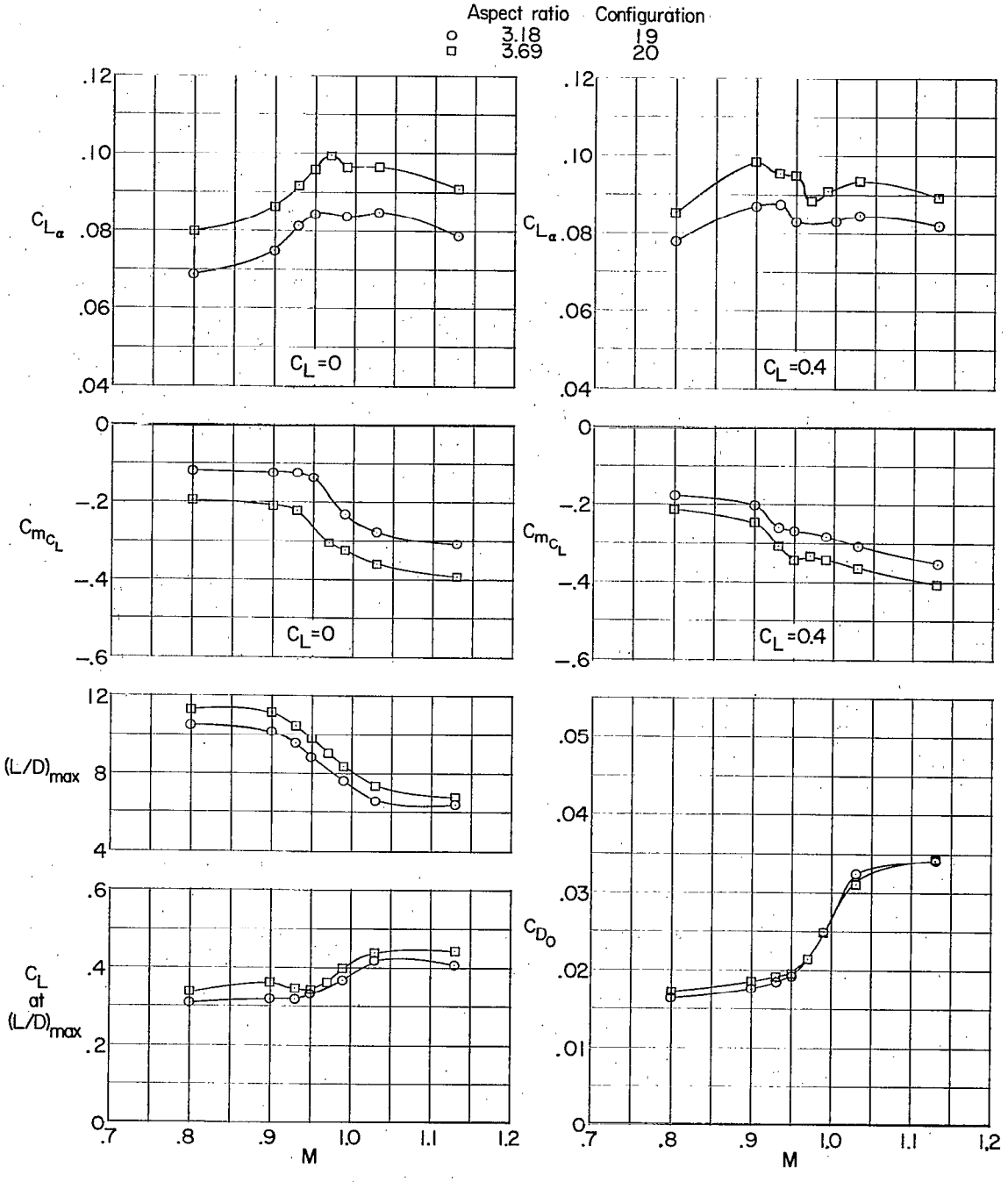

Figure 51.- Effect of wing-tip extension on aerodynamic characteristics. Complete model; $i_t = -3^\circ$; $\delta_n = -7.5^\circ$; body with M = 1 bump; drooped supersonic inlet (cruise condition).

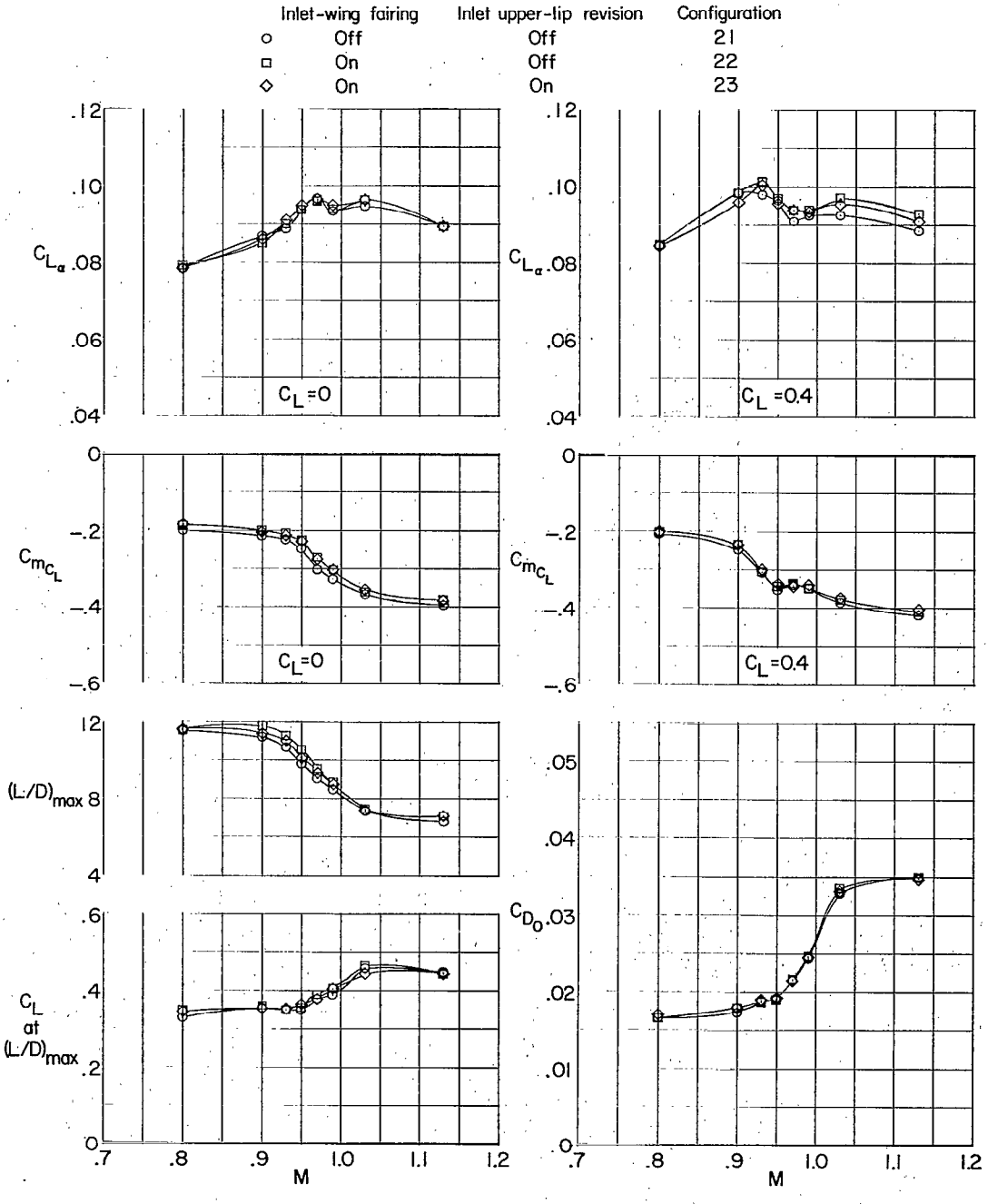

Figure 52.- Effect of inlet-wing fairing (wing modification 2) and inlet upper-lip revision (inlet modification 1) on aerodynamic characteristics. Complete model; $i_t = -3^\circ$; $\delta_n = -7.5^\circ$; body with supersonic bump; A = 3.69; drooped supersonic inlet (cruise condition).

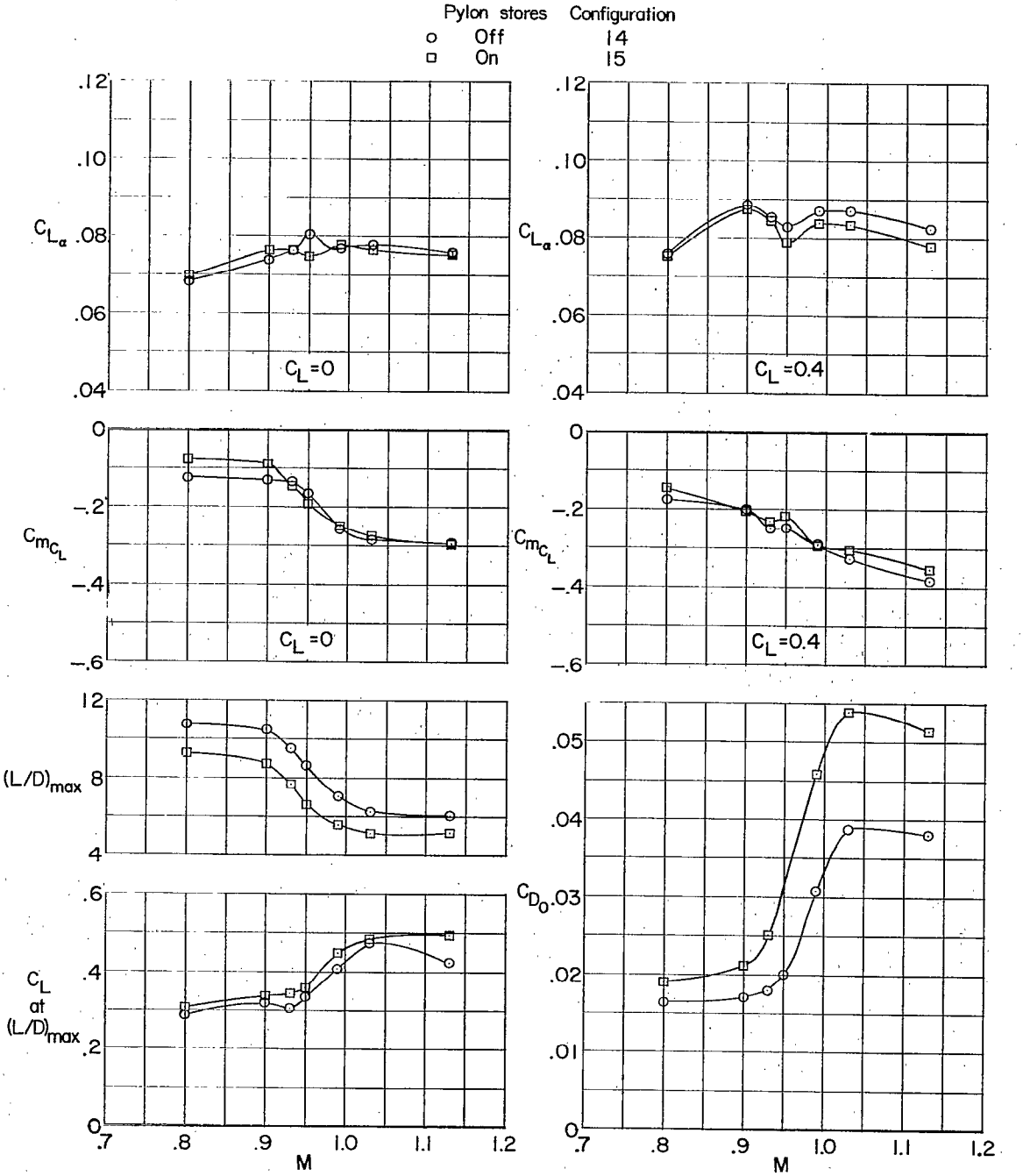

Figure 53.- Effect of pylon stores on aerodynamic characteristics. Complete model; $i_t = -3^\circ$; $\delta_n = -7.5^\circ$; A = 3.18; drooped supersonic inlet (cruise condition).

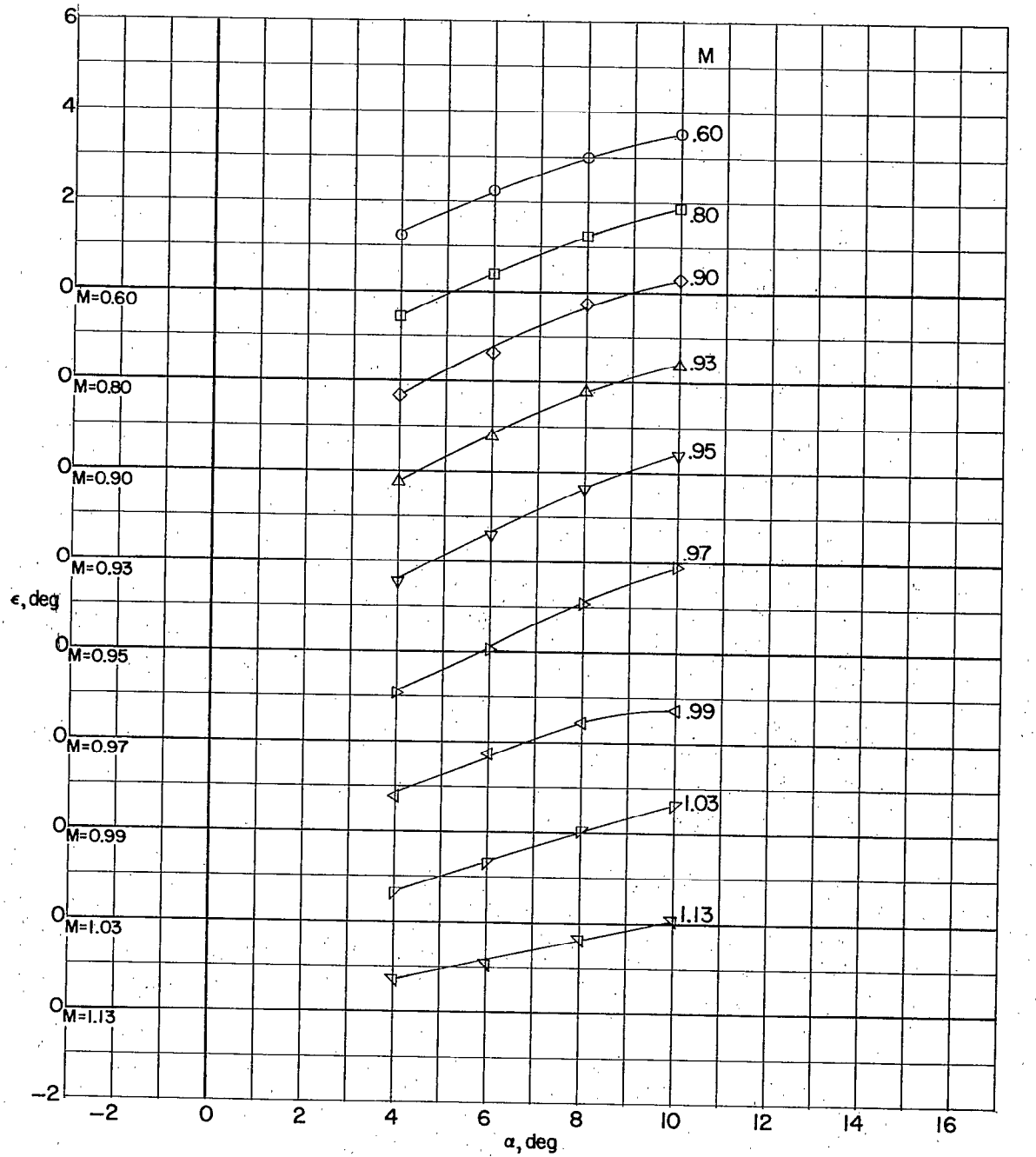

(a) Complete model; transonic inlet.

Figure 54.- Variation of effective downwash angle with angle of attack. Complete model, A = 3.18, and complete model less wing.

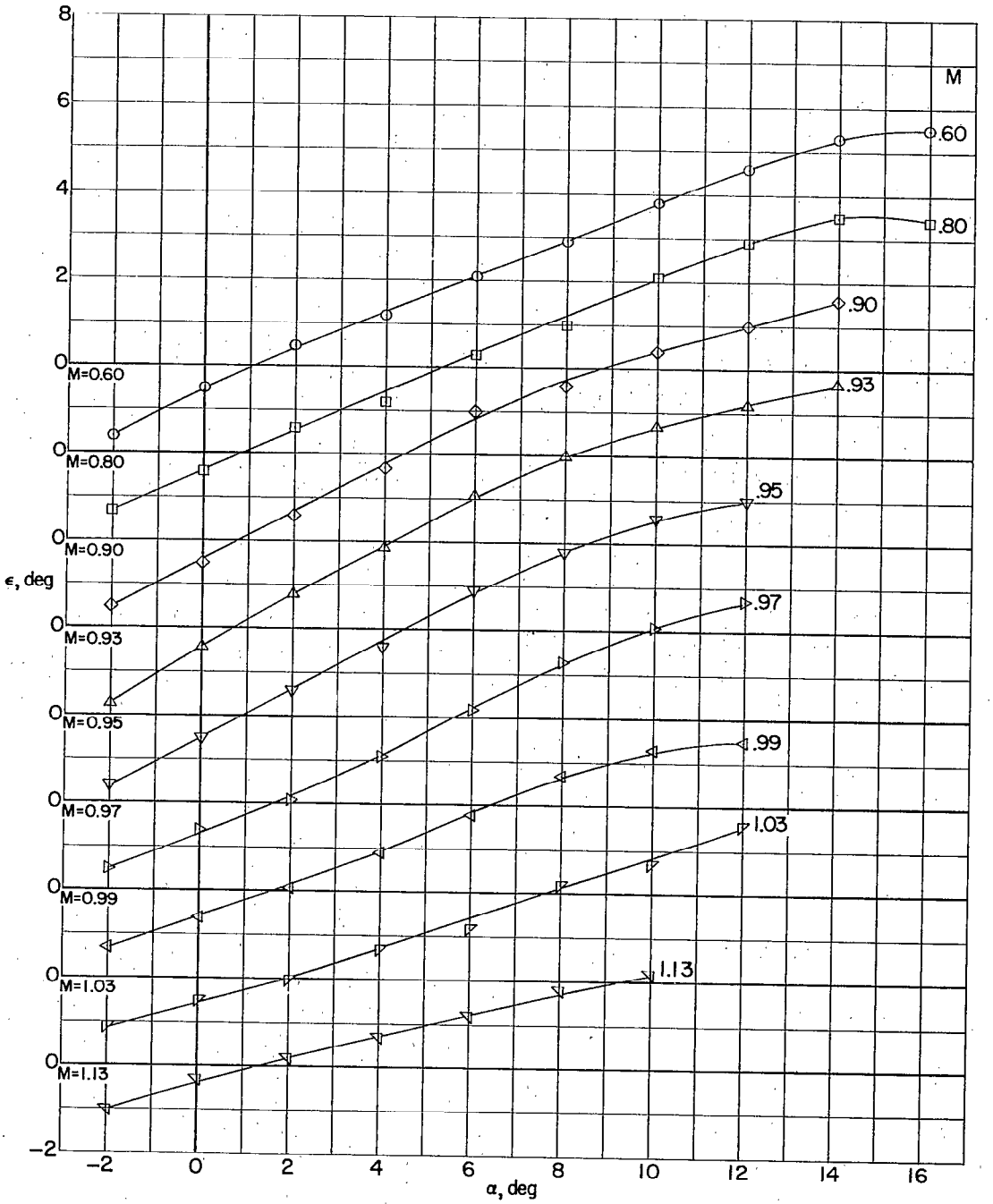

(b) Complete model; supersonic inlet (cruise condition).

Figure 54.- Continued.

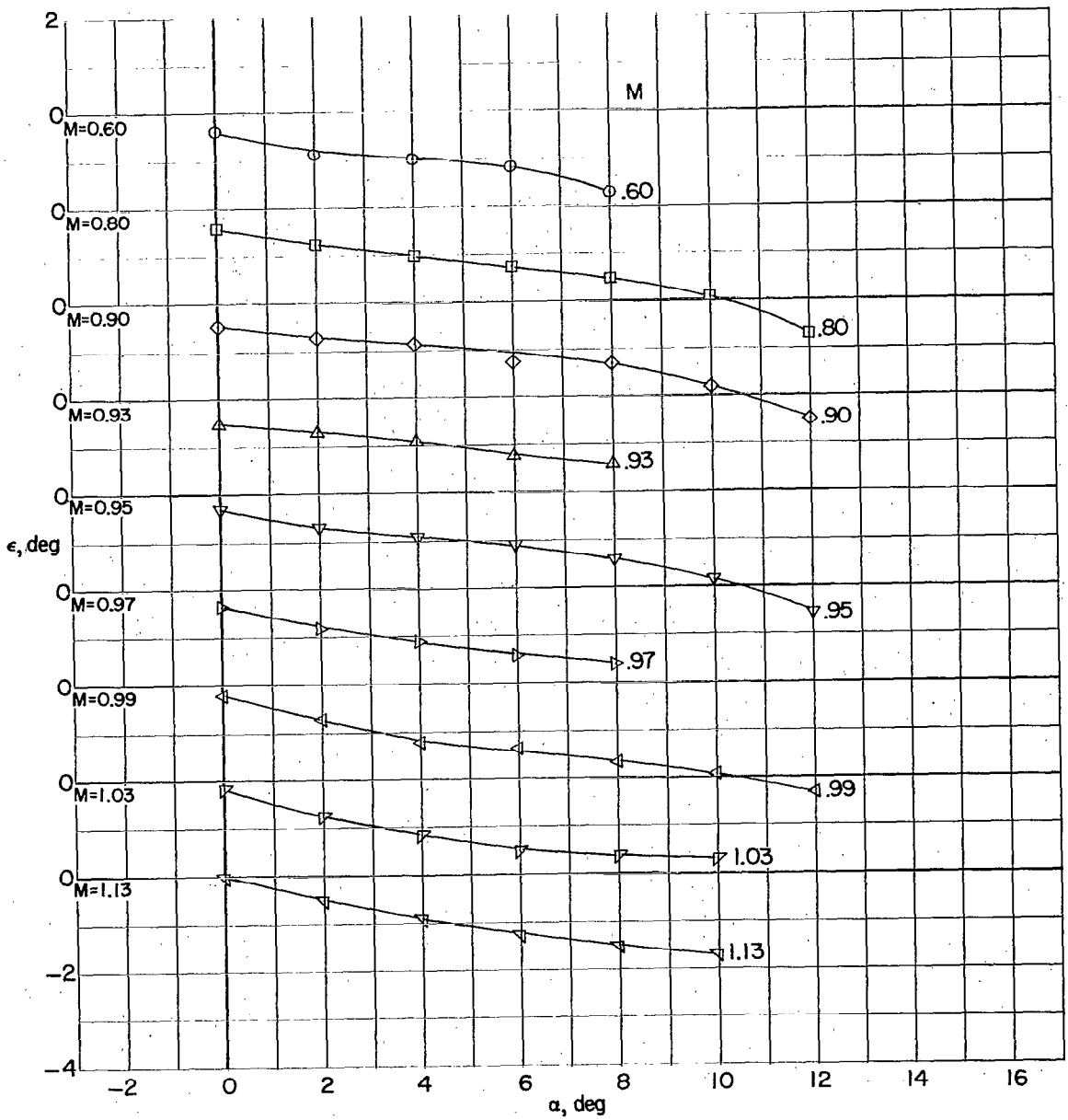

(c) Complete model less wing.

Figure 54.- Concluded.

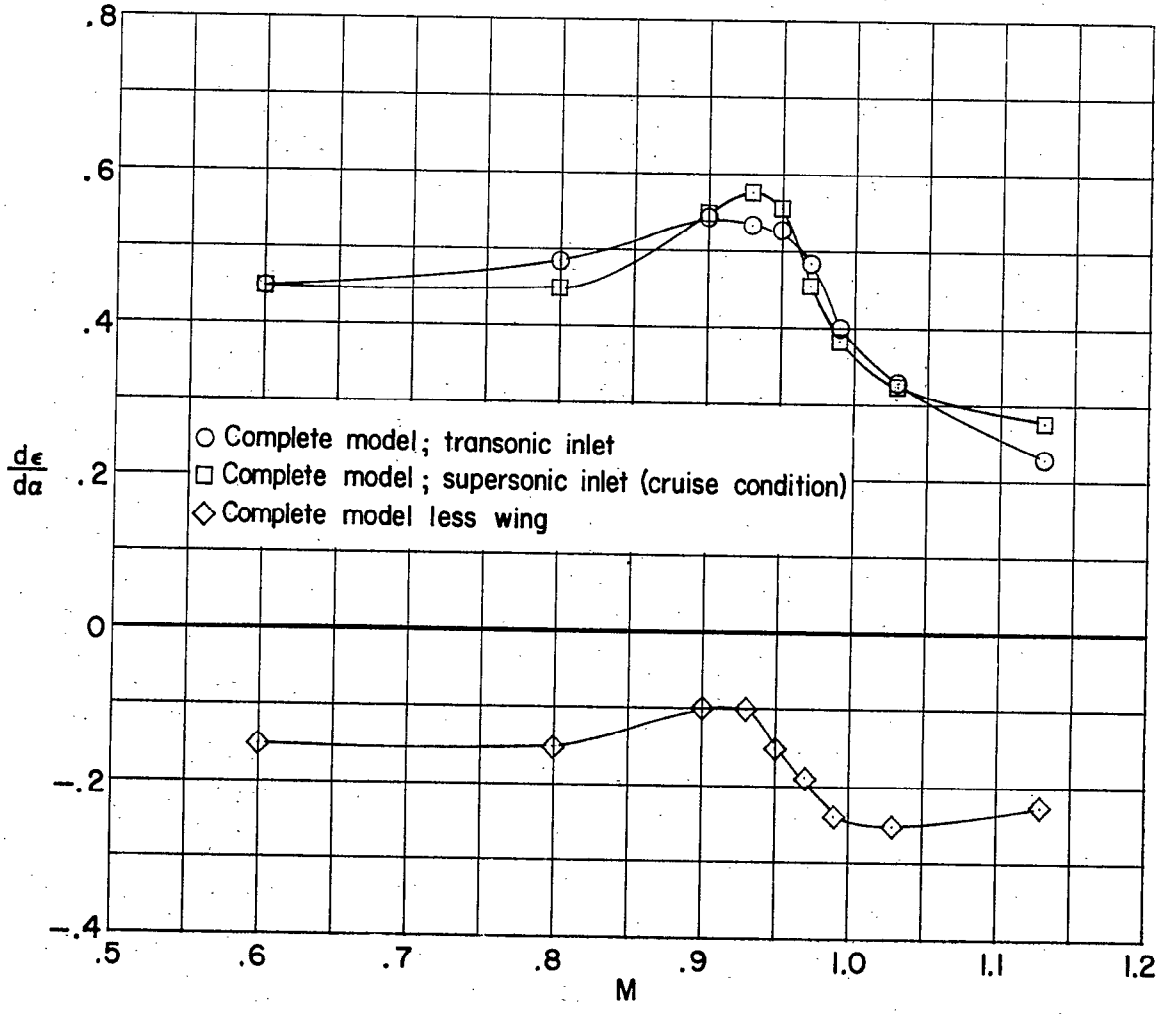

Figure 55.- Variation with Mach number of rate of change of effective downwash angle with angle of attack. Complete model, A = 3.18, and complete model less wing.

INDEX

ABSTRACT

This paper contains longitudinal stability and control and performance characteristics of a 1/22-scale model of the Republic F-105 airplane at Mach numbers from 0.60 to 1.13. The angle-of-attack range varied from approximately -2° to 16° at the lowest Mach number to -2° to 9° at the highest Mach number. No serious pitch-up difficulties were evident at a constant Mach number. An afterbody bump markedly reduced the transonic drag.